acta physica slovaca vol. 65 No. 2, 65 – 152 **April 2015**

PHOTONIC PLATFORM AND THE IMPACT OF OPTICAL NONLINEARITY ON COMMUNICATION DEVICES

Md Shakil Ahmed and Ivan Glesk[1]

Department of Electrical and Electronic Engineering, University of Strathclyde
Royal College Building, 204 George Street, Glasgow G1 1XW, United Kingdom

Received 5 June 2015, accepted 8 June 2015

It is important to understand properties of different materials and the impact they have on devices used in communication networks. This paper is an overview of optical non-linearities in Silicon and Gallium Nitride and how these nonlinearities can be used in the realization of optical ultra-fast devices targeting the next generation integrated optics. Research results related to optical lasing, optical switching, data modulation, optical signal amplification and photo-detection using Gallium Nitride devices based on waveguides are examined. Attention is also paid to hybrid and monolithic integration approaches towards the development of advanced photonic chips.

PACS: 42.79.Sz, 42.82.Gw, 85.60.Bt, 42.70.Nq

KEYWORDS: Optical Nonlinearity, Broadband Communications, Optical Waveguides, Photonic Chips, All-optical Switching, GaN Platform, Refractive Index, CMOS Compatibility, Hybrid Integrated Platform, Nonlinear Effects

Contents

[1] E-mail address: ivan.glesk@strath.ac.uk

1 Introduction

The use of photons instead of electrons is the main motivation for a development of future photonic devices which will be faster and consume less power to operate. But the question is, 'How to achieve it and how far away we are from this goal?' First of all, continuing the present efforts of making faster electronics will still go on, thanks to the support of the multi-billion dollars well established industry. The difficulty we are facing is that the silicon (Si) is running out of 'steam' [1,2] and already imposes bandwidth limitations on electronics, electronic devices and copper-based interconnects in broadband communications. It is therefore essential to replace copper-based interconnects with a fibre optic solution. At this stage very limited numbers of currently available optoelectronic devices are used in places, where both the optical and electronic domains meet in order to achieve the best possible performance. But here again, the limitation is the need for controlling these optoelectronic devices by the bandwidth limited electronics. The only way to change this is to develop all-optical chips and devices, where only light signal is used to control light carrying data.

It has been possible today to transmit and receive multi Tb/s of aggregate data throughputs over a single optical fibre, but is it possible to do the similar at a much smaller scale when using optical waveguides? Here, Si will be used as the waveguide core supported by the cladding layer made of a lower refractive index material of SiO_2 for confinement. This approach is known as Silicon on Insulator (SOI). Due to the high contrast in the refractive indices of the core and cladding layers, the waveguide is used as an effective light guiding medium and the manipulation of light via optical nonlinearity is possible to achieve. The goal is to develop "waveguide-based devices" to perform functions like all-optical switching, wavelength conversion, data detection and amplification in the optical domain. Other desired functions such as optical lasing and direct intensity and phase modulations are difficult to achieve by using only Si photonics, mainly due to its centrosymmetric crystal structure and narrow band-gap properties [3]. Therefore exploring other semiconductor material platforms such as GaN photonics were considered. Importantly, GaN is also CMOS compatible.

The principal objective of this paper is to explore how far the GaN platform can be taken to underpin the all-optical devices for photonic chips fabrication for their use in broadband optical communications.

The paper is organized into eight chapters. The **second chapter** describes the concept of optical nonlinearity and how higher third order nonlinearities are being exploited in waveguides for the development of ultrafast optical devices with different targeted functionalities. The CMOS compatibility issues and GaN passive waveguide devices for optical communications are discussed in **chapter three** and **four**, respectively. In **chapter five**, GaN active waveguide devices with different functionalities are overviewed. In **chapter six**, some GaN-based building blocks needed for photonic integration are discussed together with the description of fabrication steps and application. **Chapter seven** summarizes different integration techniques of photonic devices. **Chapter eight** draws conclusions and offers some future perspectives.

2 Optical Nonlinearity Overview

Si offers optical nonlinearity, exploiting of which is possible to go beyond the switching speed of 100 Gb/s [4]. Moreover, Si is CMOS compatible. Lasers, data modulators, amplifiers, detectors are among the main building blocks for enabling fibre optics communications and signal processing in networks. However some obstacles are found in achieving these goals. First, the minimum band gap of Si does not suit optical emission, second, the centro-symmetric crystal structure of Si impedes the electro-optics modulation and third, due to high frequency generation there are fast and slow free carrier emissions which reduce the performance. But, in course of gradual improvement in technology and nano-fabrication, it is possible to overcome these problems to some extent. In this section, the mathematical derivation of optical nonlinearity is discussed and how exploiting this nonlinearity, especially its third order, can be exploited by using different means to achieve some of our goals.

In 1961, Franklin found a weak optical signal of 347.1 nm in a quartz material when influenced by a light intensity of 694.2 nm by a ruby laser [5]. Franklin deduced that, the result was due to interaction of two optical electric fields in the quartz material producing the second harmonic response. Within a year of Franklin's discovery of second harmonic generation measurements, a good number of works were carried out in formulating the probes (in the scientific fields) basing on the nonlinear concept. In fact, optical nonlinearity is a phenomenon of the optical electric field induced modification in the properties of the material. The term nonlinear means that the optically induced changes in the material depend on more than one optical field strength in the region. Normally a single source with very high optical intensity like a laser source is sufficient to produce perturbation in the optical properties of the material. This process is quite different from the conventional or linear response of the optical signal, where the changes in the reflection, propagation and absorption depend linearly with the intensity of the optical source. In other words, optical nonlinearity is nothing but the interaction of the electric field of the incident photon with the electrons of the outer shells of the medium induced electric field. As a result, some peculiar phenomenon happens, such as:

a. phase change of the incident signal
b. generation of a new frequency
c. all-optical control of light

The mathematical relation between the induced polarization (P(t)) and the electric field (E(t)) in an isotropic medium having instantaneous dielectric response can be expressed as [6]:

$$P(t) = \varepsilon_0(\chi^{(1)}E(t) + \chi^{(2)}E^2(t) + \chi^{(3)}E^3(t) + \ldots). \quad (2.1)$$

Here, $\chi^{(1)}$ represents the first order susceptibility, $\chi^{(2)}$ represents the second order susceptibility and $\chi^{(3)}$ represents the third order susceptibility. In case of centro-symmetric material and in its bulk form, $\chi^{(2)}$ vanishes and as a result, $\chi^{(3)}$ becomes the lowest term in the above polarization expression (equation 2.1).

2.1 First Order Nonlinearity

$\chi^{(1)}$ is the 1st order susceptibility which deals with dipole excitation with bound and free electrons induced by a photon. The susceptibility term $\chi^{(1)}$ is having two parts, one is real part which is associated with the refractive index and the other one is imaginary part which is associated with loss or gain. To understand the contribution of bound electrons to the susceptibility, the following equation developed by Lorentz may be presented [4]:

$$\chi^{(1)}_{\text{Lorentz}} = \omega_L^2 / (\omega_0^2 - \omega^2 + i\,\gamma_L\omega). \tag{2.2}$$

Here, it is shown that the refractive index changes strongly near a resonance. This model provides the susceptibility of bound states belonging to a density of N dipoles. In the above equation, γ_L is the damping constant, ω_0 is the resonance frequency of the bound state, ω_L is the Lorentz plasma frequency defined as $\omega_L^2 = Nq^2/(\varepsilon_0 m_e)$, where, q = elementary charge, ε_0 = permittivity of vacuum, and m_e = effective mass of dipoles. The other factor of susceptibility is free carriers, which absorb photons and has an effect on the refractive index. The susceptibility which is related to free carriers is defined as the following expression known as Drude model which was mainly derived from equation 2.2 by dropping the restoring force, i.e., $\omega_0 = 0$:

$$\chi^{(1)}_{\text{Drude}} = \omega_P^2 / (-\omega^2 + i\,\gamma_D\omega). \tag{2.3}$$

Here, the plasma frequency ω_P is defined as $\omega_P^2 = Nq^2/(\varepsilon_0 m_e)$. The plasma frequency ω_P and damping constant γ_D have different values than the corresponding values ω_L and $\gamma_L$of equation 2.2. Any kind of contribution from either bound state or free electron oscillations contributes to the complex refractive index. To sum up, the refractive index may be defined as of the following expression:

$$n^2 = 1 + \chi^{(1)}_{\text{Lorentz}} + \chi^{(1)}_{\text{Drude}}. \tag{2.4}$$

This refractive index n, changes with both wavelength and carrier concentration N. There is also a useful function for the refractive index 'n' as a function of wavelength λ, N_e and N_h. Where, N_e is the electrons concentration and N_h is the holes concentration of free-carrier contributions to the refractive index. The function is shown as:

$$n(\lambda, N_e, N_h) = n_0(\lambda) + \Delta n_f(N_e, N_h) - i\,(\lambda/4\pi)\,\Delta\alpha_f(N_e, N_h). \tag{2.5}$$

Here, $n_0(\lambda)$ is wavelength dependence of refractive index, Δn_f is the free carrier index change known as FCI and $\Delta\alpha_f$ is the free carrier absorption change known as FCA. For Si, $n_0(\lambda)$ is related to Sellmeier equation:

$$n_0^2(\lambda) = \varepsilon + \frac{A}{\lambda^2} + \frac{B\lambda_1^2}{\lambda^2 - \lambda_g^2} . \quad (2.6)$$

This equation also describes the material dispersion of Si. From the equation, it was also known that the closer the photon gets to Si band-gap energy (1.12 eV), the stronger will be the refractive index changes. A good knowledge on material dispersion and engineering the waveguide dispersion is important for efficient conversion of higher order nonlinear terms [7]. FCA produces time-dependent fluctuations of refractive index and subsequent losses in Si which translates to distortions limiting the uses of Si at low operation speeds [8].

2.2 Second Order Nonlinearity

The symmetry of GaN crystal structure is having the presence of intrinsic second order nonlinearity which is known since 1960s (Philips and Van Vechten [9], Levine [10]). In the equation (2.1), the first term represents the first order optical nonlinearity, where the susceptibility phenomena depend linearly on the amplitude of incident optical field. The other terms $\chi^{(2)}$ and $\chi^{(3)}$ represent the second and third order susceptibilities describing induced polarizations exhibiting quadratic and cubic field dependencies. However, optical nonlinear effects that are commonly seen are listed in Table 2.1 [11] where the terms in bold represent the phenomena those have been seen and predicted theoretically in GaN.

Table 2.1: Various Second and Third Order Nonlinear Optical Phenomena

Second Order Phenomena	Third Order Phenomena
Sum-frequency Generation	Stimulated Raman Scattering
Difference-frequency Generation	Optical-field induced Birefringence
Second Harmonic Generation	**Two-photon Absorption**
Parametric Amplification	Self-focusing
Optical Rectification	Phase Conjugation
Optical Field-induced Magnetization	**Third-harmonic Generation**
Linear Electro-optic Effect (LEO)	**Electric-field induced SHG**
Magneto-optic Effect	Degenerate Four-wave Mixing

To model the second-order optical response, let us consider the expression for the time dependent incident field having more than one frequency components as [11]:

$$E(t) = \sum_n \left(E_n e^{-i\omega_n t} + \text{c.c.}\right). \tag{2.7}$$

Here, the summation extends from the positive and negative frequencies of individual field components and c.c. is the conjugate of the complex field amplitude. In the second order process, the incident field is composed of two distinct frequency components ω_1 and ω_2 resulting an incident field given by:

$$E(t) = E_1 e^{-i\omega_1 t} + E_2 e^{-i\omega_2 t} + \text{c.c.} \tag{2.8}$$

Now substituting equation (2.8) into the second order term in equation (2.1) generates a nonlinear polarization source having many distinct frequency components due to the various couplings between the ω_1 and ω_2 fields:

$$P^{(2)}(2\omega_1) = \chi^{(2)}(2\omega_1; \omega_1, \omega_1)\, E_1^2,$$

$$P^{(2)}(2\omega_2) = \chi^{(2)}(2\omega_2; \omega_2, \omega_2)\, E_2^2,$$

$$P^{(2)}(\omega_1 + \omega_2) = 2\chi^{(2)}(\omega_1 + \omega_2; \omega_1, \omega_2)\, E_1E_2,$$

$$P^{(2)}(\omega_1 - \omega_2) = 2\chi^{(2)}(\omega_1 - \omega_2; \omega_1, -\omega_2)\, E_1E_2^*,$$

$$P^{(2)}(0) = 2\chi^{(2)}(0; \omega_1, -\omega_1)\, E_1E_1^* + 2\chi^{(2)}(0; \omega_2, -\omega_2)\, E_2E_2^*. \tag{2.9}$$

The terms above represent second harmonic generation ($2\omega_1$, $2\omega_2$), sum-frequency generation ($\omega_1 + \omega_2$), difference frequency generation ($\omega_1 - \omega_2$) and optical rectification (0) respectively. Each term acts as a source for new electric field which oscillates at the frequency of respective nonlinear polarization. According to Shen [12] and Yariv [13], the electric field and polarization terms in equations (2.1) and (2.7) to (2.9) are written as scalars but in general they are vector quantities. The effect of second order nonlinearity is represented by the nonlinearity susceptibility tensor $\chi^{(2)}$ as it describes the coupling interaction between the electric fields ω_1 and ω_2 and the material of interest. The independent tensor elements of the hexagonal GaN crystal are $\chi^{(2)}_{xzx}$, $\chi^{(2)}_{zxx}$, $\chi^{(2)}_{xxz}$ and $\chi^{(2)}_{zzz}$ which are non-vanishing in nature (According to Boyd [14], Shen [12], Levenson and Kano [15]). Sometimes, the second order nonlinearity coefficient is represented as:

$$d_{ijk} = \chi^{(2)}_{ijk} / 2. \tag{2.10}$$

In GaN, under $\chi^{(2)}$ susceptibility, the phenomena that are observed are Sum-frequency Generation (SFG), Second-harmonic Generation (SHG) and Linear Electro-optic Effect (LEO).

It is important to know the concept of the Linear Electro-optic Effect, as it will be instrumental in understanding the GaN Electro-optic Modulators.

2.2.1 Linear Electro-optic Effect (LEO)

The electro-optic effect, which is a second order nonlinearity, occurs with the non-centrosymmetric materials only. In this case, the nonlinear response occurs from a dc electric field induced variation in the refractive index of a nonlinear material which produces a corresponding phase or intensity variation of an optical field that is transmitted through or reflected from the electrified sample [11]. The nonlinear response of LEO effect (magnitude) is also dependent linearly on the applied electric field which can be expressed by the following equation (Boyd [14]):

$$P^{(2)}(\omega) = \chi^{(2)}(\omega : \omega, 0)\, E(\omega)\, E_{dc}\,. \tag{2.11}$$

Here, $E(\omega)$ is the optical field, E_{dc} is the dc electric field. There is an advantage of using electro-optic effect compared to frequency conversion. The phase matching condition between the fundamental and generated fields is not required because of identical frequencies of the two optical waves. Because the electro-optical effect is the nonlinear field induced change in the refractive index, this nonlinear effect is more conveniently expressed as [11]:

$$\Delta\left(\frac{1}{n^2}\right)_{ij} = \sum_k r_{ijk}\, E_k. \tag{2.12}$$

Here, $\Delta\left(\frac{1}{n^2}\right)_{ij}$ is the ij-th component of the variation of inverse refractive index, E_k is k-th component of the dc electric field and r_{ijk} which is the electro-optic tensor, is related to $\chi^{(2)}_{ijk}$ as per the following expression [11]:

$$r_{ijk} = \frac{2\,\chi^{(2)}_{ijk}}{n^4}. \tag{2.13}$$

The above equation depicts that, electro-optic coefficient r_{ijk} has the same symmetry condition as that of $\chi^{(2)}$, which in turn indicates that it vanishes in centrosymmetric materials. The expression also confirms that the non-vanishing elements of these two terms $\chi^{(2)}_{ijk}$ and r_{ijk} are identical for a given centrosymmetric material.

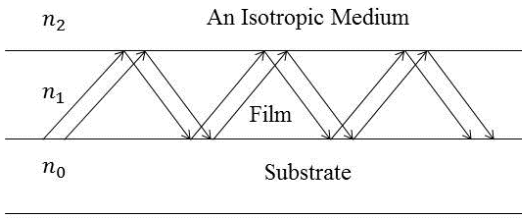

Fig. 2.1: Structure of an optical thin-film waveguide. The refractive indices of the three layers are n_0, n_1 and n_2, with $n_1 > n_0, n_2$.

2.2.2 Second Harmonic Generation in Waveguides

There are a good number of advantages in having optical nonlinearity based in waveguides [16]. First of all, a laser beam can be focused into an optical waveguide where it remains trapped over a long distance, whereas, in a bulk material, the focused beam readily diffracts from the focal point. Secondly, the phase matching in a waveguide is obtained by changing the waveguide structure which also determines the propagation characteristics of the waves. Thirdly, besides the phase matching, the nonlinear interactions of the wave can also be varied by varying the waveguide structure. Here, second-harmonic generation is used to explain the last two points. To understand this, let us go through a thin film waveguide as shown in the Fig. 2.1 [16].

For monochromatic waveguide propagation mode, we have the following expression from the theory of dielectric waveguides [16]:

$$E = \xi(x,y) \exp[i\beta z - i\omega t]. \tag{2.14}$$

$\xi(x,y)$ and $\beta(\omega)$ depend on the mode order, waveguide structure (waveguide width W, refractive indices n_0, n_1 and n_2 of three sections as shown in Fig. 2.1) and polarizations (TE or TM). For presence of both fundamental and second-harmonic waves in the guided mode, the phase matching condition is satisfied when,

$$2\beta(\omega) = \beta(2\omega). \tag{2.15}$$

For a given ω, the above equation can be satisfied by adjusting either W or one of n's. The nonlinear polarization at 2ω is also responsible for the second harmonic generation. The second harmonic generation is expected to be concentrated in those regions of the waveguide, where there is no inversion centre in the materials and $|\xi(x,y,\omega)|^2$ is strong. This has evolved into a variety of design options for phase matched second harmonic generation in photonic waveguides. However, there are some difficulties in making these kinds of waveguides. Firstly,

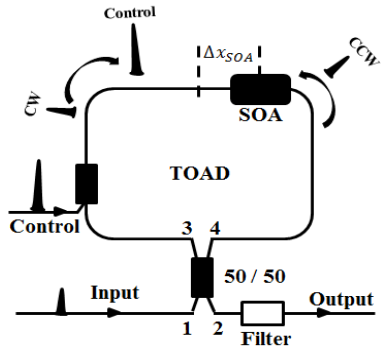

Fig. 2.2: Schematic diagram of TOAD.

the width W should be constant, or else, it will not satisfy the phase matching condition of equation (2.15) in the entire waveguide. Secondly, the surface imperfection greatly enhances the loss that is why the propagation length is limited to a few mm in a waveguide. Another reason is that, the high power laser may at times damage the waveguides. Many other nonlinear effects on the waveguides are yet to be investigated. However, the progress would depend on the rapid advances in the development of photonic waveguide technology [16]. Examples of more Second Harmonic Generation and Parametric Amplification using GaN Bragg Reflection Waveguides are discussed in Chapter 4.

2.2.3 Optical Nonlinearity in Optically Active Medium - SOA and TOAD

Semiconductor Optical Amplifier, SOA represents an active optical medium for generating optically induced nonlinearity [17]. SOA based devices now-a-days, show a great possibility of integrating with other photonic components and are used as building blocks for the development of all-optical switches, de-multiplexers, wave length converters, dispersion compensators and photonic memories [18]. One important application of SOAs is in ultrafast all optical switching in the device known as Terahertz Optical Asymmetric De-multiplexer (TOAD) [17]. The TOAD's switching window width is determined by the SOA offset from the central position of the loop. Here, the data input through a 50:50 coupler is split into CW and CCW components. The CW pulse will reach the SOA later than CCW pulse for the asymmetric position of SOA in the loop and the delay is represented by $2\Delta x_{SOA} / c_{fiber}$. Here, Δx_{SOA} is the offset of the SOA position from the centre of the fibre loop and c_{fiber} is the speed of light. In the absence of any control signal, the CW and CCW pulses propagating within the loop will experience the same unsaturated gain and then recombine at the input coupler and will emerge from the reflected port.

The introduction of a control pulse through the second coupler in CW direction (see Fig. 2.2) will change the optical properties of the SOA for which the CW and CCW components will

experience different gain saturation profiles (indices of refraction) and after the interference the data will exit from the output port as soon as they recombine at the input coupler, thus producing the switching effect. An important advantage of TOAD as a switching device is that it is not affected by temperature variations and data output stabilization is not required because the data experience the same medium of propagation [17] within the loop. The TOAD has been demonstrated as an ultrafast all optical demultiplexer, routing switch in 250 Gb/ OTDM data network [19, 20], all optical binary flip-flop circuit [21] and in other ultrafast all optical signal processing applications [22, 23, 24, 25, 26].

2.3 Third Order Nonlinearity

The third order susceptibility is important for Si photonics as it shows a good number of phenomena suitable for switching. This can be understood for an electric field E comprising three frequency components ω_k:

$$E_{(r,t)} = \sum_{k=1}^{3} E_k = \frac{1}{2}\sum_{k=1}^{3} \left(E_{\omega_k k}(r,\omega_k)\, e^{i\omega_k t} + \text{c.c.}\right) \tag{2.16}$$

Here, c.c. denotes the complex conjugate. Now substituting equation (2.16) into equation (2.1) and expanding the frequency components of the third order nonlinear term, a multitude of terms can be obtained at new frequencies for third order polarization:

$$P^{(3)} = \frac{3}{4}\varepsilon_0\chi^{(3)}[|E_{\omega_1}|^2 E_1 + ::] + \frac{4}{6}\varepsilon_0\chi^{(3)}[(|E_{\omega_2}|^2 + |E_{\omega_3}|^2)E_1 + ::] + \frac{1}{4}\varepsilon_0\chi^{(3)}[(E_{\omega_1}^3 e^{i\omega_k t} + \text{c.c.}) + ::] +$$

SPM XPM THG

$$\frac{3}{4}\varepsilon_0\chi^{(3)}[\frac{1}{2}(E_{\omega_1}^2 E_{\omega_2} e^{i(2\omega_1+\omega_2)t} + \text{c.c.}) + ::] + \ldots. \tag{2.17}$$

FWM

Here, each term refers to a particular third order nonlinear process. :: denotes all permutations of possible frequencies. Each term also corresponds to a nonlinear optical excitation. According to the energy level diagram, depicted in Fig. 2.3, it is seen how 3 photons induce dipole transitions to excitation states and then relax back by releasing a fourth photon. The relaxation process takes place instantaneously if the excited state does not correspond to the bound eigenstates of the crystal. Out of many such nonlinear processes, those maintain energy and momentum conservation

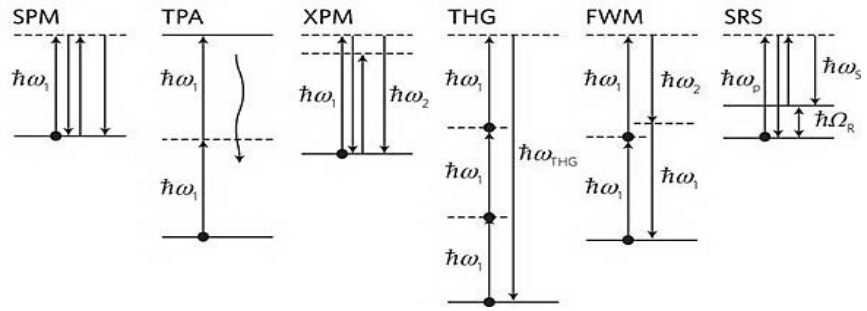

Fig. 2.3: Illustration of a dipole excitation and possible energy level diagrams.

known as phase-matching, produce efficient excitation. By choosing the energy levels and phase matching appropriately, a particular non-linear process can be selected to some degree. The first term in the above expression corresponds to a phenomenon known as self-phase modulation (SPM). This results from dipole excitations induced by three photons, as depicted in Fig. 2.3. Intensity dependent refractive index change n_2 happens due to SPM. This change in turn alters the spectral composition of the same pulse which has generated it. As a result, pulse broadening takes place and due to extreme level of SPM, there is a possibility of super-continuum generation. SPM generating photons can also excite to an energetically higher state, as shown in the two photon absorption (TPA) diagram of Fig. 2.3. TPA excitations correspond energetically to an excitation of an electron in the valance band to the conduction band and as such they are 'absorbing'. It leads to an intensity dependent contribution α_2 to the linear absorption coefficient α_0. Free carriers in the conduction band, which is the origin of FCA and FCI changes, are generated by TPA. Hence, the speed of the Si photonic devices slows down due to long lasting processes of FCA and FCI for long lifetime of the free carriers in the conduction band. Changes due to intensity dependent refractive index and the absorption associated with SPM and TPA affect the complex refractive index n by the following relationship [4]:

$$n = n_0 + n_2 I - i\frac{\lambda}{4\pi}(\alpha_0 + \alpha_2 I). \tag{2.18}$$

Here, n_2 is the Kerr coefficient, I is the intensity and α_2 is the TPA coefficient which are all related to the real and complex terms of the third-order susceptibility expressed as [4]:

$$n_2 = \left(\frac{1}{cn_0^2\varepsilon_0}\right)\frac{3}{4} Re\left(\chi^{(3)}\right), \tag{2.19}$$

$$\alpha_2 = (-\frac{\omega}{cn_0^2\varepsilon_0})\frac{3}{4} Im\,(\chi^{(3)}). \quad (2.20)$$

There is an important term called as FOM used to compare the Kerr coefficient (n_2) with the strength of TPA coefficient α_2 [4, 27]:

$$\text{FOM} = (\frac{1}{\lambda})(\frac{n_2}{\alpha_2}). \quad (2.21)$$

Higher FOM is desirable to avoid TPA related speed limitation. Si has very high Kerr coefficient $n_2 = (4.5 \pm 1.5) \times 10^{-18}$ m^2 W^{-1} at 1.55 μm, but the large TPA coefficient α_2 results in very low FOM of 0.4. Hence, the goal is to get the appropriate material with very high Kerr coefficient and low TPA coefficient α_2, so that FOM becomes high. The parameters n_2 and α_2 vary with the changes of wavelength. The Kerr coefficient in Si has maximum value in the range of 1.8 μm to 1.9 μm whereas beyond 2 μm, the TPA coefficient decreases significantly. As such, Si shows very good Kerr nonlinearity with considerable large amount of FOM in the near-infrared region.

Third Order Nonlinearity in Photonic Waveguides: To exploit the optical nonlinearity, special types of waveguides are used. The general guidelines for designing the waveguides supporting strong nonlinear interactions are mentioned as follows [4]:

a. the high optical field confinement should be provided by the waveguide
b. the waveguide material should have high Kerr coefficient
c. FOM should be high enough so that TPA is not an issue
d. phase matching should be obtained through accurate dispersion engineering or by keeping the structures very short so that dispersion is not a problem

There is a nonlinear waveguide parameter called γ which is used to "measure" the optical nonlinearity of the waveguide as follows [4, 28]:

$$\gamma = (2\pi/\lambda)\,(n_2/A^{(3)}_{\text{eff}}). \quad (2.22)$$

From the above expression, we can easily see that the high nonlinear Kerr coefficient n_2 and very small cross sectional area $A^{(3)}_{\text{eff}}$ ensure the maximum value of parameter γ. In the example as mentioned in Ref. [4], the silicon waveguide (of width from 300 nm to 1.5 μm and height from 200 nm to 1.5 μm) is fabricated on a Si substrate and due to the high contrast of Si refractive index with air; the incident light is propagated through the wave structure with high confinement. Although, here the nonlinearity parameter of $\gamma = 307{,}000$ W^{-1} km^{-1} is obtained, the FOM is only 0.4 [29]. This means that, TPA related free carriers are generated inducing FCA and FCI related losses which do not allow the speed of operation of more than 10 Gb/sec. However, the performance can be improved by using large waveguides with smaller confinement and as a

consequence, lowering the nonlinear coefficient and using the p-i-n diode structure across the waveguide to allow removal of free carriers by the application of reverse bias. Attaining a speed of 40 Gb/sec is possible with these types of devices [30].

In another approach [4], thinner waveguide was used covered with layer of high nonlinear material [27]. When the incident light is passed through these kinds of waveguides, the optical transverse magnetic mode extends far beyond the waveguide. A cladding material with very high Kerr nonlinearity is chosen. The nonlinear Kerr coefficient of this organic molecule is more than 10 times of that of Si, giving $\gamma = 108{,}000\ W^{-1}km^{-1}$. FOM of about 1.2 is possible to achieve [29]. This approach is known as silicon-organic hybrid (SOH) approach and takes advantages of many organic materials with very large Kerr coefficients.

Another approach is a slotted waveguide structure shown in the Ref. [4]. The slots not only guide the light but also enhance the intensity. The enhancement results from the continuity of the normal component of the dielectric displacement component oriented parallel to the substrate plane [31]. If the refractive index inside the slot is 1.8 and the refractive index of the Si waveguide is 3.5, then the dielectric field over the slot is enhanced by $(3.5/1.8)^2 = 3.8$ times compared to that of only Si waveguide, which is a substantial improvement. This type of slotted waveguide shows electric field distribution of the strong confinement inside the slots. As a result, a high nonlinear waveguide parameter of $\gamma = 116{,}000\ w^{-1}km^{-1}$ with FOM of 2.2 is possible with no TPA related speed limitations [29].

2.3.1 Applications of Third Order Optical Nonlinearity

All-optical switching. The nonlinear optical switch, using a fibre loop called Nonlinear Optical Loop Mirror, NOLM was first demonstrated by Doran & Wood in 1988 [32]. The device was based on loop formed by connecting the two output ports of a fibre directional coupler. In his paper, Doran & Wood showed how the optical signals in the clockwise and counter clockwise directions traveling inside of NOLM produce the phase change at the output depending on the intensity of the signal strength and the medium properties. NOLM operated based on the nonlinear phase change induced by the self-phase modulation (SPM). The device was robust, simple to construct and did not require interferometric alignment.

Using a switching concept mentioned above, many devices were demonstrated in subsequent years - for example, the switching of a 20 Gb/s pulse train at 2.5 Gb/s in an all-fibre NOLM was demonstrated [33]. The first complete nonlinear optical loop mirror with 64 Gb/s all-optical de-multiplexing was demonstrated including error-rate measurement in 1992 [34]. Although the NOLM based devices have demonstrated very high speed data rates, they have some limitations such as very long length of fibre loop (due to optical fibre low nonlinearity) and a need for very high optical power for achieving the all optical switching. Since the optical fibre long length cannot be made “integrated” this in turn was a limitation for its further development [17].

All-optical wavelength conversion. When a high power optical signal is launched into an optic medium, it gives rise to diverse non-linear effect. One non-linear effect which is due to third order electric susceptibility is known as Kerr effect. Four wave-mixing is a type of optical Kerr effect and this occurs when at least two different frequencies propagate through a nonlinear medium [35]. Suppose two input frequency components ν_1 and ν_2 due to refractive index modulation through the medium produce another two different frequencies at the output. The two new frequency components are, $\nu_3 = \nu_1 - (\nu_2 - \nu_1) = 2\,\nu_1 - \nu_2$ and $\nu_4 = \nu_2 + (\nu_2 - \nu_1) = 2\,\nu_2 - \nu_1$. At the same time the pre-existing waves at frequencies ν_3 and ν_4 can also be amplified through this process. Four-wave mixing is also related to self-phase modulation and cross phase modulation and all these originate from the same Kerr nonlinearity. Four-wave mixing occurs even for the number of frequencies less than three. Two frequencies are used here and the overlapping of same frequencies is possible which is suitable for the switching and de-multiplexing in OTDM networks. In a demonstration, it was seen that a control signal with high intensity is inserted in a data stream and the control pulses induce the same frequency out of the data-stream making the particular channel separated. This is known as de-multiplexing and this happens after four-wave mixing process due to nonlinearity in a special type of dispersion controlled single mode 14 KM fibre with filtered output. One disadvantage of this phenomenon is that the power requirement for the control signal is very high and the conversion efficiency is very low as well (i.e., on extraction of 6% data power compared to the control signal power) in comparison to other available optical switching techniques. Another disadvantage is the walk-off of the data pulses from the control pulses causing the reduction in performance. This occurs due to the differences of group velocities of both data and control pulses. However, this could be minimized with the utilization of a dispersion controlled fibre which also helps to ensure the phase-matching conditions by increasing the nonlinear interaction for the four-wave mixing processes.

Multiple channel all-optical 100 Gb/s de-multiplexing using multichannel FWM in SOA was demonstrated by Uchiyama and Kawanishi [36]. One important requirement of a multichannel de-multiplexer is the simultaneous multiple-channel operation. This required compact circuit design, low latency, easy synchronization and low insertion loss.

Supercontinuum generation. The term supercontinuum generation means, the conversion of laser light into a broad spectrum of light. This type of spectral broadening is accomplished by propagating optical pulses through a highly nonlinear device as for example, it is possible to send optical pulse of lower energy through an optical fibre of very high optical nonlinearity. The main interest is using photonic crystal fibres due to their chromatic dispersion characteristics that allow nonlinear interaction over a good length of fibre. The interesting outcome is that, with very moderate input power, very broad spectra can be obtained leading to a rainbow of lasers. At times, tapered fibres are used. An important application of this supercontinuum generation is in fibre optics communication system [37]. The optical spectra generation particularly in the vicinity of telecommunication band of 1.5 μm was of special interest mainly to facilitate wavelength division multiplexing system. These fibre based sources play an important role as an

alternative to the bulk laser sources for all the optical pump configurations related to supercontinuum generation [38]. One application of fibre based supercontinuum generation is 'Comb-like-spectrum generation' for WDM optical networks [39].

2.4 Silicon Photonics Limitations and The Emergence of GaN Photonics

A conspicuous disadvantage of Si is the absence of second order nonlinearity ($\chi^{(2)}$) due to centro-symmetric crystal structure of Si. Si is also indirect band-gap (1.1 eV) material and limits its operation to wavelengths above 1100 nm. Most importantly, it precludes the active functionalities like light emission, second harmonic generation and linear electro-optic effect (Pockle's Effect). $\chi^{(2)}$ nonlinearity is important for wavelength conversion and it is also an important requirement of producing electro-optic effect which is needed for ultra-speed modulation. However, electric modulation could be achieved in Si by injecting carriers and using first order susceptibility related FCA and FCI effects. But use of second order related electro-optic modulator is preferable as Pockle's Effect does not rely on those effects (FCA, FCI). Another limitation in using Si photonics is due to Raman Effect, as it is limited within the operation window of 105 GHz [6]. Carrier induced TPA, FCI and FCA effects are responsible for the material related speed limitations in Si. The time constants for these effects are of the order of several hundred picoseconds to several hundred nanoseconds [29]. Limitations might also add up due to the choices of resonant configurations with a ring filter, grating or photonic crystal [4]. There is an option of choosing a semiconductor photonic device which can act as better choice than Si. For example, GaN semiconductor material possesses all types of optical nonlinearity - first, second, and third order including. Due to direct band-gap configuration of GaN, TPA related absorption or losses are absent in this type of photonics. Exploiting the required nonlinear effects for different device components, there is a strong possibility of generating the lasing, electro-optics modulation, wavelength conversion, switching and photo-detection using GaN photonics, particularly in the telecommunication wavelength of 1.5 μm.

GaN based devices show better performance using inter-sub band switching. The inter-sub band absorption recovery time is very short, in the ranges of 150 - 400 fs, mainly due to the high electron-photon interaction [40, 41, 42]. That is why there is a tremendous possibility of ultrafast all-optical switching and modulation (achieving a Tb/s bandwidth). Adding to this advantage, the dielectric constant of these materials is smaller compared to the InGaAs(P) /InP based materials which make GaN platform more suitable for optoelectronic devices due to reduced device capacitance. Further miniaturization of these devices is possible (for 3 mm long waveguides) with 14 dB absorption associated with inter-subband transitions [43, 44]. In another aspect, both the GaN and AlN are wide band gap materials (for GaN 3.4 eV and for AlN 6.2 eV), with large index of refraction differences and for these reasons the bulk GaN/AlN materials are favourable for the fabrication of waveguides having low insertion loss at telecommunication band [45]. These nitrides are also robust in nature against very high temperature and radiation effects. GaN/AlN devices can be tuned at arbitrary wavelengths by engineering the confinement of

electrons i.e., by adjusting the thickness of quantum wells. In conventional InGaAs/AlInAs devices, the conduction band offset is only 0.52 eV, which limits the device fabrication having wavelengths of more than 3.5 μm. Whereas, in GaN/AlN, the conduction band offset is close to 1.8 eV which is enough to tune inter sub band resonance wavelength within the telecom band.

3 Towards CMOS Compatible GaN Photonics for Broadband Communication

In a semiconductor, there is a band gap where no electron states are allowed. At low temperature, below the gap it is full of electrons whereas, above the gap it is empty. As the completely filled in or empty band carry no net currents, these are known as insulators at absolute zero [46]. But at room temperature, these can show some conductance that can be controlled by introducing impurities or doping and by applying electric field. The CMOS technology, which is core to the present day computing, is based on the ability to switch a semiconductor material like Si between its conduction and non-conduction states. On the other hand, the semiconductor materials like GaN, AlN are the kind of compound materials made of elements from group III and V of the periodic table. These are more costly than Si and the processing technology is not mature enough. But these materials have functionalities which are not available in Si, including second order optical nonlinearity we discussed earlier. Also an important feature of GaN platform is the property of a direct band gap (ranging from ultra violet to infrared region) which means that the electrons can relax to the lower energy level by recombining with holes with conserved momentum. GaN also possess some properties such as: high thermal conductivity, chemical inertness, mechanical stability, high breakdown voltage. Because of these exceptional properties, GaN materials are very promising for opto-electronic devices with enhanced speed and some functionality. However, for GaN to function "jointly" in both microelectronic and optical domains for ultrafast signal processing, GaN material needs to be CMOS compatible.

3.1 CMOS Compatibility Issues and GaN Photonics

Different substrates, such as sapphire, SiC, GaAs and Si are currently used for the growth of GaN. But considering the need for the CMOS compatibility and large scale integration with Si based integrated circuits, Si substrates are desirable. Si substrates have some merits such as thermal stability at high temperatures and large size growth of GaN with top down electrode formation. Moreover the price of Si is lower compared to other substrates.

Optical wave-guiding in GaN, where the refractive index is 2.3 at wavelength of 1.5 μm, requires cladding layers of lower refractive index to confine light through the GaN core layer. In case of Si photonics, this confining of light wave is fulfilled by the utilization of Si thin films on top of low refractive index SiO_2 buffer layer, which is thermally grown on bare Si substrate. Such Si on insulator substrate with CMOS compatibility is the main reason for the success of Si photonics. On the other hand, integration of GaN on CMOS compatible substrate is challenging to fabricate. High quality GaN growth by the conventional method of MOCVD is carried out only on closely lattice matched substrates named as sapphire, SiC and Si (111). To form GaN on Si substrate using the techniques of epitaxial growth and lift-off, encounter difficulties while separating the grown film from the substrate for the reason of strong bonding at the interfaces. As per reference [47], a robust bonding process that allowed to realize photonic structure in GaN thin films at the top of SiO_2 on Si (100) substrate was demonstrated which can be illustrated as

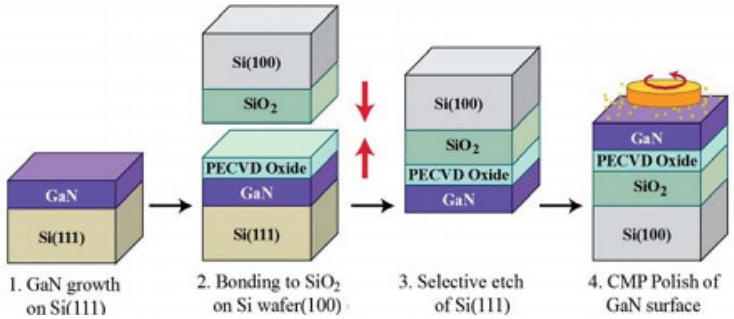

Fig. 3.1: GaN photonic circuits are built on 'GaN on SiO_2 on Si' (GaNOI) substrates. Reproduced with permission from Ref. [47].

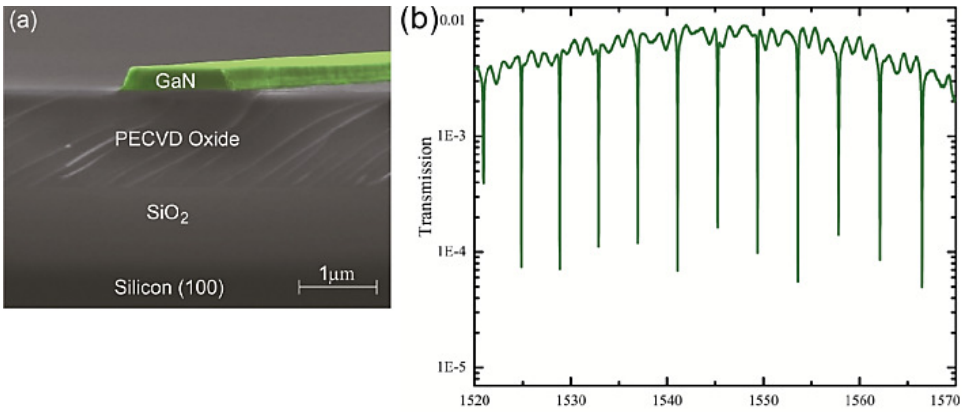

Fig. 3.2: (a) Scanning Electron Micrograph of a cross section of a GaNOI waveguide (b) Optical transmission of a GaN microresonator. Reproduced with permission from Ref. [48].

per the Fig. 3.1(a). Here, GaN photonic circuits are built on 'GaN on SiO_2 on Si' substrate (GaNOI). This GaNOI process works as: PECVD oxide is initially deposited on commercially available GaN on Si (111) wafers to assist the bonding process. Later on, the Si (111) layer is removed after bonding and new GaN surface undergoes a chemical-mechanical polishing (CMP) step reducing the GaN layer thickness.

Waveguides are formed in the top layer of GaN by electron beam lithography and dry etching in the medium of inductively coupled plasma chloride. As described in ref [48], scanning electron microscopic (SEM) image of a cross-section of this type of waveguide can be seen, as in Fig. 3.2(a).

A GaN microring resonator with 40 μm radii coupled with an input waveguide of width 860 nm was fabricated as mentioned in the paper. These two elements were separated by a 150 nm gap. These kinds of microrings are coupled critically at the telecommunication band of 1550 nm having extinction ratio of approximately 20 dB. By launching light from a tuneable infrared laser source and amplified with EDFA and by output light measurement using InGaAs photodetector, the optical response of this kind of photonic circuit can be estimated. It was also possible to get the phase matching between the fundamental light and the second harmonic light by waveguide width tuning. The technique used was 'multi-mode matching technique' [47].

3.2 Fabrication of GaN Waveguides on Silicon

Si substrates are low cost, extensively available in large diameter and have very good thermal and electrical properties. But still Si is not popular as substrate for the GaN photonics mainly due to cracking of GaN film for stress generation. This kind of stress is not so prominent for the SiC and sapphire substrates. The lattice mismatch between GaN and Si is about 16% which causes the dislocation density in the GaN layers but the important problem is high thermal mismatch which is about 54%. Again, Si has resistivity up to 10^4 ohm-cm which is very less than the resistivity values of SiC or sapphire and that is why there is a possibility of parasitic capacitance effects at high frequency [49]. To make GaN based waveguides, membranes with high refractive index contrast is essential in between GaN and cladding layer mainly due to its low refractive index (it is 2.3 at 1.5 μm). However, for SOI based waveguides, the lower refractive index of SiO_2 compared to Si provides sufficient refractive index contrast to confine the light within the waveguide. Although the common substrates used in GaN waveguides are SiC, Si and sapphire but considering the under-etching technique, Si and SiC are better. SiC shows lower lattice mismatch (3.5%) compared to Si (17%) as substrate. But, the cost of SiC is comparatively higher. The use of Si is important for the goal of making integration of photonics and electronics in the same chips for their advantages of well-established technology, low cost and special optoelectronic properties of GaN. In case of GaN on Si technology, the refractive index of the underlying layer (n_{si} = 3.47) is higher than the GaN core (n_{gan}= 2.3) layer at near-IR region. This will stop the guiding of light through the waveguide unless there is some mechanism of suspended wire waveguide where the Si layer under the GaN wire is removed by dry etching. These wire waveguides are mechanically supported by the use of well-designed tethers.

According to ref [50], the process of fabricating GaN photonic structure by under-etching the Si substrate is enumerated. The steps are shown as in Fig. 3.3. The complete structure, including the wire waveguide and the photonic crystal lattice, is fabricated in a single lithographic and in single subsequent etching steps. As a result, the total processing time is reduced. Firstly, the process in initiated by the growth of a thin AlN buffer layer of 60nm on Si (111) and it is followed by a layer of 330nm GaN along the c-axis (0001) by the process of MOVPE. It is noteworthy that, this kind of thin GaN/AlN growth on Si is affected by strain induced by the difference of thermal expansion coefficients of the layers. Then a thick layer of 100nm SiO_2 is

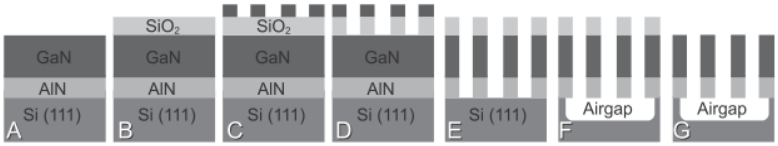

Fig. 3.3: Fabrication process of a GaN based photonic crystal waveguide. Reproduced with permission from Ref. [50].

deposited on top of the structure by the process of PECVD. This SiO_2 layer acts as a hard mask for the entire fabrication process thereby protecting the GaN surface and the degradation of the pattern is stopped. Then, to pattern the previously spun positive photo-resist ZEP-520, the E-beam lithography is carried out. After the development of the resist, first the pattern is transferred to SiO_2 by the process of fluorine-based Reactive Ion Etching (RIE). Then the pattern is formed into AlN/GaN stacked layers by the process of chlorine based ICP (inductively coupled plasma) etching. By the dry process of fluorine based RIE, the membrane is released of the Si (111) substrate. Air gap in the order of 3 μm is achieved in this process which is sufficient to avoid the light loss through the substrate in the 1.5 μm band. At the final stage, the SiO_2 layer is released using the solution of hydrofluoric acid. This is the most critical stage for the fragility of the structure and very careful manipulation is required to avoid collapsing of the waveguide.

3.3 Optical Properties of GaN Waveguides

As per ref [51], a study has been carried out, to find the optical characteristics of GaN waveguides with Si substrate. Measurement of refractive indices for TE and TM modes were performed on the GaN on Si films for different wavelengths ranging from ultraviolet to infrared such as 450nm, 532nm, 633nm, 975nm and 1539nm. It was shown that GaN on Si had good optical property compared to that of GaN on Sapphire [52]. In the same study, the GaN structure deposited on Si was analysed using TEM, SEM and AFM methods. It was seen that the optical properties like refractive indices for TE/TM mode of GaN on Si are familiar to those for GaN on Sapphire. Moreover the optical measurements showed very good waveguide properties in terms of index and its relationships with temperature and showed good prospects for future GaN on Si based waveguide devices as it is seen presently for GaN based waveguides on Sapphire devices.

4 GaN Passive Waveguide Devices for Broadband Communication

In optical communication systems the ability of data manipulation / switching is important. There is a strong requirement to improve the speed of switching. There is a growing need for chip level optical systems where the data can be generated, modulated, and manipulated all-optically in the ultrafast fashion. The electro-absorption characteristics of GaN photonics have properties which can support very fast relaxation times suitable for ultrafast switching and properties to support lasing in the communication band. Moreover, as discussed in chapter 3, the GaN photonics is also CMOS compatible and the existing setups at factories might be used for mass production of devices.

4.1 Waveguide Basics

An optical waveguide is formed of a non-absorbing dielectric layer whose thickness is comparable to the wavelength of passing light and is deposited on a planar substrate. The thin film of the dielectric layer has the refractive index higher than the refractive index of the substrate. A variety of techniques are used for the growth of thin films such as metal organic chemical vapour deposition (MOCVD), molecular beam epitaxy (MBE), pulsed laser deposition, sputtering etc. These kinds of dielectric waveguides are used in various optical devices such as modulators, lasers, couplers, splitters etc. Typically, a GaN based novel dielectric waveguide is made of GaN semiconductor materials grown on sapphire. Waveguide structures can be constructed with GaN as the core with higher refractive index and $Al_xGa_{1-x}N$ as the cladding layer with lower refractive index. Here $Al_xGa_{1-x}N$ is made by engineering the band-gap energy of GaN and AlN alloys with different Al concentrations. Through this process, direct band-gap GaN semiconductor material and its alloys are used for the development of LEDs, lasers, photodetectors using the waveguides which are transparent for the spectrum of communication wavelength (1.5 μm). Importantly, the refractive indices of GaN materials and their alloys are important parameters for the design, fabrication and modelling of the above mentioned devices. There are different structures like buried rectangular, ridge and slab optical waveguides. These are shown in Fig. 4.1 [53].

It is important that the waveguides exhibit very low scattering, radiation and absorption losses for device efficiency. These are actually the three mechanisms of propagation loss of light wave through the waveguides and minimizing them is important to get the best performances. Splitters, combiners, Mach-Zehnder interferometer configurations are developed from the waveguides, which are the basic opto-electronic components using materials of GaN compounds. Splitters like Y-beam splitter is used to split a light signal travelling through the waveguide. This type of splitter is made of an input which is a transition zone formed by an adiabatic symmetric taper and two mono-mode waveguide outputs sufficiently separated in such a way that the coupling loss between them is negligible. Again, various types of splitters are available such as

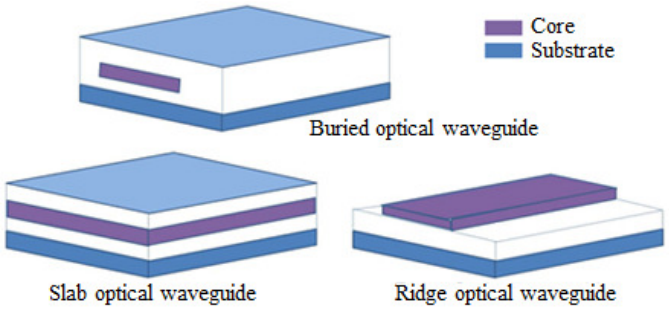

Fig. 4.1: Examples of waveguides.

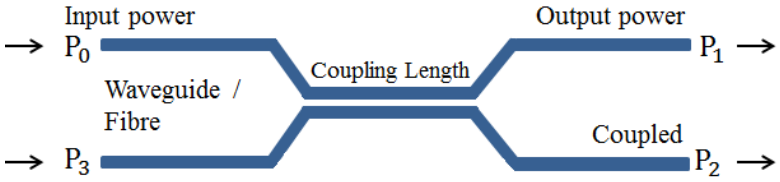

Fig. 4.2: A 2×2 directional coupler.

Y-branch beam splitters, tuneable TE/TM polarization splitters, power splitters and 1 × N integrated splitters. All of these have versatile applications. For example, a single mode 3 dB Y-junction splitter which is symmetric has an important role in the development of integrated optics. This can be utilized in the splitting regions of the input and output ends as Mach-Zehnder interferometer. Waveguide couplers can be thought of connecting two Y-junction splitters connected oppositely.

A directional coupler is used to split or combine optical signals in a network. Figure 4.2 shows a 2×2 directional coupler. It has two input ports and two output ports. The figure shows that the power from one input port P_0 or P_3 can be split into two output ports P_1 and P_2.

4.2 Exploitation of Material Refractive Index in GaN Waveguides

Knowledge of the material refractive index in the operating wavelength is important for designing an optically guided waveguide device. R. Hui et al. [54] followed a measurement technique in the design, fabrication and characterization of a single mode ridge optical waveguide device based on GaN/AlGaN hetero-structure. In his design initiative, a number of $Al_xGa_{1-x}N$ film samples were grown on sapphire substrate through the process of MOCVD. The

film thickness ranges were from 1.1 to 1.5 μm and Al molar fraction ranges were from x = 0.1 to x = 0.7. The optical transmission spectra were then measured to evaluate the refractive index on each film. The optical transmission efficiency was wavelength dependent due to Fabry-Perot (FP) interference caused by two facets of the film (one is between $Al_xGa_{1-x}N$ and the air and the other is between $Al_xGa_{1-x}N$ and sapphire). The film refractive index can be obtained from the knowledge of the film thickness, by best fitting the measured optical transmission spectrum to a well-known FP transmission equation. For several different Al molar fractions, the measured refractive indices of $Al_xGa_{1-x}N$ are shown in Fig. 4.3(a). In the figure, the continuous curves are the numerical fittings using the first order Sellmeier dispersion formula as:

$$n(\lambda) = \sqrt{1 + \frac{(B_0 + B_1 x + B_1 x^2)\lambda^2}{\lambda^2 - (C_0 + C_1 x)^2}}. \tag{4.1}$$

The coefficients for best fit are shown in Fig. 4.3(a) and their variations versus Al molar fraction (x) are shown in Fig. 4.3(b).

For calculation of the refractive indices in 1550 nm wavelength, the information can be taken from Fig. 4.3. The following polynomial expression can be obtained for Al molar fraction (x) which has a dependence on the refractive index at 1550 nm:

$$n\ (1550\ \text{nm}) = 0.431x^2 - 0.735x + 2.335. \tag{4.2}$$

Here, the monotonic decrease of refractive index of $Al_xGa_{1-x}N$ with the increase of Al molar fraction helps for the design of the single mode waveguide devices.

A schematic diagram of a single mode waveguide cross-section based on GaN core and $Al_xGa_{1-x}N$ cladding is shown in Fig. 4.4. A 4μm thick epitaxial film of $Al_xGa_{1-x}N$ is grown on a sapphire surface and a 3μm thick GaN is deposited on top of $Al_xGa_{1-x}N$ layer. The optical waveguide structures are formed by the process of lithographic pattern and inductively coupled plasma dry etching.

A 2×2 waveguide coupler fabricated in this process is shown in Fig. 4.5. The uses of these waveguides are suitable in the infrared region because of their material wide band-gap. For this reason, the optical gain and absorption are negligible in the GaN based waveguides. That is why the device is transparent and can be used in the communication band of 1.5 μm. Again it is

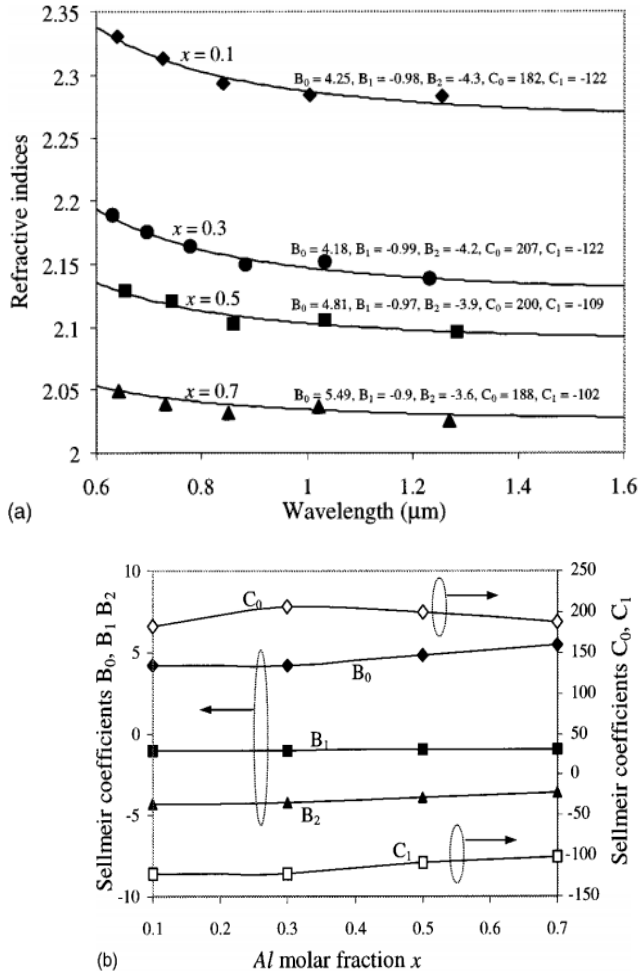

Fig. 4.3: (a) Refractive indices of AlGaN vs wavelengths for different Al molar fractions. (b) Sellmeir expression coefficient vs Al molar fractions. Reproduced with permission from Ref. [54].

known that the material refractive index is a function of carrier density. Through the carrier injecttion, the refractive index can be modulated. The hetero-structure waveguides are therefore suitable for optical phasors like Mach-Zehnder modulators and AWGs. The refractive index of

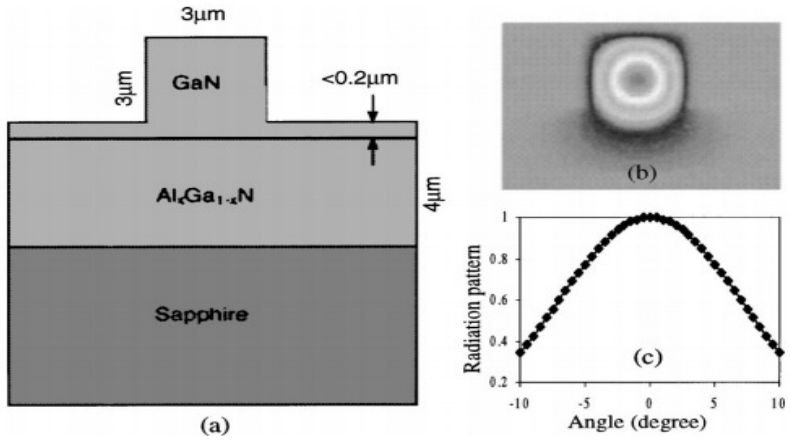

Fig. 4.4: Optical waveguide design using GaN/$Al_xGa_{1-x}N$ hetero-structure grown on sapphire substrates: (a) Waveguide Cross-section, (b) Single mode simulation, (c) Radiation pattern vs exit angle. Reproduced with permission from Ref. [54].

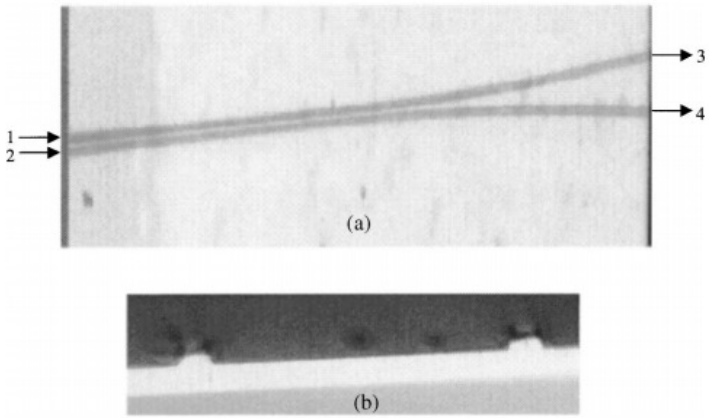

Fig. 4.5: Optical microscope image of GaN/$Al_xGa_{1-x}N$ hetero-structure optical waveguide. Coupler: (a) Top View (b) Cross-section at the output. Reproduced with permission from Ref. [54].

GaN is smaller and the optical absorption is lower compared to those of InP. Moreover, the carrier induced refractive index changes are independent of the signal polarization state. This is superior to the devices made of $LiNbO_3$ where the polarization dependencies are prevalent [54].

4.2.1 Birefringence of GaN Waveguide

In planar light wave circuits, it is important to have knowledge about refractive index changes, but at the same time the knowledge about birefringence of material is also important in the design and performance of waveguides. The birefringence of GaN film on sapphire was reported when a 4% refractive index change was observed due to changes of polarization of incident signal from perpendicular direction to the parallel direction to the c-axis crystal in the long wavelength (800nm) [55]. Again for the wurtzite crystalline structure, GaN possesses hexagonal configuration on c-axis. Due to variation of optical propagation direction on c-plane, the efficiency of optical propagation emission changes periodically. Hui, R. et al. investigated the birefringence on single mode GaN-AlGaN waveguides operating in 1550 nm telecommunication band [56]. They found that, the refractive index depends on the state of signal polarization and also on the direction of optical propagation in the c-plane. However, to avoid the need for polarization controller, birefringence in the waveguides needs to be minimised. Different ways to eliminate the effect of birefringence are: polarization compensation, introduction of tensile and compressive built-in stress during the process of growth and special waveguide cross-sectional design as mentioned in ref [56]. Stress engineering is the best option as it does not depend on device functionalities and configurations. This kind of stress may be caused by lattice mismatch, dislocation and impurity doping in the film. In the report, it is also mentioned that, with the variation of Al content, the light polarization in AlGaN film varies and the polarization property of AlN is different from that of GaN. This indicates another option of polarization control by the process of bandgap engineering [56].

4.2.2 Carrier-induced Index Change in GaN Waveguide

The carrier-induced refractive index change is the basic tuning process of PHASER based optical switching devices and it is faster than thermal tuning based devices [56]. To understand the efficiency in carrier based index changes in GaN semiconductors, three main carrier effects such as bandfilling, bandgap shrinkage and free carrier absorption will be discussed. By the term bandfilling, we understand the optical absorption decrease at energies slightly above the bandgap by the process of free carrier injection and impurity doping [56]. Optical absorption is a function of carrier concentration due to bandfilling. The carrier induced change in absorption coefficient can be expressed as [56]:

$$\Delta\alpha\,(N, P, E) = \alpha\,(N, P, E) - \alpha_0\,(E). \tag{4.3}$$

Here, $\Delta\alpha$ (N, P, E) denotes the absorption coefficients at doped semiconductor with carrier injection and α_0 is the intrinsic material absorption without injection. N and P denote the concentration of free electrons and holes. E and É are the energy of ground and excited levels respectively. The change in refractive index influenced by bandfilling can be expressed as:

$$\Delta n\,(N, P, E) = \frac{2c\hbar}{e^2}\,\mathfrak{R}\int_0^{\infty}\frac{\Delta\alpha(N,P,\acute{E})}{\acute{E}^2 - E^2}\,d\acute{E}. \tag{4.4}$$

Here, c, e and $\mathfrak{R}$ are the speed of light, electron charge and principal value of integral respectively. Because bandfilling decreases the absorption coefficient at a particular energy for all the cases, the material refractive index decreases due to bandfilling as well.

Bandgap shrinkage is caused by free injected carrier solely and not by doped carriers. For the increases of free carrier concentration for current injection, the conduction band energy decreases and the valance band energy increases. This happens as a result of the overlapping of electron wave functions, where a lower energy level gas of interacting electrons is formed at the bottom of conduction band and at the same time, a higher energy level gas of interacting holes is formed at the top of valance band. As a result, shrinkage of bandgap takes place for which a red shift of the absorption curve is generated.

The third carrier effect is known as free carrier absorption or plasma effect. In such a situation, a free carrier can absorb a photon and within the conduction band can move to a higher energy level. The changes in refractive index can be expressed as follows [57]:

$$\Delta n = \frac{-6.9\times10^{-22}}{nE^2}\left\{\frac{N}{m_e} + P\left(\frac{m_{hh}^{1/2} + m_{1h}^{1/2}}{m_{hh}^{3/2} + m_{1h}^{3/2}}\right)\right\}. \tag{4.5}$$

Here, n is the material refractive index, m_e, m_{hh} and m_{1h} are the respective effective masses of electrons, heavy holes and light holes.

In Fig. 4.6, the curves show the refractive index changes vs wavelength due to bandfilling, band shrinking and carrier absorption effects. These calculations were carried out at three carrier injection levels of N = 7×10^{18} cm^{-3} as solid line, N = 3×10^{19} cm^{-3} as dashed line and 6×10^{19} cm^{-3} as dotted lines. For the cases of both bandfilling and bandgap shrinking, the curves are anti-symmetric around the bandgap and the values tend to reduce much towards the higher wavelengths. However, in the region of infrared wavelengths, free carrier absorptions are the influential effects. The Fig. 4.7 also shows the combined effect of carrier induced refractive index change vs signal wavelengths and the refractive index change at 1550 nm vs carrier density change. It is deduced that in the infrared region which is far away from bandgap, the refractive index change increases monotonically with the wavelength mainly due to absorption of free carriers [56].

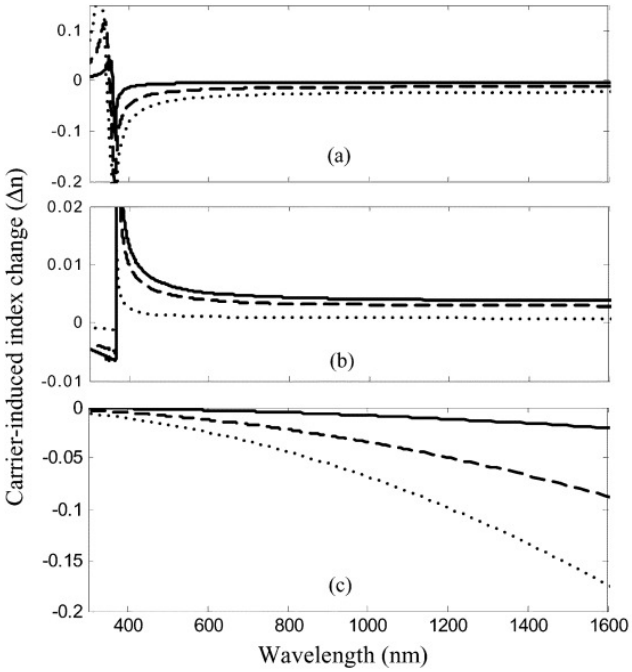

Fig. 4.6: (a) Index change for bandfilling, (b) Band shrinking, (c) Free carrier absorption at N = 7 × 10^{18} cm^{-3} as solid line, N = 3 × 10^{19} cm^{-3} as dashed line and 6 × 10^{19} cm^{-3} as dotted lines, Reproduced with permission from Ref. [56].

4.3 AWG for Multiplexing and De-multiplexing using GaN/AlGaN Hetero-structures

AWG is important for optical communication because of its uses for wavelength multiplexing, de-multiplexing and add/drop. Prior to the uses of GaN/AlGaN based AWG, some other devices such as Silica PLC (Photonic Lightwave Circuits) were used commercially [56]. Due to the passive nature of these devices, thermal tuning was used for making wavelength switching. In these devices, a small resistor is used in between each waveguide branch to induce a thermal effect by changing the refractive index for inducing an optical delay [58, 59]. However, the major disadvantage is the slowing down of the tuning process which is not suitable for fast packet based optical networks. Another kind of device is InP PLC where carrier injection methods are used for wavelength tuning [60, 61]. But this also has some disadvantages; - its refractive index is higher (3.5) than silica and that is why the waveguide cross section has to be

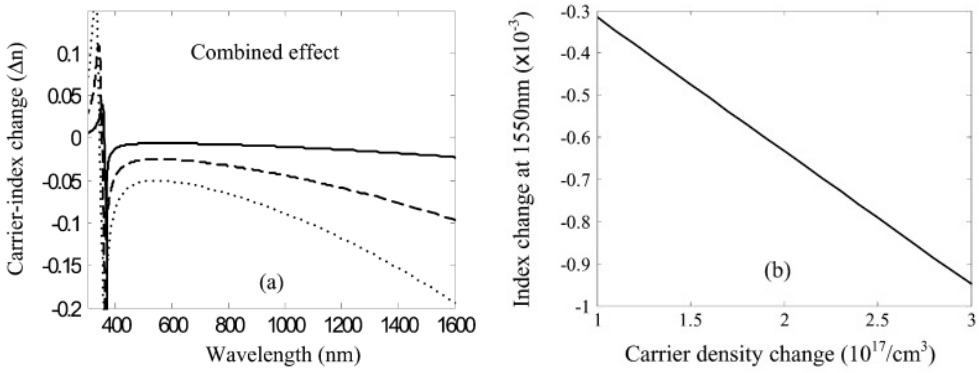

Fig. 4.7: (a) Overall index change vs wavelength at three carrier density levels (N = 7 × 10^{18} cm^{-3} as solid line, N = 3 × 10^{19} cm^{-3} as dashed line and 6 × 10^{19} cm^{-3} as dotted lines). (b) Overall index change vs carrier density at 1550 nm. Reproduced with permission from Ref. [56].

small in size which is difficult to materialize. Here, the interface between InP waveguide and optical fibre is difficult to achieve because of refractive index mismatch and mode spot size mismatch. The other disadvantage is the temperature sensitivity of refractive index which is about 10 times higher than that of silica. As such, the InP based AWGs are very sensitive to temperature changes and very meticulous temperature control is required for which these kinds of devices were not materialized commercially. GaN/AlGaN based AWGs are very advantageous compared to silica PLC and InP PLC for the application of wavelength tuning optical devices. In this case, the refractive index is less than 2.3 which is much close to that of silica and the intrinsic loss is less because of wide band gap in relation to the telecommunication band of 1.5 μm. In GaN/AlGaN materials, it is possible to make the hetero-junctions suitable for carrier injections. The application wavelength of 1.5 μm is far beyond the material band-gap and so; the optical loss at this wavelength will not be affected much by the carrier density change. However, the effective refractive index will be a function of carrier injection mainly due to free carrier absorption. That is the reason for materializing the fast tuneable GaN/AlGaN based AWG.

4.4 GaN Bragg Reflection Waveguides

Bragg Reflection Waveguides (BRW) are interferometric waveguides possessing core and periodically cladding of high and low index acting as Bragg reflectors and thereby confining energy into core. BRW shows the characteristics of strong phase and group-velocity dispersion. This is because of the strong spectral dependence on the stratified cladding layers. Hence, the BRW can be designed in such a manner that the waveguide dispersion is strong in those areas

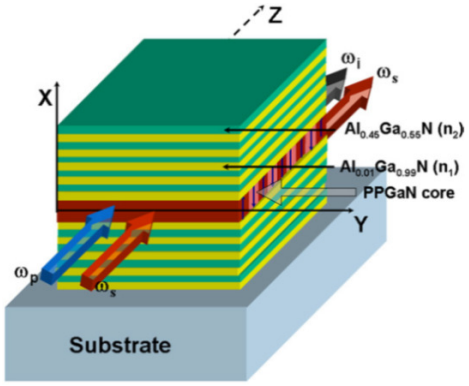

Fig. 4.8: Schematic diagram of a Bragg Reflection Waveguide. Reproduced with permission from Ref. [62].

where the material dispersion is weaker especially at low frequency. Thereby, BRW features strong dispersive mode at low frequency in order to counter the strong dispersive mode at high frequency. This mechanism conserves the phase matching condition for Optical Parametric Amplification (OPA) over a broad range of wavelengths. Here, the $\chi^{(2)}$ nonlinearity is used for the generation of OPA with a goal of exploiting the entire available bandwidth (S, C, L) of communication band (1450-1600nm) [62].

A schematic diagram of Bragg Reflection Waveguide (BRW) geometry for non-degenerate OPA process having periodically poled GaN as core and periodic cladding layers of $Al_{0.01}Ga_{0.99}N$ (n_1) and $Al_{0.45}Ga_{0.55}N$ (n_2) is shown in the Fig. 4.8. GaN is chosen here as a potential material operating in a wide spectrum (365 nm – 13.6 μm), high nonlinear coefficient comparable to $LiNbO_3$, high damage threshold and possibility of periodic poling to get Quadra Phase Matching (QPM) conditions. Another advantage is that GaN does not exhibit photorefractive properties, which shows that these devices can be pumped with high-power visible radiation. In another example of a study on high index core symmetric Bragg reflection waveguide (BRW), efficient phase matched second-harmonic generation (SHG) was experimented [63].

4.5 GaN Photonic Crystal Waveguides

The term, 'Photonic Crystal' was first coined by Yablonovitch in the article published in 1983 [64] and he referred to the structured dielectric material as photonic crystal. The term broadly refers to the 2D or 3D photonic structures having very high refractive index contrast (>2) which is different from the conventional one dimensional layered structures. Fabrication and measurement of 2D photonic crystal in the near infrared region was first reported by Krauss and co-worker [65, 66]. The optical fibres where the band-gap effect was implemented, is newly

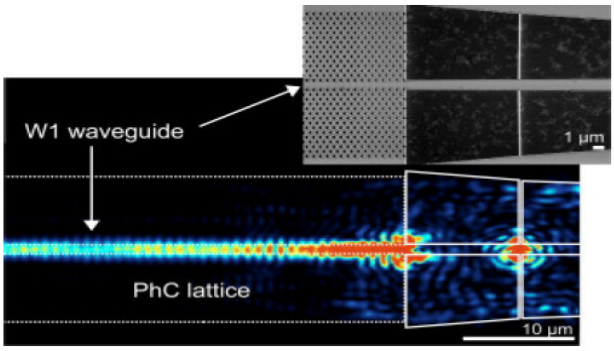

Fig. 4.9: Light propagation through a GaN photonic crystal waveguide. Reproduced with permission from Ref. [67].

named as photonic crystal fibres (PCF) [68]. In a perfectly periodic lattice, the effect of impurity states also showed interesting properties in the band-gap which leads to the possibility of optical cavities for confining light in the photonic crystals [69]. In course of time, the idea of planar 2D photonic crystals was there [70, 71]. The photonic crystal effects act in two dimensions and that is why these are called 2D photonic crystal devices. The total internal reflection acts in the vertical dimension. To create a waveguide mode in a photonic crystal, it is possible to create a line defect by removing a row of holes from it. As a result, a mode of guidance through the spatial region is created from one end to the other end of the crystal within the waveguide but confined by the crystal lattice [72, 73]. This guided band which is discrete in nature falls inside the band gap. This is labelled as W1, W2 or Wn photonic crystal waveguides depending on the number of rows removed.

This photonic crystal W1 waveguide is important in the family of photonic crystal devices and shows a property of slow light near the band edge. It is also used effectively to couple the light in between the cavities embedded in the crystal lattices. A W1 photonic crystal waveguide based on GaN was designed and fabricated as shown in Fig. 4.9 [67].

4.6 GaN Nanowires as Waveguides

Nanowires are defined as wires of diameter in the range of nanometres [74]. In fact, GaN based nanowires are the quasi one dimensional nanostructure having the diameter of 10 to 100 nm and the length in the range of hundred microns. These nanostructures are a new kind of semiconductor materials on which light generation, detection, amplification and modulation are investigated. At this scale, their material properties do not follow the characteristics of bulk ma-

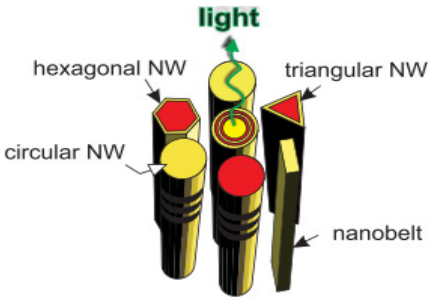

Fig. 4.10: Different structures of nanowires. Reproduced with permission from Ref. [75].

terials but only one dimensional characteristic. Their diameters are large enough that the quantum size effect is ignored and are not quantum wires. They can be found in the cross section of triangular, rectangular, hexagonal or cylindrical shapes as shown in Fig. 4.10 [75].

In a way, nanowires are very high quality unidirectional waveguides with high refractive index contrast from 2.5 to 3.5 between the wire and the surrounding layer, typically air [76]. Due to this high contrast, nanowires are very good waveguides with very small in diameter and length. It is possible to grow nanowires with or without epitaxial connection with a substrate [77]. In case of nanowires grown epitaxialy on a substrate, the crystal orientation of the substrate is automatically transferred to the nanowires that determine the direction and orientation of the nanowire growth. For this attribute, the lattice matching condition is greatly relaxed compared to the thin film growth. As such a higher strain can be tolerated. On the other hand, for the nanowire synthesis without epitaxial connection to substrates, the lattice matching condition is reduced further as any kind of substrate can be used for nanowire growth. For this reason of substrate insensitivity, nanowires open up new uses which are not common in planar systems. This strain relaxation of nanowire growth improves the design flexibility for the development of hetero-structure devices. This can be understood with the example of nanowire growth on Si as it will remain as preferred platform for different kinds of applications [46]. Si is available with large wafer area with very high crystal quality and purity. It is also mechanically stable and its material characterization is well known because of extensive investment made on Si technology. So, it is important to have a union between GaN material and Si which could render CMOS compatible devices with diversified functionalities. However, it is not easy to get the high quality growth of GaN thin films on Si. But, the mismatch problem has less consequence in crystal quality nanostructures because a very small diameter allows the strain to be relaxed laterally in contrast to the planar growth where the strain can only be relaxed along the one dimension [46].

The ability to manipulate the pulses of light beams within the submicron volumes by using nanowires is important for the development of different light based devices [78]. The concept is to make or assemble different nanowires that perform different functions like generation of light, routing and detection. The important step is to develop nanowire waveguides that interconnect

these elements of different functionality and provide flexibility for the development of complex logic operations. Using the commercial micro-manipulators, the nanowires with sufficient lengths and strengths can be bent, pushed and shaped under optical microscope. Wires are flexible and can be reshaped to a coil of radii close to 5 μm which is not possible in case of bulk forms. Moreover, the nanowires can be easily shaped on the chosen surfaces with the support of wired substrates to avoid elastic recoil. These kinds of chemically synthesized nanowires are the building blocks for the making of nano-scale optoelectronic devices. In this way, the flexible nanostructures with precision positioning, optical waveguide linking and manipulation on surfaces with other nanowire elements are utilized to form optical networks and component devices.

To have an in-depth understanding of GaN nanowire growth, it is important to understand the crystal structure of GaN. GaN has the wurtzite structure as bulk under the ambient condition which is also thermodynamically stable. Wurtzite structure is hexagonal unit cell with two lattice constants c and a [79]. The stacking order or the order of GaN and N atom layers on top of another layer in c direction can be represented by $Ga_AN_AGa_BN_BGa_AN_AGa_BN_B...$.

Various growth processes, such as Laser assisted growth, Chemical Vapour Deposition (CVD), Anodic alumina template synthesis and Molecular Beam Epitaxy (MBE) are there for GaN nanowires [79]. These can be performed with the help of metal catalysts or without of them. For Chemical vapour deposition method, nanowires grow along the a-axis of wurtzite phase, whereas, in MBE method, nanowires grow along the c-axis. More often than not, small particles of a foreign material are used to help the nanowire growth in these methods. This growth mechanism is also named as catalytic growth and it has two techniques namely, vapour-liquid-solid (VLS) or vapour-solid-solid mainly depending on the particle (liquid or solid) phases. As for example, in case of VLS, the growth starts from liquid metal catalyst [79, 80]. Here, the metal catalyst of nanometre size is deposited on a substrate utilizing the techniques like laser ablation, thermal annealing, electrochemical deposition, colloidal dispersion etc.

VLS can give good advantage in controlling the diameter of the nanowires. Nanowires are ideal crystals which are free of defects and crystalize differently in structures compared to bulk phases. Nanowire epitaxy offers greater freedom in the design of more complex structures in comparison to planar one.

5 GaN Active Waveguide Devices for Broadband Communication

Quantum wells are the structures consisting of thin well materials sand-witched by two layers of barrier materials. Optical properties of quantum well depend on the photon energy of two materials (well and barrier materials) and their thickness. In the materials, lattice mismatch produces the straining effect. Due to excess strain, the material quality is degraded as it develops cracks. This critical value of strain depends on the thickness of the layer and also on the magnitude of the lattice mismatch. It seems that the thick layer needs to be accurately lattice-matched but the thin layer as seen in the quantum wells can be severely strained without significant degradation of the material quality (Page: 2-3, The Handbook of Photonics, 2nd Ed, Mool C. Gupta, John Balloto) [81]. In GaN/AlN quantum wells, GaN is the 'well' and it is sandwiched by AlN 'barriers'. In the wells, both electrons and holes see lower energy. This layer is very thin and electrons and holes may be considered as waves. The allowed states in the structure correspond to the standing waves working in perpendicular direction of the layers. Using the Multiple Quantum wells (MQW) of such materials, two types of all-optical switching can be performed - one being 'Inter-band transition by inter sub-band transition' and the other is 'Inter sub-band transition by inter sub-band transition' [82].

5.1 GaN Waveguides with Quantum Wells and Characteristics

GaN based quantum well (QW) waveguides evolved, due to the requirement of ultra-high switching speed platforms at very low input threshold power, using the electro-absorption techniques. This is a great advantage compared to the GaN based waveguides without quantum wells. Yan Li demonstrated the optical processes in GaN/AlN quantum well waveguides [83]. The waveguide considered in the experiment was a 30 repetition of GaN/AlN quantum wells as these were sandwiched by the 1.5 μm AlN cladding layer and 0.6 μm cap layer of GaN at the top. The scanning electron microscopy (SEM) image of the facet of the device is shown in Fig. 5.1 [84]. The 30 repetitions of quantum wells show strong inter-subband absorption peak at 1.5 μm telecommunication band. Using the RF plasma assisted molecular beam epitaxy, the materials of waveguide are grown on a c-plane sapphire substrate. The optical mode is mainly confined to the higher indexed GaN cap and in the QWs, which is then decayed evanescently into lower indexed AlN cladding layer. Here, the optical mode has small amplitude at the sapphire-semiconductor interface where high structural defects produce optical propagation losses in significant amount. To maximize the overlap factor between the guide mode and the active layer of QW, the 0.6 μm thickness of GaN cap layer is selected. This 0.6 μm thickness is more or less close to the wavelength of the telecommunication band (1.5 μm). Using this principle of design, the inter sub-band saturation power measured was found lower than the data observed in other previously attempted similar experiments [85]. Here, the characteristics of this

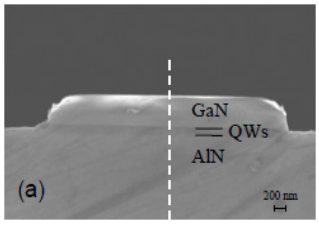

Fig. 5.1: A SEM image of the facet of a GaN/AlN QW waveguide. Reproduced with permission from Ref. [84].

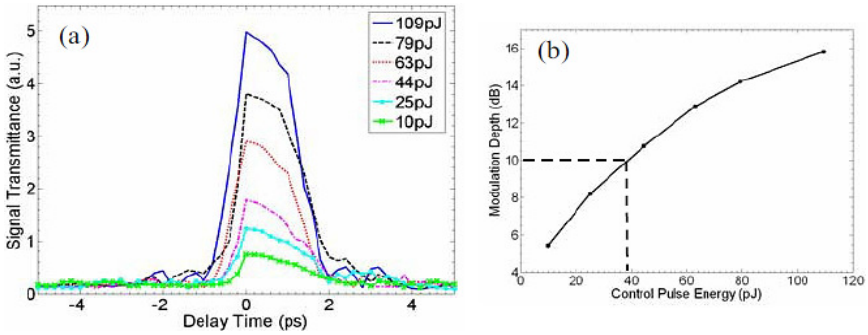

Fig. 5.2: (a) Signal transmittance through a GaN QW waveguide versus signal-control delay time for different.

type of waveguide are discussed. The inter sub-band (ISB) transition of this type of QW in the near-infrared band shows: (i) ultrafast relaxation lifetime, (ii) very large conduction-band offset, (iii) large optical nonlinearity and (iv) promises of monolithic integrated platforms [83]. High power control pulses were used to modulate the ISB absorption losses of a weaker input optical signal. Both the signal and control pulses are generated by the same mode-locked fibre laser having 160 fs pulse width and TM polarization mode. The plot for signal transmittance versus signal control delay time through the waveguide (1 mm long and 3 μm wide) is shown in Fig. 5.2(a) [83]. This plot was traced for different energies of control pulses. The signal modulation depth versus control pulse energies is also plotted as shown in Fig. 5.2(b). From the plot, it is seen that the switching requirement to obtain 10-db modulation depth is about 38 pJ.

This shows great improvement compared to other previously obtained data as mentioned in ref [85]. For the confirmation of ISB originated all optical switching, it was found that there was no modulation of signal transmittance by the control signal if one of them is TE polarized. In Fig. 5.2(a) above, the traces of temporal width were 1.6 ps and these were suitable for all-optical gating at several hundred Gb/s bit rates. The temporal widths were affected by certain degree of

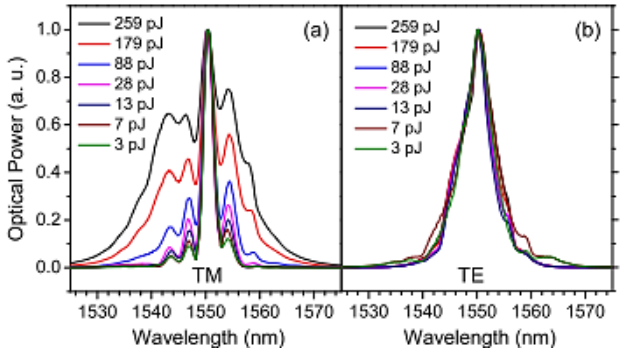

Fig. 5.3: Signal Transmittance versus signal-control delay time for different control pulse energies. Reproduced with permission from Ref. [83].

timing jitter seen in the measurement mainly due to the laser source. With better laser source, faster ISB relaxation time is expected in the QW of the waveguides. The absorption saturation in these types of quantum well waveguides is generally accompanied by ultrafast refractive index modulation which is related to same inter-subband carrier dynamics. A plot of self-phase modulation is shown in the Fig. 5.3 [83]. Here the optical spectra of transmitted ultra-fast pulses through the waveguide for different energies of input pulses are shown. However the shapes are governed by the interaction of the dispersion and nonlinear refraction. Spectral broadening with the increases of input pulse energy occurs if the pulses are TM polarized and coupled to ISB transition. Here the inter sub-band refractive index modulation or phase modulation induced by the pulses takes place. On the other hand, there is no change in the spectral shape if the pulses are TE polarized which also confirms the ISB nonlinear process in the QW waveguides. This refractive index nonlinearity can be further used for optical switching platform by utilizing an interferometric configuration to convert phase to amplitude modulation [83].

5.2 Optical Nonlinearity in GaN/AlGaN Quantum Wells

For optimum utilization, the ultrafast absorption in the multiple quantum wells of GaN/AlGaN in all-optical switching techniques, first and foremost, we need to understand the very high second order nonlinear susceptibility in those materials. Compared to the widely known GaAs based materials, GaN materials have the properties of wide band-gap, large piezo-electric coefficient, strong macroscopic polarization and strong atomic bonding, which suit the getting of strong optical nonlinearity in the quantum wells. In structures with inversion symmetry, the even order susceptibility vanishes. Hence, the second order susceptibility can only be achievable by breaking the symmetry of the conduction band potential. Because of large conduction band

offset in the interface of GaN/ AlN in the wavelength of 1.3 μm and 1.5 μm suitable for optical communication networks utilizing the ISB transition and very high relaxation time in quantum wells, these support the terahertz level optical switching platform. Quantum wells basing on (0 0 0 1) oriented wurtzite nitride semiconductors show remarkable spontaneous strain-induced piezoelectric polarization and breaks the symmetry of GaN/AlGaN quantum wells and show very high value of $\chi^{(2)}$. Liu et al. [86] analysed the second order nonlinearity susceptibility theoretically in GaN/AlGaN quantum wells where it was shown that $\chi^{(2)}$ depends on well width, Al content and pump photon energy. In course of time, Passeri and co-operators [87] measured the second harmonic generation susceptibility tensor in GaN/AlGaN materials and on the $Al_xGa_{1-x}N$/GaN QWs. The results portrayed, that the non-centrosymmetric structure and quantum confined effect enhance the second order optical nonlinearity. More recently, Chen et al. [88] experimented on the nonlinear optical absorption in GaN/AlGaN QWs. The important derivation of their finding is that properties like structure of QW, the quantum confined effect and the carrier relaxation rate can tremendously influence the nonlinear absorption properties of the sytem.

5.3 GaN Waveguide Switches and Modulators

Various materials are proposed for the inter sub-band transition such as InGaAs/AlAsSb MQW, InGaAs/AlAs MQW, ZnSe/BeTe MQW and GaN/AlN MQW. But GaN/AlN MQW are promising, mainly due to large conduction band offset of 2 eV. Moreover, large electron mass and large LO photon energy in this kind of material make the inter-sub band transition energy relaxation extremely fast - close to a few hundred femtoseconds [40, 89]. The components used for the modulation are important since they deal with the changes in the optical properties such as intensity, frequency, phase shift and polarization of waveguides [90]. The waveguides utilize the saturation of inter sub-band absorption and require high switching pulse power to pump the inter sub-band absorption to a saturated state [91]. On the other hand, absorption depends on the number of quantum wells and the waveguide confinements. Basing on this, the new design of waveguides will be requiring less switching pulse energy. This kind of design is performed by using the crystalline growth technology and two parameters are mainly considered in the design. The first one is optical confinement of MQW which should be as high as possible for the best utilization of inter sub-band absorption to ensure less pumping power to reach a saturation level and the second one is the mode of operation which should be single mode for the ultrafast and reliable operation. Suzuki et al. [92, 93] first predicted the feasibility of inter sub-band (ISB) transition concept in the telecommunication band (1.5 μm). They found the relaxation for ISB to be 80 fs at 1.5 μm which was around 30 times shorter than that of other similar type materials such as InGaAs quantum wells. As such, they proposed for GaN/AlGaN quantum wells (QWs) for the Tb/sec all-optical switching platform. Waveguide structures suitable for MQW switching, need to be fabricated on low refractive index material mainly to produce high confinement waveguide with cladding materials. Optical confinement can be further enhanced by inserting

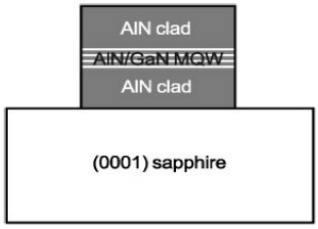

Fig. 5.4: An AlN waveguide structure. Reproduced with permission from Ref. [95].

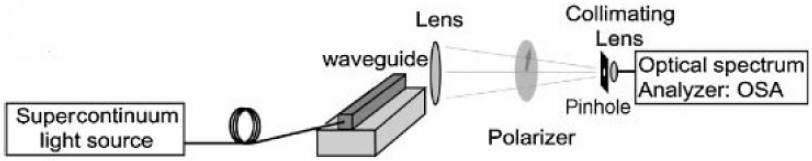

Fig. 5.5: Schematic diagram of measurement setup. Reproduced with permission from Ref. [95].

high refractive index guiding layer as the waveguide core. This waveguide structure can be achieved by growing AlN as cladding layer followed by GaN as guiding layer. But the growth of this kind of structure with high crystalline quality is very difficult to achieve because of large lattice mismatch between GaN and AlN which is about 2.6%, as such improvement on the growth technique is required to realize these types of waveguides. Using the GaN waveguides, ultrafast switching based on ISB absorption was demonstrated [94]. These switching waveguides still require high switching pulse energy for their application in photonic networks. In such cases, AlN waveguides are an alternate to reduce switching energy because of its low refractive index which is suitable for the fabrication of high optical confinement waveguides having low propagation losses. It also has good carrier confinement in quantum wells and can induce strong built-in electric field. Basing on this, Chaiyasit Kumtornkittikul and et al. [95], demonstrated an AlN waveguide for GaN/AlN MQW switching platform. In his paper, an AlN waveguide structure was studied consisting of bottom AlN cladding layer, a GaN/AlN MQM layer and upper AlN cladding layer as shown in the Fig. 5.4.

A waveguide measurement technique using ultra wide spectrum light source was used in the experiment to find ISB absorption in the waveguide (shown in Fig. 5.5). The light from the super-continuum source is coupled to the input of the waveguide using a tapered fibre. The light that comes out from the other side is focused onto a small point using a 100× lens. To reduce noise, a small pin hole was used as a filter. The light was then coupled to a larger diameter fibre using a collimating lens making it suitable for measurement using an optical spectrum analyser.

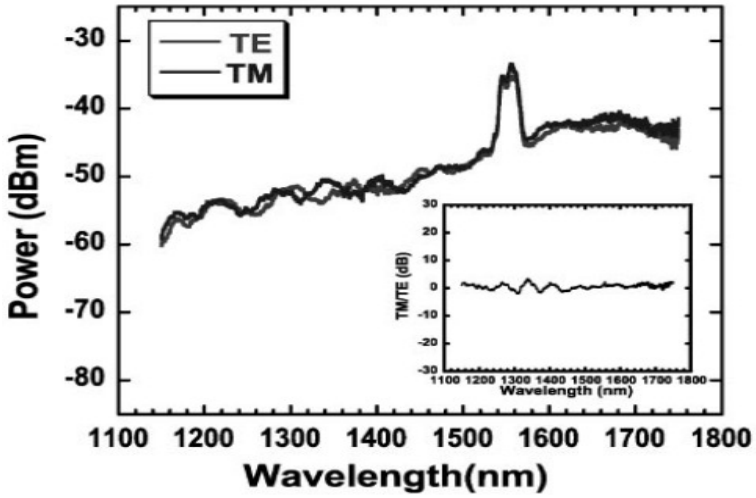

Fig. 5.6: TE and TM polarized transmission spectra in an AlN waveguide without GaN/AlN quantum wells. Reproduced with permission from Ref. [95].

The polarized TM and TE mode of light was obtained using polarizer in between the waveguide and the pin hole.

With this setup, the transmission spectra for both TE and TM mode light in the wavelength range of 1.1 – 1.7 μm could be obtained. With the calculation of power ratio of TM to TE mode or by getting the difference of log scaled transmission spectra between the modes of TM and TE, the absorption spectra of the waveguide can be achieved. Now we can have a comparative look at the different phenomena among the 'waveguides without quantum wells', then 'waveguides with quantum wells having AlN as cladding layer' and finally 'the waveguides with quantum wells with GaN cladding layers'. As first observation, a 1 mm long and 2 μm wide AlN waveguide without quantum well was placed in the experimental setup. According to the Fig. 5.6, by analysing the TM and TE mode transmission, it was found that there was no absorption in the waveguides since no difference between the transmitted powers of TM and TE modes along the scanning range was observed.

Analysing the spectra for the AlN cladding waveguide with quantum well, we see the transmission spectra for TE and TM mode in Fig. 5.7(a) and also the inter-subband absorption in Fig. 5.7(b). This shows that, the AlN waveguide had the highest level of absorption at the wavelength of 1.3 μm with extinction ratio of 20 dB. For the purpose of comparison, the measurement of ISB absorption for GaN waveguide was also carried out. This GaN waveguide also contained two 2-nm thick GaN quantum wells and was fabricated with the same structure but the cladding material was changed to GaN. The AlN barrier thickness was set to 3 nm for this GaN waveguide to achieve the high quality waveguide. With this kind of waveguide, it was

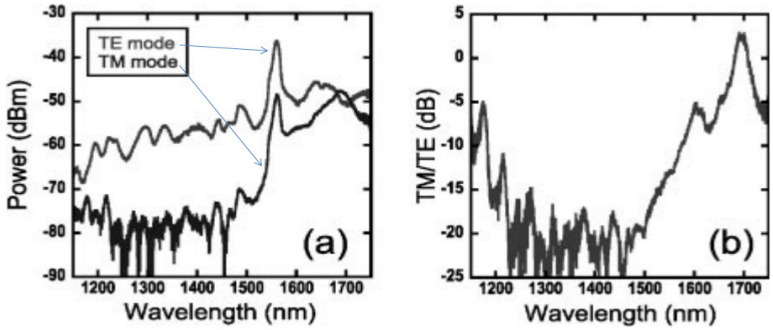

Fig. 5.7: (a) Transmission spectra in an AlN waveguide with GaN/AlN quantum wells, (b) Inter-subband absorption spectrum. Reproduced with permission from Ref. [95]

found that the absorption spectrum was seen to shift towards longer wavelength with decreasing number of quantum wells. For example, with 40 number of quantum wells, it had the inter-subband absorption at 1.55 μm, whereas the absorption shifted towards 1.7 μm with 2 quantum wells in the setup. The reason behind this shift is the weakening of built in electric field in the quantum wells since the barriers are comparatively thin. However, for GaN waveguides, the thickness of barrier is difficult to adjust for critical thickness limitation of AlN on GaN. As such, the red shift of absorption for GaN waveguide is difficult to compensate. On the other hand, for AlN waveguide, the absorption wavelength does not vary with the number of quantum wells. Moreover, the wavelength can be varied by changing the barrier thickness. The main reason is that the AlN cladding layers and the barriers are very thick in comparison to GaN quantum wells. As such the built in electric field is very strong for each quantum well and the variation in the number of quantum wells does not affect much in the electric field strength.

Modulators are required to change the signals from electrical domain to optical domain in conjunction with the continuous waves or mode locked lasers. Modulators are made by exploiting a different kind of physical effects, which use changes in electric field to change the optical properties of a medium for the control of light flow. Some methods of modulation are: (1) Electro-absorption Modulation (EAM), (2) Electro-refractive or Electro-optic Modulation (EOM), (3) All-optical Modulation, (4) Modulators using Quantum Cascade Stark Effect (QCSE), (5) SiGe Modulators. The discussion here is on the first two methods which use the GaN/AlN waveguides. In comparison to EAM, normally, EOM has lower chirp, higher optical saturation power and wider (100nm) optical bandwidth [96].

5.3.1 GaN/AlN Electro-absorption Modulators

Electro-absorption modulators modulate light either by passing or preventing light through them. These kinds of modulators are based on the modulation of the material absorption by the electric

field that is induced by the applied voltage on the semiconductor. Using the bulk semiconductor, it is possible to perform electro absorption modulation through Franz-Keldysh Effect (FKE) or in quantum well through quantum confined Stark effect (QCSE) [96]. The light modulation performance can be characterized by a term known as 'extinction ratio'. This is the ratio between the maximum and the minimum power outputs of the modulator. The higher absorption ratio is related to the higher light absorption by the creation of more electron-hole pairs in the active regions. The band-gap energy of the quantum well structure is changed by applying an electric field through the QCSE. Quantum well based modulators have better extinction ration than the bulk modulators mainly due to higher strength of QCSE. The modulators absorb light when a reverse bias is applied in the p-i-n junction. As small current passes in the reverse bias condition, the modulation speed is limited due to the time required to charge and discharge the capacitance of the electro absorption modulator. Higher extinction ratio might be achieved by the uses of longer waveguides or by an increase in the number of quantum wells or higher voltage swing operation but, the modulation rate is seriously affected since longer modulators create higher capacitance and an increased number of quantum wells also increases the carrier extraction time. It is desirable to integrate an electro-absorption modulator into a waveguide with strong optical mode mainly due to compatibility with the fibre optics system. Figure 5.8 below shows a GaN ridge waveguide inter-subband modulator [97].

In Fig. 5.8(b), the active region consists of a 3 period GaN well of thickness 1.3 nm with AlN barrier of thickness 3 nm inserted in the core of an $Al_{0.5}Ga_{0.5}N$ waveguide layer of thickness 1 μm. According to the Fig. 5.8(a), for device operation, it is seen that the modulator is transparent at negative applied bias since the 3 quantum wells are depleted. On the other hand, at positive applied bias, the electron population of wells allows rise in inter subband absorption at 1.5 μm wavelength. Figure 5.9 given below, shows the transmission through the waveguide under different bias conditions.

This was measured with an injection-lensed fibre with a tuneable semiconductor laser diode. The transmission is flat for TE polarized light, as it does not depend on the bias. Whereas, for TM polarized light, there is an ISB absorption which increases with the increase of bias from –9 to +5V as a result of the population of the ground state of QWs. The modulation depth of the order of 14 dB for bias voltage of -9V/+6V and 10 dB for voltage swing of 5V can be obtained. It is important to mention here that a 12dB is required for optical modulation to achieve 10^{-12} bit error rates in the present fibre optic communication system.

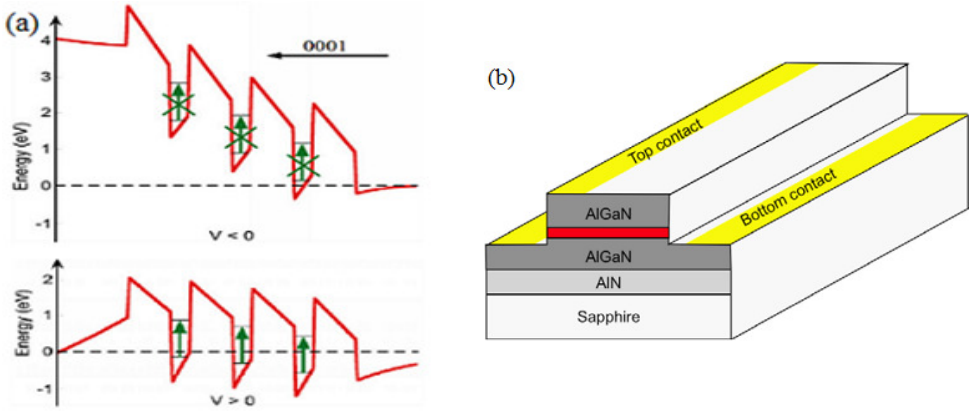

Fig. 5.8: (a) Principle of operation of depletion modulator (b) Ridge waveguide modulator device. Reproduced with permission from Ref. [97].

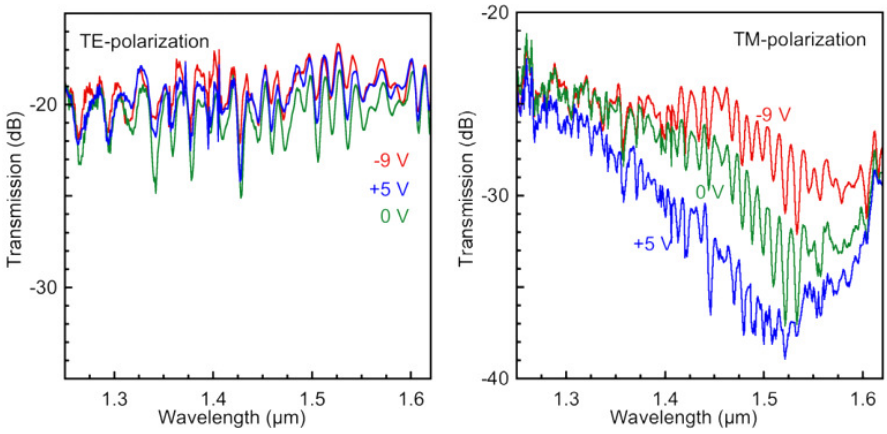

Fig. 5.9: Waveguide transmission spectra of the depletion modulator for TE and TM polarized light. Reproduced with permission from Ref. [97].

The optical bandwidth for EAM is narrow for FKE based devices (10 nm) and very narrow for QCSE based devices [96]. QCSE based EAMs have lower ON-OFF voltages (2 V or less) and small size due to interaction length of less than 500 μm. Hence integration of this device with the source is possible where the optical bandwidth is closely matched with that source and this kind of device is known as electro-absorption integrated laser (EAL) with better compactness [96].

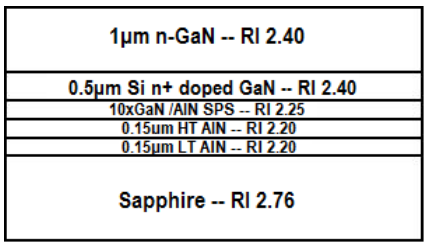

Fig. 5.10: Schematic diagram of the waveguide structure.

5.3.2 GaN/AlN Electro-Optic Modulators

Electro-optic modulators are mainly used for ultrafast information processing system [54]. It is possible to make modulators from bulk electro-optic materials but it requires high driving voltages and the modulation bandwidth (30 GHz) is also narrow. However, to improve the properties of electro-optic modulation, materials with high electro-optic coefficient, good transparency, low dielectric constant, low optical loss and single mode waveguide operation are needed. Using proper design, GaN and its alloy based optical modulators open the new initiative to make new generation optical waveguides suitable for active and passive devices such as modulators and switches [98, 99, 100]. Optical and electro-optic characteristics of a GaN optical waveguide studied by Arnaud STOLZ and et al. [101] are discussed below. The schematic diagram of the waveguide structure is shown in Fig. 5.10

Optical confinement exists at the top layer due to refractive index contrast of GaN (2.40) compared to buffer layer (between 2.20 for AlN and 2.25 for GaN/AlN short period superlattice) and substrate (1.76). Using Scanning Electron Microscopy (SEM), it was found that the two GaN layers were undistinguishable from each other. The buffer layer, specially the AlN/GaN short period superlattice (SPS) acting as barrier layer had a strong influence in suppressing the dislocation propagation of the 1.5 µm GaN film. From the Ref. [101] data, optical loss at 1.5 µm was found to be 0.5 dB/cm. This value is found lower than InP based ridge waveguides where, the loss is about 1 dB/cm [102]. The temperature dependence of the waveguide was found low and it is even lower compared to InP [101]. To understand the electro-optic characteristics, some parts of the n- GaN top layer were etched with RIE-ICP to allow biasing on both sides of the GaN film. A standard Ti/Al/Ni/Au metallization was deposited on etched n+ GaN for ohmic contact and schottky type Au pad contacts were deposited on top of n- GaN film. The front and back contacts were connected to a voltage generator for electro-optic characterization using the soldered wires. The electro-optic structure is shown in Fig. 5.11. In the experiment, the reflected

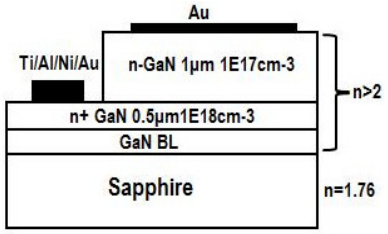

Fig. 5.11: The electro-optic structure on GaN/sapphire.

optical intensity was measured as a function of voltages in the range of 0-35 V. It was seen that index modulation Δn of n- GaN waveguide was about 2×10^{-3}. This was a clear indication of active behaviour of GaN material as an electro-optic modulator. The result was not impacted by thermal effects [101].

From the physical point of view, both the EOM and EAM exploit the modulation of the refractive index of the material which is induced by the electric field. In EOM, the real part n_r and in EAM, the imaginary part n_i of the refractive index are exploited. But n_r and n_i and their variation with the applied field are related (Kramers-Kronig relation). This kind of inter-dependence is the main cause of chirp in EAM. Here, the intensity modulation of the device creates some amount of phase modulation also. However, in case of EOM, due to low absorption coefficient, this kind of variation has no significant influence on the performance of the devices. In EOM, chirp originates from the design geometry and asymmetry of the device [101].

5.4 Lasing in GaN Nanowires

Recent research focuses more on the application of nanowires as light sources compatible to very large scale integrated (VLSI) circuits. To make this photonic VLSI circuits, lasers of nanoscale dimensions will be required. Moreover, lasers with very small dimension and low-threshold will allow the development of many high speed communication devices, optical interconnects and information processing. In comparison to commercially available vertical cavity surface emitting lasers (VCSELs), nanowire lasers show small dimension (diameter close to 100 nm) thereby, requiring much less power consumption and larger integration density. Defect free nanowires can be grown on Si substrates which also allow the monolithic integration of light emitters with other photonic and electronic components on a chip. The principle of the nanowire operation lies on the simultaneous confinement of carriers and photons in a one dimensional nanoscale cavity. A better carrier confinement in these structures helps them to move freely along the direction of axis only. On the other hand, the spontaneous emission rate is significantly enhanced due to optical confinement in the miniaturized optical cavities. The spontaneous emission is directly proportional to the electromagnetic density mode with which an emitted spontaneous photon is coupled to. In this way, a quantum electrodynamics in cavity can generate the low threshold

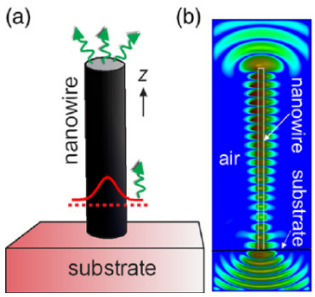

Fig. 5.12: (a) Schematic diagram of a single nanowire Fabry-Perot (FP) cavity, (b) Laser intensity profile. Reproduced with permission from Ref. [75].

lasing from nanowire based cavities [75]. Nano-lasers must have the feedback mechanism and gain medium to compensate the cavity losses for its sustained laser outcome. This fundamental operating principle of nanowire laser can be depicted further by using Fabry-Perot (FP) cavity. The smallest FP type cavity which can effectively provide the positive feedback of stimulated emission can be represented by a single crystalline semiconductor (GaN) nanowire of lengths in the order of light wavelengths. Figure 5.12(a) shows a diagram of a single nanowire laser which represents FP nano-cavity and this nanowire can be fabricated from one dimensional GaN nanostructure [75]. In such nano-cavities, two crystalline nanowire facet ends act as reflecting mirrors.

Nanowire cavity is similar to gain medium terminated by two reflectors. So, the threshold condition can be determined by the balance between the round trip gain and losses inside the cavity. On the other hand, the optical field propagating along the longitudinal direction is amplified and absorbed inside the nanowire. Part of the light is reflected back to cavity from the facets of the nanowire and the remaining light is emitted to the outside medium from the facets (Fig. 5.12b). To improve FP based nanowire lasers, different research groups are engaged globally. In 2002, two research groups of the Lawrence National Laboratory (USA) and University of California, Berkeley, first developed optically pumped single GAN NW at room temperature [103]. The NW was grown using the MOCVD process and its length was about 40 μm mainly to reduce the mirror loss. The same group later developed optically pumped core-sheath ($GaN/Al_xGa_{1-x}N$) quantum wire lasers in the UV range [104]. Vapour-liquid-solid (VLS) process was followed for the development of cylindrical GaN core of 5nm diameter with 50 to 100nm $Al_{0.75}Ga_{0.25}N$ cladding layer. It is seen that GaN nanowires with diameter less that 100nm are too leaky to sustain the laser cavity mode. Hence wrapping the GaN core with material of lower refractive index and higher band-gap creates a structure with simultaneous exciton and photon confinements. Here, the core provides the gain medium and the sheath works as FP cavity under optical pumping. The lasing threshold was observed to be 10 times higher than the

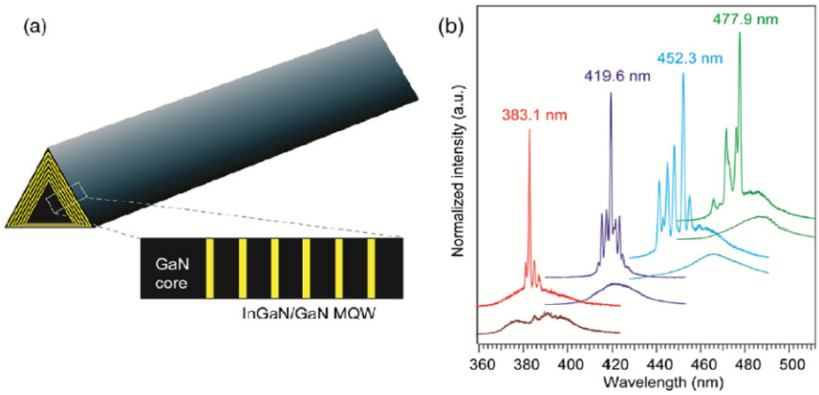

Fig. 5.13: (a) Diagram of a GaN/InGaN nanowire showing the cross-sectional magnified view of NW facet with MQW structure (b) Normalized PL spectra collected from four representative 26 MQM nanowire structures. Reproduced with permission from Ref. [75].

larger unclad GaN nanowire lasers [103]. In 2008, a new type of tuneable nano-laser was reported by Qian et al. [105], where multiple quantum well core/shell hetero-structure was used. The structure consists of GaN nanowire as core acting as optical cavity which is surrounded by InGaN/GaN MQW (consisting of 3- 26 quantum wells) shell (Fig. 5.13a) which acts as tuneable gain medium. The dimension of this NW was 200 – 400 nm diameter and 20 – 26 μm length. Interestingly, by varying the In content, the wavelength could be tuned in between the wavelengths of 365 and 494 nm (Fig. 5.13b).

Most nanowires suffer from lasing at multiple frequencies simultaneously due to LO mode seen in native Fabry-Perot cavities. Laser emission in multiple frequencies can lead to temporal pulse broadening and false signalling. This problem can be avoided by controlling the laser oscillation in single frequency mode. As such, a concept named ‘cleaved coupled cavities’ is introduced, where two Fabry Perot nanowires are axially coupled with an air-gap to produce single mode emission [106]. Single-mode lasing can be obtained when the spectral spacing between the modes (free spectral range) is larger than the optical gain bandwidth [107, 108, 109]. The free spectral range can be increased by radiatively coupling two Fabry-Perot cavities axially with an air-gap. The two cavities can be made by cutting a single nanowire thereby ensuring their axial alignment. However, the range of air-gap width is limited due to diffraction losses. Using focused ion beam (FIB) milling and defining the optical cavities on a single crystal GaN nanowire, the cleaved-coupled nanowires can be designed as shown in Fig. 5.14a [106].

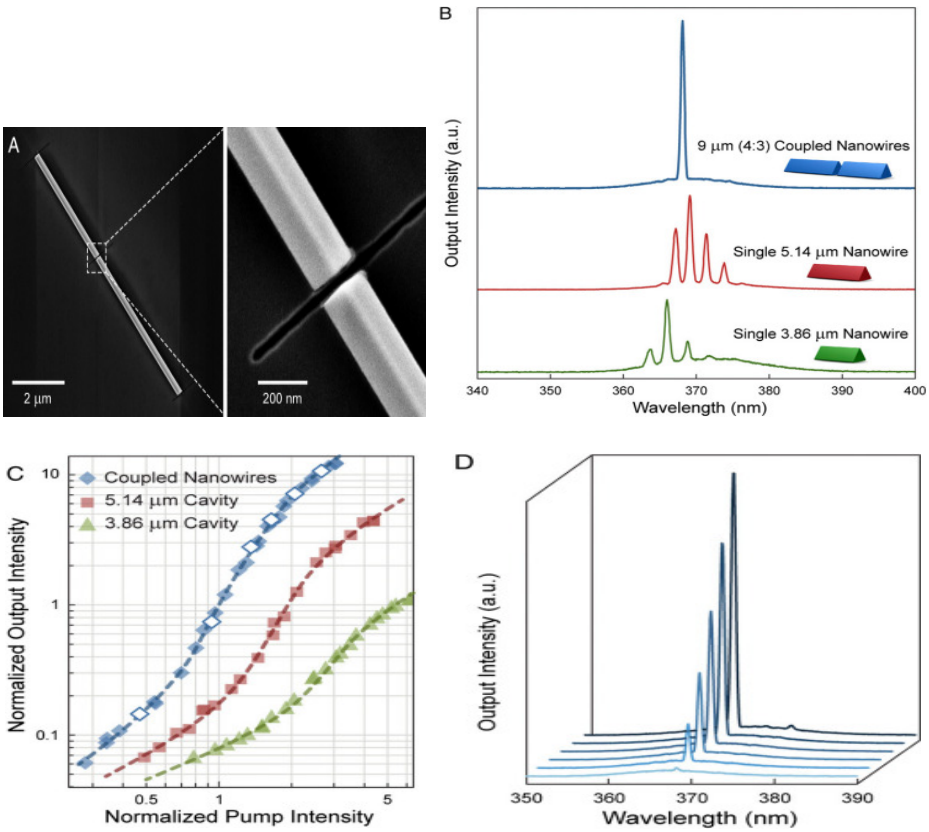

Fig. 5.14: (a) Single mode lasing in 9 µm (4:3) cleaved-coupled nanowire; (b) single wavelength lasing in coupled cavity (blue line) and each component nanowire lasers at multiple wavelength when they are separated; (c) Showing the lasing pump intensity occurring at lower pump intensity in cleaved-coupled nanowire lasers; (d) Stable single mode operation over a good range of pump intensities. Reproduced with permission from Ref. [106].

To prevent the degradation of the photoluminescence during the FIB milling, a metallic protection layer is used. The smooth end facets and the gap facets obtained due to milling also help to reduce the diffraction losses of the cavities. The lasing spectra of individual nanowires of lengths 3.86 µm and 5.14 µm, with multiple Fabry-Perot modes are observed as in Fig. 5.14(b). However, as soon as the two cavities are aligned axially with a 40nm gap, a single mode lasing is obtained from 9 µm (4:3) cleaved coupled cavity as shown in Fig. 5.14(b). The lasing transition

occurs comparatively at low pump intensity in cleaved-coupled nanowire in addition to the reduced number of lasing modes as in Fig. 5.14(c). It also shows stable single mode operation over a good range of pump intensities (Fig. 5.14(d)).

GaN based nanowires have some advantages compared to their planar types. Planar type lasers grown on sapphire and SiC show very high dislocation densities and reduced performances due to large lattice mismatch and related strains. As such, very high threshold current densities, of about 10kA/cm^2 is required to emit the lasing action over 500nm wavelength in particular. On the contrary, nanowire based devices show very reduced dislocation densities and polarization fields which support better device engineering. Subsequently, these kinds of devices require very little threshold current densities and the power consumption is also less. Most importantly these nano-structured lasers with reduced cavity volumes can operate at higher modulation speeds [110]. The lasing thresholds of these lasers vary with the characteristics of the nanowire cavities, nanowire dimensions, nanowire qualities and coupling of the nanowires with the substrates.

Although, there has been good progress in the development of optically pumped nanowire lasers, but there has been no progress so far in the development of electrically pumped nanowire lasers. These types of electrically pumped nanowires are required for the practical device applications. To get electrically injected nanowire lasers, some issues need attention. Almost defect-free nanowires with controlled doping need to be grown. It will also be required to have high active regions with large gain. From the fabrication point of view, it is difficult to get nanoscale level low resistive contact points (metal-semiconductor) without degrading the optical confinement in the devices. It is interesting to explore the nanowire based lasers with high speed optical modulation which is very important for telecommunication devices. Another important drawback of recently developed nanowire lasers is that the output lasing power is not high enough for some practical device applications. But with reduced coupling losses, optimized hetero-structures, better carrier injection and better thermal management, the output power can be increased to a sufficient scale [75].

6 Overview of Selected GaN Based Devices for Broadband Communication

GaN and AlN semiconductor devices are utilized so far in the application of blue and UV lasers and diodes. Through using these, high capacity blue-ray DVDs and GaN-based LED lights are some of the exciting inventions of modern days. But GaN based devices have also the utility in the spectral region which is far from the blue i.e., in the infrared region. One important advantage of utilizing GaN semiconductor materials in the long wavelength region is that it has the transparency in this region but its refractive index can be changed by carrier injection. As such, it is possible to make all-optical switches in the pico-second level basing on optical phasors. On the other hand, SiO_2 based conventional waveguides do not provide this type of tuneability. Several devices are possible to materialize in the mid and far infrared spectral region basing on other techniques like the inter-subband (ISB) transition in multiple quantum wells (MQW) using the waveguides. Examples of some of these devices are quantum cascade lasers, quantum well photo-detectors etc. These ISB transition characteristics are also suitable for the development of ultrafast switches and modulators towards photonic platforms mainly for the sub picoseconds relaxation time and high optical nonlinearity. It is expected that these devices will play an important role in the ultra-wide band signal processing and all-optical fibre optics communication system especially in the telecommunication band of 1.5 μm.

6.1 GaN Photodetector

Photodetectors detect the light and by the definition of detecting light we mean to generate an electrical signal as a function of the incident light intensity. The incident photons generate electrons in photodetector. The number of electrons passing through the photodetector is relevant to the number of photons. This relevance is known as the overall efficiency and is shown by the following expression [111]:

$$\eta_{\text{tot}} = \frac{N_e}{N_p} . \tag{6.1}$$

Due to the difficulty in determining the number of electrons and photons, to measure the ratio of output electrical current per incident optical power, a parameter is used which is known as responsivity ℜ, the expression for which is:

$$\Re = \frac{I}{P_i} = \frac{\lambda e}{hc}\frac{N_e}{N_p} = \frac{\lambda e}{hc}\eta_{\text{tot}} . \tag{6.2}$$

Here, e, h, c and λ are the electron charge, the Planck's constant, the speed of light and the incident light wavelength respectively. The diagram of a typical photo-detector is shown in Fig. 6.1.

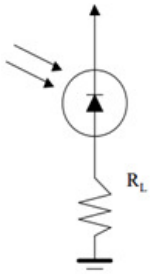

Fig. 6.1: A typical photodetector.

As already known that, for the cases of fibre based optical data transmission, the opto-electronics components have reached to their intrinsic speed limit. For this reason, the future generation telecommunication components will require the detectors of ultra-high frequency ranges which do not suffer from parasitic capacitance effects. Semiconductor materials in the infrared wavelength can be made optically active by engineering the electron quantum confinement in the quantum well (QW) layers [112]. Different types of GaN based photodetectors are available such as Quantum well infrared photodetectors (QWIP), Quantum cascade detectors (QCD) and Terahertz Inter-subband photodetectors. The main uses of QWIPs are in the high speed detectors for the optical communication platform. DeCuir E A and et al. [113] reported the infrared photodetector based on cubic GaN/AlN QW superlatices. These kinds of devices, exhibit photo-voltaic effect and is influenced by the dark current at the temperature of 215K. Dark current originates from high density of dislocations from GaN/AlN devices near IR wavelengths. Large dark currents provide low yield for these photo-voltaic devices. Hofstetter et al. [114] first studied the operation of GaN/AlN based QWIP devices in the telecommunication band and the working principle of this type of photovoltaic ISB detector was based on resonant optical rectification in asymmetric QW [114]. Another application for the photovoltaic ISB photodetectors is known as 'multi-spectral detectors' operating in different wavelengths. Hofstetter et al., in an experiment [115, 116], have combined the optical interband and ISB transition with a photo conductive ultra violet interband detector based on AlGaN thin film and a photo voltaic near infrared ISB detector based on AlN/GaN superlattice as in Fig. 6.2. The two detectors exhibited narrow responsivity curves enlarging the UV to visual rejection ratio and improved the noise in infrared detector at room temperature.

Another type of high performance photodetector named 'Quantum Cascade Detector (QCD)' is available. In comparison to QWIP, QCDs are photo-voltaic devices and work on zero bias condition. In QCDs, the absence of dark current is important to improve its signal to noise ratio. A one period of QCD is formed of a quantum well (ISB absorption happens here) and an extractor stage to transfer the photo excited electrons to the next period. This kind of charge transfer produces the photocurrent if connected to a load resistance. The extractor design stage

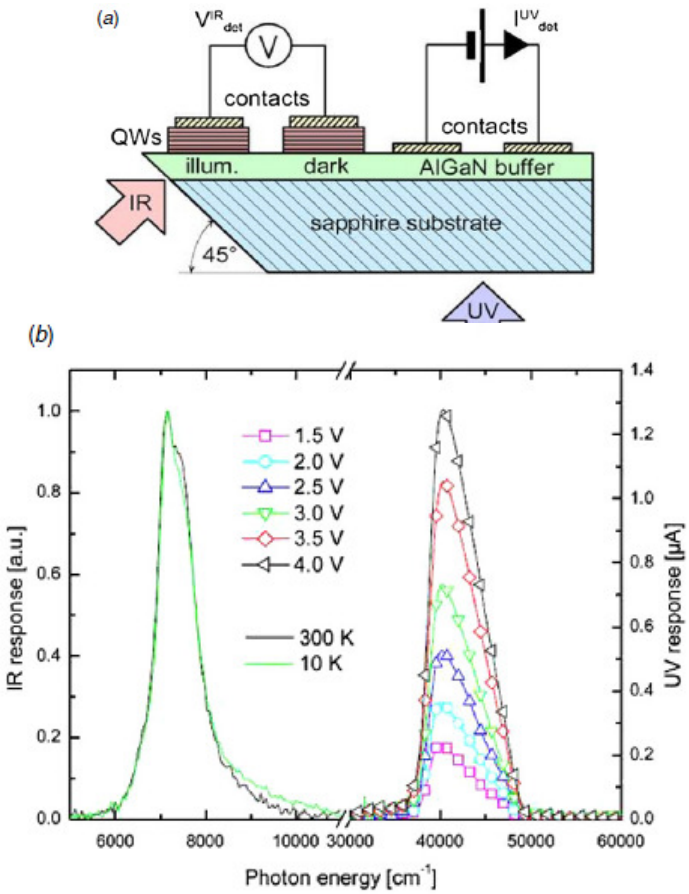

Fig. 6.2: (a) Schematic cross section through the sample showing the relative positions of the UV and the IR detector. The QWs are used as the detection layer for the IR, while the AlGaN buffer is the detection layer for the UV radiation. (b) Spectral responsivity curves measured for the UV (1.5 to 4.0 V in steps of 0.5 V). Reproduced with permission from Ref. [116].

depends on the thickness of multiple quantum wells which is chosen to get a ladder of ground states separated by the energy of one longitudinal optical (LO) phonon. The design also enables efficient electron transfer through extractor by the enhanced electron-LO phonon interactions.

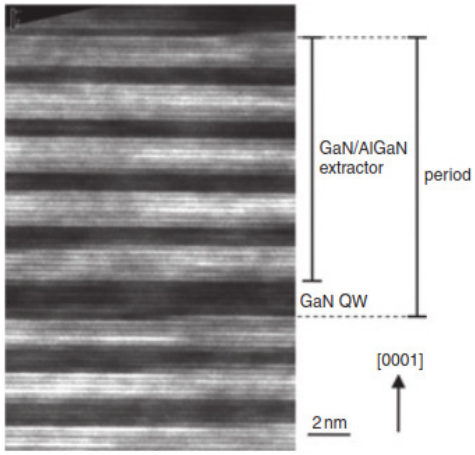

Fig. 6.3: TEM Image of hetero-structure dark, grey and bright regions which correspond to GaN, AlGaN and AlN respectively. Reproduced with permission from Ref. [120].

GaN based QCD was first demonstrated by Vardi et al. in 2008 [117]. An important feature of the GaN QCD is their intrinsic ultrafast response [118]. This intrinsic speed limit is determined by the carrier transmit time from one period to the subsequent one across the extractor stage. Vardi et al. in 2008 [118] also reported the operation of GaN QCD having –3 dB cut-off frequency of 11.4 GHz which was limited by extrinsic RC time constant. A significant improvement of GaN waveguide based QCD at 1.55 μm band was shown by Sark et al. [119] in terms of responsivity and bandwidth. It reached 9.5 ± 2 mA W^{-1} for 10 × 10 μm^2 devices at room temperature and 1.5 μm peak detection wavelength having BW_{-3dB} frequency response of about 40 GHz. In his experiment, the enhanced responsivity was achieved by illuminating the side facets of QCDs owing to good coupling between TM polarized waveguide propagating light and ISB transition. On the other hand, the bandwidth frequency was improved by reducing the contact layer resistivity and the top contact resistance. The device capacitance was improved by increasing the number of periods which was also advantageous for increased resistance at zero bias. In the experiment by Sark et al. [119], a sample was grown on 1 μm thick AlN layer on c-sapphire template by the process of plasma assisted molecular beam epitaxy. Here, the active region is formed of 40 periods of thick active GaN QW n-doped with Si. This is then followed by an extractor formed of 5 periods of thick $Al_{0.3}Ga_{0.7}N$ QW with an AlN thick barrier of 1.5 nm. To allow multimode propagation in the plane, the 40 period active region is sandwiched by two $Al_{0.3}Ga_{0.7}N$ contact layers with Si doping. A transmission electron microscopy image is shown in Fig. 6.3 which shows abrupt interfaces with good reproducibility of the layers [120].

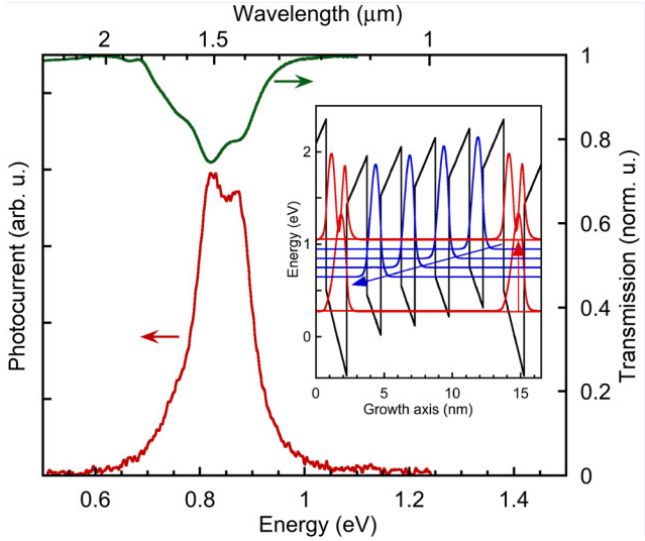

Fig. 6.4: Photocurrent spectrum of 700 × 700 μm^2 QCDs and transmission spectrum of the sample in multi-pass waveguide configuration with 450 polished facets at room temperature. Conduction band diagram and squared envelope functions of one QCD period. Reproduced with permission from Ref. [119].

The above Fig.6.4 shows the conduction band profile of one period of the device (using Schrodinger-Poisson solver) in the inset. From the polarization discontinuity between GaN, $Al_{0.3}Ga_{0.7}N$ and AlN, the band bending of the extractor originates. The band profile is engineered to provide fast electron relaxation from the upper state of active QW to the ground state of active QW in the following period [119]. By using the Fourier transform infrared (FTIR) spectrometer, the light transmission through the sample was measured in multi-pass configuration with 45^0 angle polished facets. The spectrum shows two peaks at 1.42 and 1.50 μm (Fig. 6.4) which are only available for TM polarized light. The photocurrent spectrum (measured on 700 × 700 μm^2 device) is also shown. Using a 1.55μm fibre laser diode, the estimated responsivity of the illuminated top surface of the sample was 25 ± 8 μA/W. From the experiment [119], it was further deduced that the performances of GaN/AlGaN QCDs were comparable to those of waveguide based InGaAs or Ge p-i-n photodiodes at telecommunication band and were also prospective for ultrafast QCDs at mid-infrared and THz spectrum.

6.2 GaN Optical Amplifier

GaN based devices with erbium doping have important applications in the telecommunication wavelength. There is a great demand for optical source. Particularly, integrating the optical

sources with the existing micro-electronics is growing mainly to fulfil the ever increasing bandwidth requirement for the devices used in telecommunication networks. Luckily, there is a coincidence of spontaneous emission of Er at 1535 nm with the low loss window in the absorption spectrum of optical fibre. This is the driving force behind the recent development of erbium doped materials especially in silica optical fibre and other semiconductors. In course of time, the development of erbium doped fibre amplifier (EDFA) exploited the transition of $^4I_{13/2} \rightarrow {}^4I_{15/2}$, for which it was possible to do transmission and amplification of optical signals in the band of 1530 to 1560 nm without the need for opto-electronic conversion [121]. It is also advantageous to have the optical signal gains at different wavelengths simultaneously which is suitable for WDM system using EDFA. In this way, the silica based EDFA is successful for its utilization in long haul telecommunication networks and this technology is improving further for the increasing demand of bandwidth [122]. Research activities are also going on to utilize erbium for the light emission from different semiconductors like Si, GaAs and importantly GaN. Here Si is the preferred semiconductor as the microelectronics industry is based on it and the integration of electronics with optics will definitely allow the realization of low cost ultra-high speed circuits. But the indirect band gap of Si has obstructed these kinds of integration. As such, the present opto-electronics technology relies on III-nitride based hetero-structures, the processing of which are complex and expensive.

GaN possesses a good number of properties making it suitable for visible and infrared emitting rare earth ions. A wide direct band-gap, thermal and chemical stability, high field transport properties, incorporation of rare earth ions with high concentrations are important to note. GaN is also insensitive to high presence of defect concentration which enables emission from materials having defect densities of similar band-gap materials. In fact, defect can play an important role in activation of rare-earth emission. Engineering of the defect centres can enable to produce tailored channel activation and emission bands. Fortunately, this is an advantage because of difficulty in producing defect-free GaN waveguides. In this section, an example of erbium doped waveguide amplifier operating in the telecommunication band is discussed. There is a strong requirement of compact and inexpensive erbium doped waveguide amplifier (EDWA) as it is an important component for the realization of local and wide area networks, 'fibre to the home' application platforms, where amplification of optical signals are required at different stages. The optical signal absorption is negligible in GaN based waveguides since the band-gap of this material is far from the signal wavelength. A report [123] mentioned first the MOCVD grown AlGaN/Er : GaN/AlGaN hetero-structure and their processing into strip waveguides as a potential EDWA. Their low optical loss properties were measured and optical enhancement at 1.5 μm under the LED excitation was demonstrated. These types of strip waveguides were fabricated using the technique of optical lithography and inductively coupling plasma dry etching as shown in the Fig. 6.5(a). The width of the waveguide is 5 μm with etch depth of 2 μm. The facets of the waveguide were made by polishing with diamond paste. The waveguide length was 3 mm. An atomic force microscopy (AFM) image of the array of fabricated waveguide is

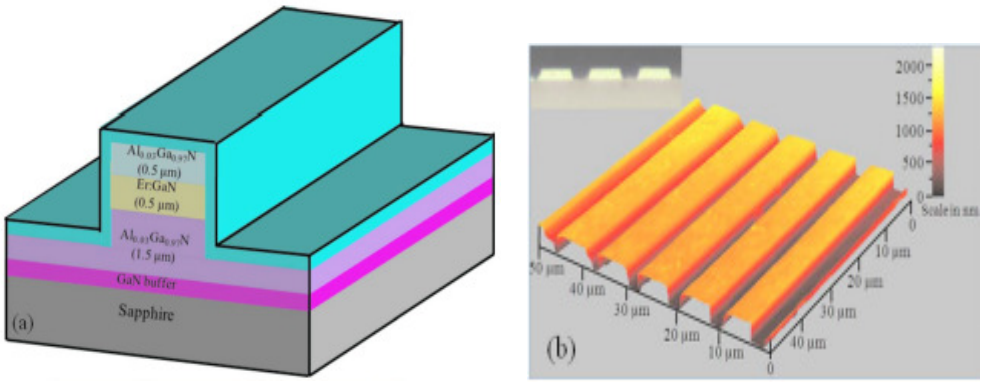

Fig. 6.5: (a) Schematic diagram of an Er-doped GaN Waveguide Amplifier (Here GaN:Er is used as optical gain medium with $Al_{0.03}Ga_{0.97}N$ as top and bottom cladding layers; (b) Atomic Force Microscopy Image of the devices. Reproduced with permission from Ref. [123].

shown as Fig. 6.5(b) where the polished waveguide facets (AFM image) are shown in the inset of the same figure.

To measure the optical loss in the waveguide, one side of the waveguide facet was illuminated by a 371 nm laser beam from the top to excite Er^{3+} ions and thereby generating light emission at 1.54 μm within the waveguide. Here the beam spot size was about 10 μm diameter. Subsequently, the 1.54 μm light was propagated through the waveguide and was collected at the other side of the waveguide using a tapered fibre coupled with a monochromator and a detector made of InGaAs. The following Fig. 6.6(a) shows the PL spectra measured at the other end of the waveguide at the room temperature. The inset shows the measurement setup. The PL spectra peaks at 1.54 μm as it corresponds to the transition of intra-4f Er^{3+} from level $^4I_{13/2}$ to the ground level of $^4I_{15/2}$. The PL emission intensity as a function of laser excitation spot distance d (collected at the other end of the waveguide) is plotted as shown in the Fig. 6.6 (b).

The emission intensity at the output facet of the waveguide can be formulated by the following expression:

$$I_t = I_0 e^{-\alpha t}. \tag{6.3}$$

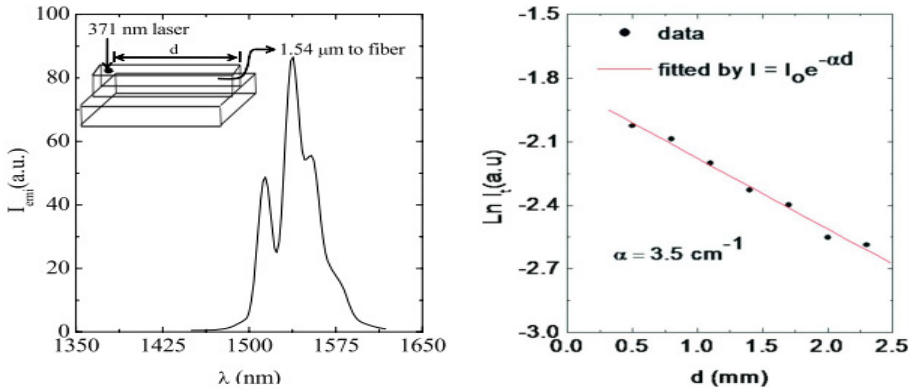

(a) (b)

Fig. 6.6: (a) Photoluminescence spectra of Er-doped GaN waveguide amplifier, (b) Plot of 1.54 μm peak intensity vs laser excitation spot distance d. Reproduced with permission from Ref. [123].

Here, I_0 is the PL intensity which is measured at the laser excitation spot, d denotes the optical path length, α denotes the optical loss of the waveguide. From the slope of the plot in Fig 6.6(b), it is possible to measure the optical loss of Er-doped GaN waveguide at 1.54μm and it is close to 3.5 cm^{-1}. This kind of optical loss is mainly due to light scattering by the sidewalls of the waveguides. The loss can be reduced by techniques like wavelength selective coating, wet etching after plasma etching etc. However, this optical loss is less than the measured loss of 4.45 cm^{-1} taken earlier [98] from an un-doped GaN waveguide. It is expected to see small value of optical losses in the Er-doped GaN waveguides since 1.54 μm is far from the GaN band gap which is 362nm. The low optical loss at 1.54 μm wavelength demonstrates the proof of Er doped GaN waveguide amplifier in the telecommunication networks. For further understanding the amplification process, the waveguides were tested by noting the relative changes in transmission signal intensity through them at telecommunication band. A 365 nm GaN LED was used as the optical excitation from the top. A signal at 1.54 μm wavelength was coupled at the input of the waveguide using a tapered fibre with focussing lens at the tip. In the same way, the transmitted signal is received at an InGaAs detector at the other side of the waveguide through the uses of tapered fibre and collecting lens at the tip. The following Fig. 6.7(a) shows the transmitted signal spectra at different LED excitation of 365 nm. Figure 6.7(b) shows the measurement setup.

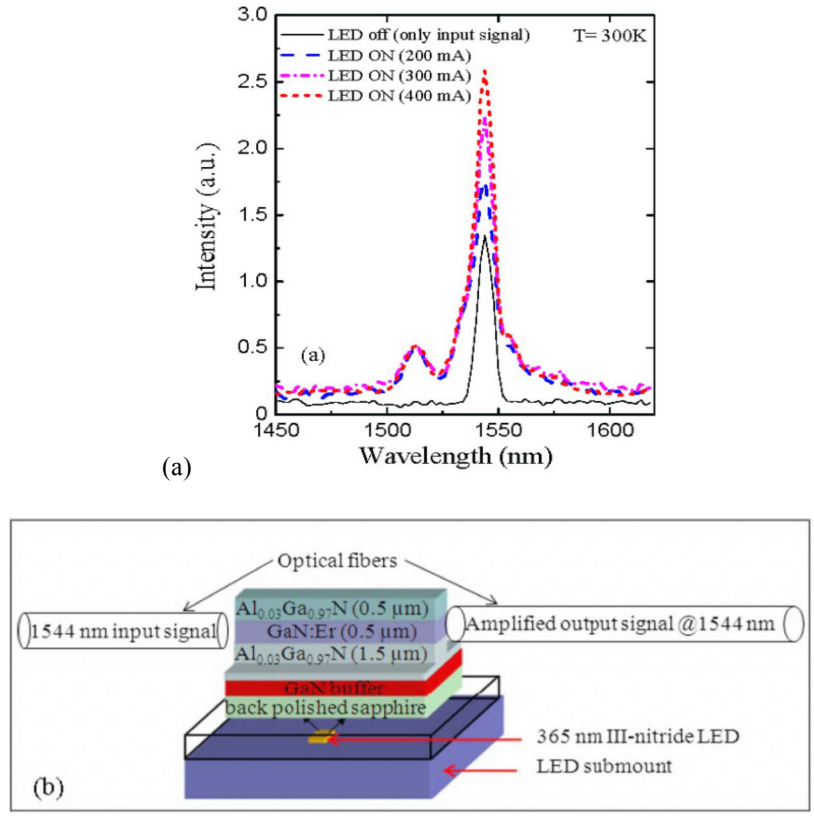

Fig. 6.7: (a) Spectra of the transmitted 1.54 µm signal emerged from the Er-doped GaN waveguide, (b) Schematic of the optical amplification property measurement setup. Reproduced with permission from Ref. [123].

This clearly proves that the GaN based waveguide amplification process, where we could see the increases in the relative signal intensity at 1.54 µm with increasing excitation from a 365 nm LED. The relative signal enhancement was measured to be 8 dB/ cm for a 3 mm long GaN waveguide which was excited by a 365 nm LED at 400 mA [123].

It is possible to realise planer waveguide amplifiers and emitters in the communication band of 1530-1550 nm by the process of monolithic integration of Er-doped InGaN GaN/ epilayers with nitride LED and Laser diodes as we have seen in the above experiments. These waveguide amplifiers are expected to have better performance than Er-doped silica glasses or InP in terms of linear gain, low noise and temperature stability [124, 125].

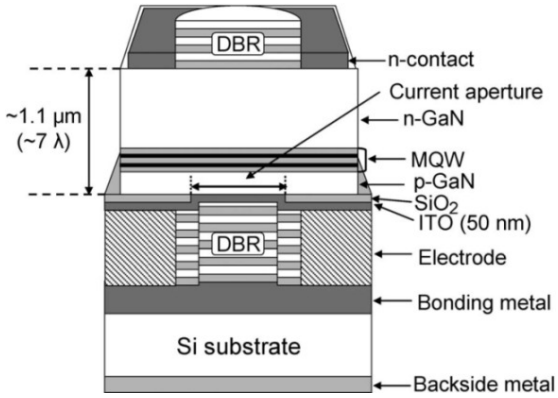

Fig. 6.8: Schematic cross-sectional diagram of a GaN-based VCSEL with vertical current injection feature. Reproduced with permission from Ref. [129].

6.3 GaN VCSEL

The term vertical cavity surface emitting laser, stands for a lasing structure where the surfaces of epitaxial layers form the vertical cavity and the light output is taken from one of the surfaces mirror [126]. The Gb/sec LANs are utilizing VCSEL based optical transmission system since 1999 [126]. Current-injected GaN based continuous wave VCSEL was first demonstrated in 2008. For strain relaxation, an n-side DBR having superlattice interlayers and p-side Ta_2O_5 / SiO_2 DBR at a low temperature of 77K were utilized [127]. An AlGaN electron stopper layer was missing in this hybrid concept which was added later with an additional thinner indium-tin-oxide layer for current injection. The maximum power of this kind of GaN VCSEL was about 37 μW at the wavelength of 412 nm [128]. The room temperature continuous wave GaN VCSEL was developed by another group, Higuchi et al. utilizing dielectric Nb_2O_5 / SiO_2 DBR at both the sides of the cavity [129]. The schematic diagram with cross-section of this kind of GaN-based current injected VCSEL is shown in Fig. 6.8.

An n-type GaN, a MQW of 2 pair InGaN /GaN and a p-type GaN were grown epitaxialy on c-plane sapphire by the process of MOCVD. The detailed fabrication process of the sample is depicted in ref [129]. The sample was later mounted on a Si substrate which was highly conductive and using the laser lift-off, the sapphire substrate was removed. From the current vs light output and voltage characteristics as shown in the Fig. 6.9(a), threshold current of 7.0 mA and threshold voltage of 4.3 V were obtained. The threshold current density estimated was ~13.9 kA/cm^2. Figure 6.9(b) shows the spectral emission at different current injections. It is seen that by increasing the driving current, the peak intensity increases and the spectrum width also become narrower.

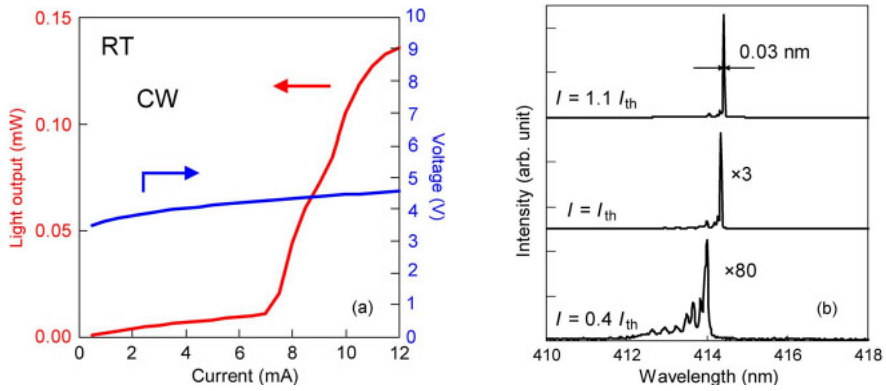

(a) (b)

Fig. 6.9: (a) Current vs light output and voltage characteristics of GaN-based VCSEL. (b) Spectral emission at different current injections. Reproduced with permission from Ref. [129].

GaN based VCSELs are expected to have some advantages over their edge-emitting devices such as single longitudinal mode operation, beam of circular and low-divergence, high modulation speed, wafer level testing, low manufacturing cost, low threshold, longer lifetime, high density two dimensional arrays [130]. But GaN based VCSEL still face some challenges compared to edge-emitting lasers. One is the poor quality of AlGaN / GaN DBR for lattice mismatch in between AlN and GaN [130]. For edge-emitting laser, the output facet reflectivity due to change of refractive index at the cleaved semiconductor-air interface is typically 30%, whereas, for VCSEL, reflectivity requirement is more than 99% where Bragg mirrors with alternate refractive index characteristics are used. VCSELs are becoming popular day by day for the applications of data communication and optical interconnects. The integrated (monolithic) platform requires single run epitaxial growth which is easier to fabricate. The high mirror reflectivity and minor active volume ensured the very low threshold in VCSELs (few microamperes) [131]. The outcome is reduced device heating and decreased power consumption. Due to small size and surface emission, it is possible to fabricate two dimensional dense arrays of VCSEL for multi-channel modules of parallel transmission [132]. It is also possible to monolithically integrate them with other optoelectronic devices such as photodetectors since they are not required to be cleaved [133]. Moreover, light is emitted from VCSEL in a circular beam shape with low divergence which suits very good coupling with optical fibres allowing relaxed alignment tolerances and thereby reducing the installation cost. The wavelength of VCSEL can also be tuned by varying the cavity length mechanically.

The vast growth of internet data transmission is pushing bandwidth requirement for the fibre networks especially in the metro area network (MAN) and local area network (LAN) to a high

pace. Low cost, single mode, long wavelength VCSEL which can be directly modulated and easily coupled to fibre with easy packaging characteristics are essential to materialize this goal. However, for 850 nm GaAs based VCSEL at 100 Mbps (presently available), the transmission distance is 7 to 8 km. At 10 Gbps, the transmission distance is only 50m which is not suitable even within the building LANs. So far, InGaAsP /InP DFB lasers have been the source for long haul 1.5 μm optical backbone networks. But their cost is extremely high to meet the tens of thousands of laser requirements for MAN or LAN networks. GaInNAs is a good option for long wavelength emission. Here, the combination of N and In produce dramatic decrease in bandgap to reach the long wavelength of 1.3μm or 1.5 μm [134]. However, using GaN based VCSEL, to reach the long telecommunication band has not been materialized as yet.

7 Hybrid Integrated Platform Towards Photonic Chips for Broadband Communication

7.1 Use of Ga and Its Alloys for Lasing on Si

In major initiative towards the development of Integrated Photonics the conventional waveguides are fabricated on Si, this technology approach is known as Si on insulator (SOI) [135]. Si is having advantages over the other semiconductors mainly due to the following reasons: (1) extensive availability and easy to process it in purified condition, (2) mechanical and thermal stability, (3) existence of state-of-the-art chip processing facilities. Thanks to the gradual miniaturization of Si integrated circuits known as CMOS technology, in the last few decades, has been possible to improve the performance of computers at reduced cost. But this gradual miniaturization has led to some undesirable side effects for CMOS chips as the clock pulse width has also been gradually decreasing. The electrical cross-talk forced introduced relative "increases" of the total length of electrical connections per unit chip area in complex IC structures, RC delay due to increased metal line densities are some of the known drawbacks [136]. To overcome these difficulties, there is a global effort to find novel solutions for the development of improved CMOS fabrication techniques and photonic chip designs. At the same time, the means of communication via optical fibre has improved significantly. This has led to thoughts of utilizing the photonics 'into' semiconductor devices/chips for improving the speed of the signal processing. The key enabler is to have a 'chip level' lasing capability (i.e., the light source). At present, the lasing at the 'chip level' is provided by lasers formed of III-V semiconductors – a hybrid non-CMOS compatible solution, also more expensive compared to Si based devices. Moreover, the needed optical chip level alignment between III-V laser(s) and Si based waveguides are cumbersome, expensive and also could be time-consuming. On the other hand, having an efficient light source integrated on Si chip will be ideal for supporting a chip-to-chip or within-the-chip communication.

But it is a great challenge to have integrated lasers on Si substrates. Si is an indirect band gap material for which emitting light is difficult to materialize. Free electrons tend to recombine with holes emitting phonons (heat) instead of light [137]. Moreover free carrier absorption hinders the population inversion which is a must for having stimulated light emission and gain. At the same time, the Auger recombination retards the density of emitted photon as shown in Fig. 7.1 [136].

Scientists have been trying to improve the weak photo-luminance of Si by using approaches such as Si nano-crystals [138] or using rare earth materials with Si [139] since 1990. But intense luminance is yet to be materialised. A demonstration of lasing on Si has been achieved using Raman amplification in 2004 [140] however this approach requires another optical pump source for Raman amplification and as such *practically* does not solve the described lasing needs in connection with Si waveguides. Alternatively, there is an option of fabricating individual lasers on a Si die and then ensure an appropriate alignment. But this has some drawbacks, such as, increased assembly time for attaching more number of lasers for more channels. Some approaches of attached III-V based laser sources on a Si photonic chip are schematically shown in Ref. [141].

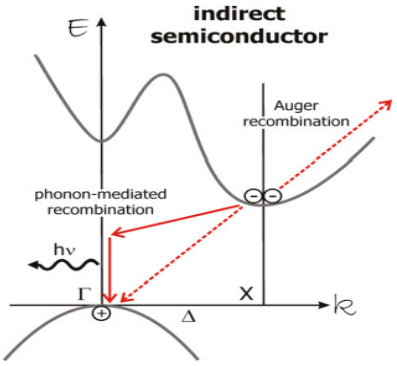

Fig. 7.1: Indirect band-gap structure of Si. Reproduced with permission from Ref. [136].

The Off-chip and On-chip methods are the most straight forward approaches for injecting fibre-coupled laser light into a Si photonic waveguide. One advantage of choosing the Off-chip method is its flexibility. The second advantage is a better thermal management of the photonic devices since the laser is separated from the chip. However, among disadvantages are the high cost of the laser and a large size of non-integrated packaging. A better approach seems the On-chip method where low cost lasers can be attached with the Si chips using mechanical stops and metal patterning with alignment of lasers. Still this approach has increased assembly time [141].

7.1.1 Hybrid Lasers

A fundamentally different approach is using so called hybrid lasers. Here a wafer bonding process is used. An unprocessed wafer made of Ga and its alloys (III-V materials) is bonded to Si wafer which is patterned with optical waveguides. By way of planar fabrication process, multiple lasers can be fabricated all at the same time across the wafer. One important advantage of this technique is that it does not need a laser alignment with the Si waveguides since they are patterned before the laser fabrication. Here, the lasing is guided by the Si waveguides but the electrical pumping and emission of light take place in the quantum wells (AlGaInAs) of the III-V materials [141]. The optical gain can be varied by the adjustment of the height and width of the Si waveguides. The bonding process is done at low temperature (about 300 °C) which allows the different thermal expansion coefficients of the two material types to 'settle', thereby avoid any kind of stress in the bonding outcome. In fact, the key to this bonding technique is using the thin oxide glue that is used for bonding these two materials together. Such a laser device was proposed in [141]. With 65 mA of driving current at room temperature, continuous wave (cw) having about 1.8 mW of output power and 12.7% quantum efficiency was experimentally observed.

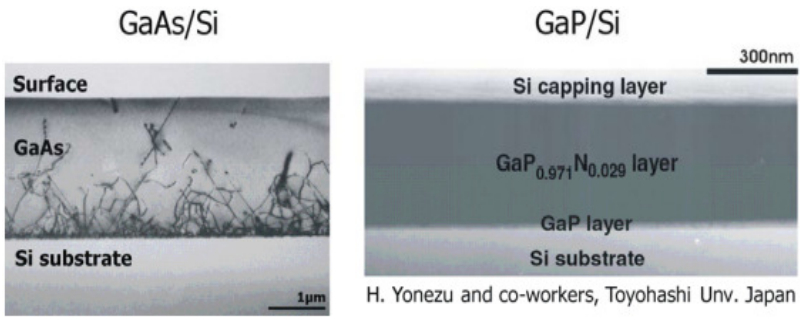

Fig. 7.2: Transmission Electron Microscopy (TEM) images of lattice mismatch due to dislocations formed in the GaAs layer grown on Si (Left), Contrarily GaP/GaNP layers can be formed on Si without any threading dislocations. Reproduced with permission from Ref. [142].

However, these kinds of hybrid devices have some disadvantages such as, device's reliability and issues related to fabrication. Required different fabrication steps for Si chips and III-V lasers, including the alignment issues are not only expensive but also consume a lot of time. Moreover there is an upper limit on the integration density of lasers per a Si chip [143]. A new concept called monolithic integration [143] shows very good promise in solving the above problems.

7.1.2 Monolithic Optoelectronics Integrated Circuits (OEIC) on Si

There is a strong interest in growing monolithic integrated circuits on Si substrates but as we have already shown, it is quite difficult to achieve lasing 'in' Si due to its indirect band gap characteristics. Therefore direct band-gap III-V materials such as GaAs and InP are studied intensively. But high dislocations between these III-V materials and Si due to large lattice mismatch are observed in the epitaxial films of III-V materials as seen in the Fig. 7.2.

The reason behind these dislocations can be understood if we study the energy bandgap vs lattice constant of III-V materials and Si (see Fig. 7.3 [136]).

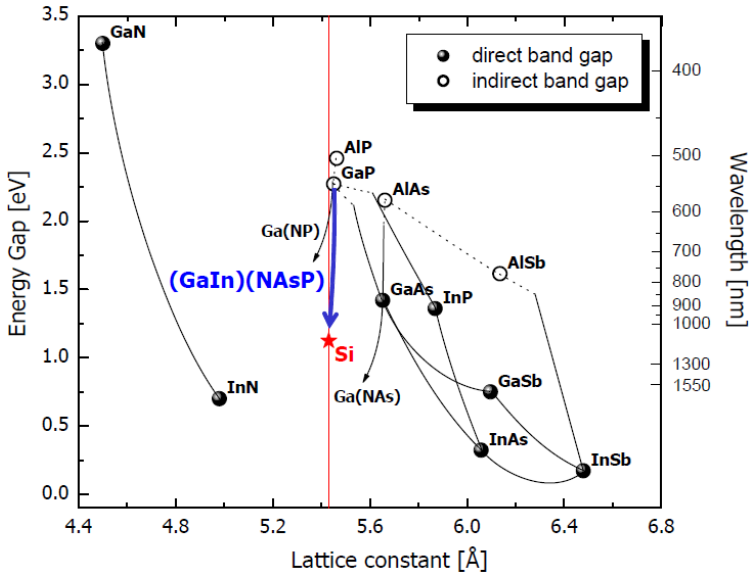

Fig. 7.3: Plot for the energy gap vs lattice constant of common III-V materials compared to Si. Reproduced with permission from Ref. [136].

We can see that GaAs and InP have lattice constants which are larger than Si by 4%. The question is how to suppress the formation of dislocations by optimising the epitaxial growth conditions in III-V layers. It can be also seen from the same plot that GaP (indirect band gap material) has a lattice constant very close to that of Si. At the same time, the Ga(NP) which is ternary material system can be grown on Si with lattice matching with the N content of only 2%. This was demonstrated by Yonezu, et al. [142]. Base on this, one can grow the lattice matched direct band-gap materials on GaP then transfer them on Si substrates. This approach was undertaken as a new concept by the Material Science Centre of Philipps University Marburg in Germany. Adding In, As and N helped to modify the band structure and transform it into a direct band-gap material. Here we note that the direct band-gap characteristics are important for optical gain and lasing action [136]. The combination of N with In and As helped with the important adjustment required for the compound material (GaIn)(NAsP) to be in line with the GaP lattice constant as seen in the Fig.7.3. The important task was to find the right composition of (GaIn)(NAsP) which supports the pseudomorphic growth of good quality films on GaP substrate showing direct band-gap structure and luminescence efficiency. Finally, Arsenic (As) rich nitride material Ga(NAsP) was introduced which can perform the above characteristics as reported in [136]. The transmission electron microscopy (TEM) of Ga(NAsP) quantum wells grown on GaP substrate show the absence of any dislocations (seen in Fig. 7.4) [136].

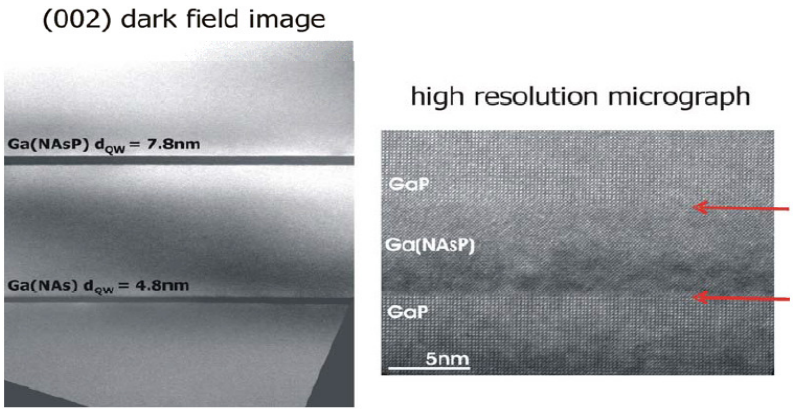

Fig. 7.4: Transmission electron microscopy (TEM) images of Ga(NAsP) quantum wells grown on GaP substrate. Reproduced with permission from Ref. [136].

This compound material shows direct electronics band structure for As rich composition. The thin multiple quantum well structure of Ga(NAsP) works as an excellent light emitter. Utilizing this material, a demonstration of electrically injected lasing action in a device at low temperature was shown by B. Kunert and et al. [144]. A forecast was also made on the development of such lasing materials on Si microelectronics since Ga(NAsP) deposited on GaP can be transferred via deposition on Si because of similarity of lattice constants in between them [142, 145].

7.2 Use of Hybrid Waveguides for Photonic Integrated Chips

Optical interconnect system requiring chip level integration of electronics and optics are very promising to meet the ever growing bandwidth requirement in the telecommunication network devices. In the conventional optical domain, different devices perform the specialized purposes such as, III-N based devices like InP or GaN are good for lasing, $LiNbO_3$ based devices are good for electro-optic modulators and Si based devices are good for waveguide devices. But the problem of developing integrated optics is that all the above mentioned differently functioning devices are not compatible to each other. Not one common substrate material is optimum to function for all of the above mentioned devices with their respective best performances. Hence, a compromise must be there for the fabrication of integrated optics to fulfil the goal of realizing ultrafast all-optical signal processing as it is done in the present day electronics chips. The salient components of an integrated optical system may be shown as follows [146]. All of these components need to be fabricated on the same chip. The optical modulator has two inputs – one, on-chip or off-chip source of laser and the other is electrical input from a CMOS driver as in Fig. 7.5. Here the optical couplers are used to inject light into the optical device components.

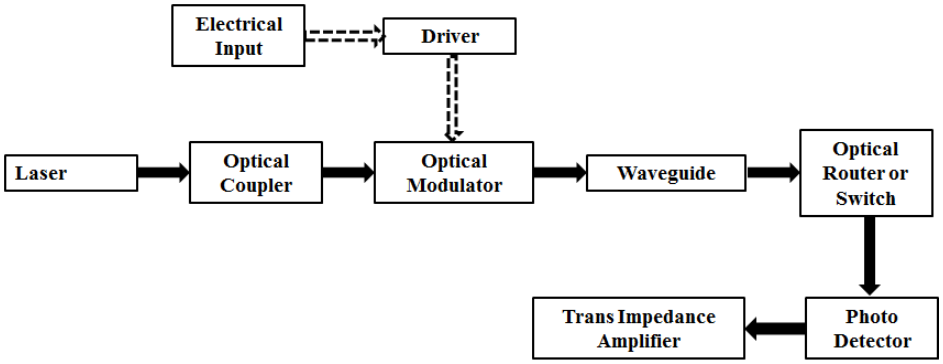

Fig. 7.5: Different components in an integrated photonic chip (dashed arrows indicate electrical signals and solid arrows indicate optical signals).

Modulators convert the electrical signals into the optical domains. Optical information signals are then fed into the optical routers or switches using the waveguides. These optical switches route the optical signals to different directions according to needs. At the receiver side of the system, a photo-detector is used to detect light and convert optical pulses into photo currents. An amplifier is used to amplify the photo-current and make the digital signals in the form of electrical signal domains. However, the route for making the integrated optical chips is either to make all the component devices using the same material such as GaN or using different specialized device components like lithium niobate modulators, gallium nitride or Indium Phosphate lasers to be monolithically integrated using the same substrates. Earlier write-ups show that it is possible to make GaN based lasers, modulators and couplers. But to exploit the best performances of the respective highly efficient devices, the second option of monolithic integration is preferable.

To achieve low cost and compatibility with mature microelectronics manufacturing technology, using Si as fundamental building material for the development of integrated optics was initiated since 1980 [147]. But Si based photonics has different kinds of drawbacks like poor emission of light, low electro-optics effect and propagation loss in the waveguides in the telecommunication bands. Extensive research initiatives have been made during the last few decades to overcome these limitations [148, 149, 150]. In the table below, the material properties of semiconductors are mentioned in Table 7.1 [151]. Light guiding through the GaN core requires cladding layers with refractive indices lower than that of GaN. For Si based waveguides, SiO_2 as cladding layer proved to be a great success. It was possible to fabricate Gallium Nitride on Insulator (SiO_2 as cladding layer) waveguides as depicted in section 3.1. There, a bonding process was described to realize GaN thin film at the top of SiO_2 on Si substrate [47].

Table 7.1: Material properties of Si, GaAs, GaN and InP.

Properties	Si	GaAs	GaN	InP
Crystal Symmetry	Diamond	Zinc Blende	Wurzite	Zinc Blende
Lattice constant (Å)	5.43	5.65 (4%)	3.19(a) /5.189(c)	5.87 (7%)
Thermal Exp. Coeff. ($10^{-6}K^{-1}$)	2.6	5.7	5.59(a) /3.17(c)	4.60
Thermal Conduct. ($W.cm^{-1}.K^{-1}$)	1.3	0.55	1.3	0.68
Youngs modulus (GPa)	130	85.9	181	61.1

(Data from 'semiconductors on NSM' via http://www.ioffe.rssi.ru/SVA/NSM/Semicond/)

7.2.1 Lithium Niobate Waveguide Devices as LNOI

For most applications, the performances of nonlinear devices operating on third order nonlinear susceptibility $\chi^{(3)}$ cannot compete in principle with the performances of devices based on second order susceptibility $\chi^{(2)}$ [152]. Due to non-centrosymmetric crystal configuration of Si, it does not have the $\chi^{(2)}$ susceptibility. Hence, a hybrid platform which has the CMOS compatibility with low loss and strong light confined waveguide and uses $\chi^{(2)}$ nonlinearity as the core of the waveguide is preferred instead of Si. In this case, $LiNbO_3$ with strong second order nonlinearity is one of the best options. As a crystal, it possesses large electro-optic coefficient (r_{33} equal to 31 pm/V and r_{13} equal to 8 pm/V), wide wavelength window from 0.4 to 5 μm and large bandwidth. The second order nonlinearity helps to control the refractive index changes in the medium through the electro-optic (EO) effect. Using this kind of nonlinearity, it is also possible to mix optical signals at different wavelengths for the requirement of parametric amplification, generation of second harmonics, and conversion of wavelengths [153]. In the present industrial context, $LiNbO_3$ waveguide based modulators are chosen as the best option for its modulation bandwidths of 100 GHz [154]. This extremely high modulation is possible mainly due to its capability of producing pure phase modulation without any significant changes in the optical absorption and thereby, the vector signal modulation can be attained in advance telecommunication fields and applications with negligible chirps [155]. Application of $LiNbO_3$ as a platform of integrated optics depends on the ultra-compact optical circuits using the material. But $LiNbO_3$ waveguides are bulk in size and unable to bend sharply. $LiNbO_3$ modulators are normally 4 to 5 cm long and 10 μm wide. To achieve nonlinear applications with efficiency, the devices must be short in length due to pump sources of low intensity in the large cross-section of the waveguides. For these reasons, $LiNbO_3$ is not so prominent for integrated optics compared to other options [156]. However, a novel method of realizing compact size $LiNbO_3$ devices on Si substrates was demonstrated in the reference of [156]. The platform may be seen schematically as in Fig. 7.6. The structure consists of a thin layer of $LiNbO_3$ as core, SiO_2

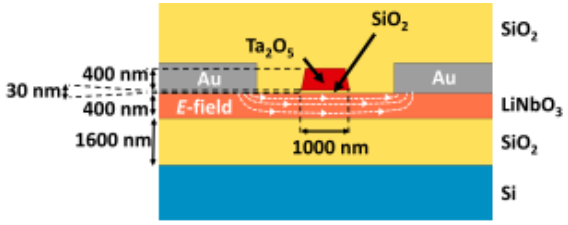

Fig. 7.6: Cross-section of a $LiNbO_3$ on Si waveguide. Reproduced with permission from Ref. [156].

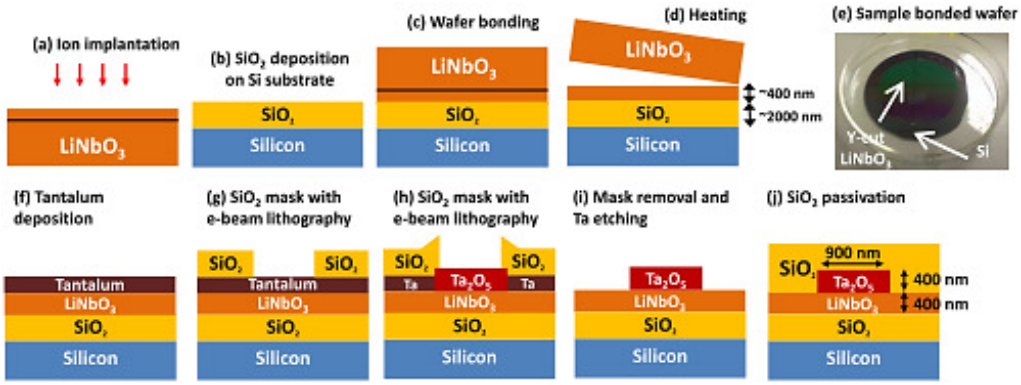

Fig. 7.7: (a) to (d) Processing steps for the fabrication of $LiNbO_3$-on-Si wafers; (e) A successful bonding of a 3" $LiNbO_3$ wafer bonded to a 4" Si wafer; (f) to (j) SORAM process of submicron $LiNbO_3$ ridge waveguide on Si. Reproduced with permission from Ref. [156].

as lower cladding and Ta_2O_5 as rib region on top of $LiNbO_3$ layer. It is to be mentioned here that the refractive index of Ta_2O_5 is close to that of $LiNbO_3$. Thereby, the difficulty of etching $LiNbO_3$ directly can be avoided for the formation of ridge waveguide. Moreover, the platform helps in producing the high index contrast waveguides having low bending loss with submicron layers of $LiNbO_3$ and Ta_2O_5 on Si substrates. Here $LiNbO_3$ acts as active region.

In demonstrating the fabrication process of this type of waveguide [156], first a $LiNbO_3$ wafer is ion implanted to high doses of H_e^+ ions. Then a Si wafer is coated with a buffer layer of 2 µm thick SiO_2. These two types of wafers are polished and attached together as in Fig. 7.7(c). After initial bonding at room temperature, a 200 ˚C heating process is provided for improved bonding. At the time of heating, the implanted ions create high pressure Helium (He) gas at the layer of implantation which forces the crystal slicing accurately. An image of 3" film bonded to 4" Si wafer can be seen in Fig. 7.7(e) with no traces of cracking. Next the ridge waveguides (Ta_2O_5 as ridge layer and $LiNbO_5$ as slab layer) are created using the 'Selective Oxidation of

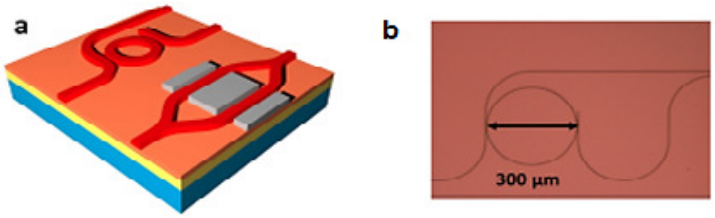

Fig. 7.8: (a) A schematic of microring resonator and Mach-Zehnder modulator, (b) A top view of a high magnifycation optical microscope image of a fabricated ring resonator with input and output bent bus waveguides. Reproduced with permission from Ref. [156].

Refractory Metals (SORAM)' method [156]. For passivation, the device is then covered with SiO_2.

To make Electro-Optic modulator, metal electrodes are added on this device following the usual fabrication method as in Fig. 7.6. This is the cross-section of the waveguide at one arm of the Mach-Zehnder modulator as in Fig. 7.8(a), with RF electric field in the active region of $LiNbO_3$. Mentionable here, the importance of submicron and tightly confined waveguide is the advantages of placing electrodes much close to the waveguide without significant optical absorption by the electrodes. This is helpful in applying much lower voltages to obtain the same electric field for electro-optic modulation. The simulated results showed, that the gap can be as small as 4 µm without overlap in between the optical mode and the electrodes, which is smaller by a factor of 5 compared to the conventional $LiNbO_3$ modulators [156]. Figure 7.9(a) shows that, the Q of the ring resonator is 4.5×10^4 which is higher than the previously obtained results [157]. The linear propagation loss is more or less equal to 5dB/cm. On the other hand, the Mach-Zehnder modulator was tested using a saw-tooth modulation voltage (at 1 kHz) through the electrodes having a gap of 7 µm (Fig. 7.9(b)). V_π was 6.6 V corresponding to a half-wave voltage-length of 4 V-cm for 6 mm long electrodes which is lower than $V_\pi.L$ of diffusion based modulators [158]. The extinction ratio for the modulator is 20 dB. The above discussion makes the way for the possibility of a noble integrated photonic platform based on thin film $LiNbO_3$ on Si substrate, at room temperature.

7.2.2 Lithium Niobate Microrings Using Gallium Nitride Waveguides

Microring resonators are considered to be one of the most important elements in the integrated optical chips. The materials considered for micro-ring resonators need to have the ability to change their resonance spectrum upon some external effects such as thermal effect, electric field or carrier injection. Non-centrosymmetric materials are best suited as materials for the microring resonators as they have high nonlinear and electro-optic properties which are advantageous for ultrafast electrical tuning of the spectral response. The following Table 7.2 shows a list of non-centrosymmetric materials which are related to electro-optically tuneable micro-ring resonators.

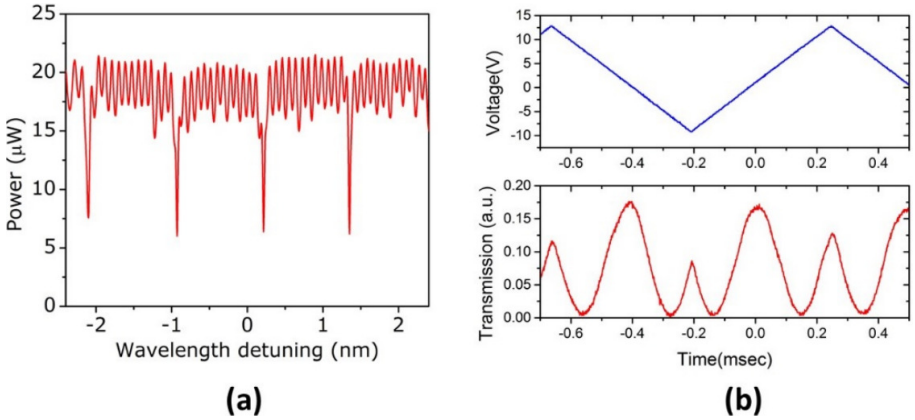

Fig. 7.9: (a) Transmission spectrum of a microresonator (300 μm dia) for TE mode at telecom band. The resonance linewidth is 2.7 GHz; (b) Sawtooth electrical signal applied and the measured modulation response of the Mach-Zehnder modulator. Reproduced with permission from Ref. [156].

From the table, it is seen that, the electro-optic coefficients and figure of merits (required for electro-optic switching) for GaN/ AlN are low. Compared to that, $LiNbO_3$ shows larger nonlinear optical coefficient and electro-optic constants and is stable and possess large transparency from the infrared to ultraviolet regions. It is also suitable for VLSI optics as it can be fabricated on Si substrates.

But GaN is important for its many utilities – such as lasing, amplification, photo-detection, coupling etc. Interestingly, the refractive index of GaN (2.28 at 1.55 μm) is very close to that of $LiNbO_3$ (2.21) which allow almost symmetrical coupling between these two devices. Ring and port/ bus waveguide sometimes serve different roles, hence it is desirable to fashion them differently [159]. Moreover, GaN shows low absorption in the wavelengths in the visible and near infra-red region. Considering this, an approach for building hybrid integrated optics using GaN waveguide as port waveguide which is laterally or vertically coupled to a $LiNbO_3$ micro-

Table 7.2: Materials for electro-optic microresonators [160]

Material	Wavelength [nm]	Dielectric constant ϵ_j	Refractive index n_i	Electro-optic coefficient r_{ij} [pm/V]	Figure of merit $r_{ij}n_i^2/\epsilon_j$ [pm/V]
$LiNbO_3$	633	28	2.2	31	5.4
GaAs	1020	13	3.5	1.2	1.1
GaN	633	11	2.35	1.9	1.0
AlN	633	10	2.0	1.0	0.4

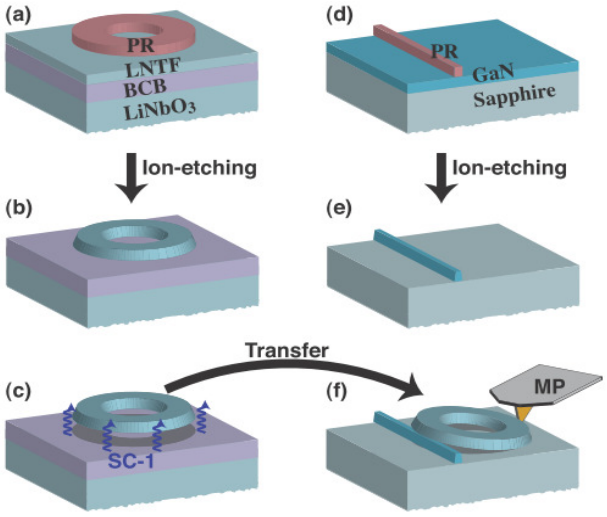

Fig. 7.10: The fabrication process of realizing the hybrid microring resonator. Reproduced with permission from Ref. [160].

ring resonator was demonstrated [160, 161]. A noble technique of fabricating a free standing microring from $LiNbO_3$ thin film was depicted first. This microring was later vertically coupled to a GaN port waveguide. The principal steps of fabricating hybrid microring resonator are depicted in Fig. 7.10.

In the first step, samples of ion-sliced $LiNbO_3$ (z-cut) thin films were prepared which were obtained by bonding the thin film on $LiNbO_3$ substrate using a low refractive adhesive type polymer like benzocyclobutene (BCB) as an intermediate layer. The thickness of $LiNbO_3$ has been reduced to 600 nm by Ar^+ ion-etching mainly to reduce the scattering losses in the waveguides by reducing the surface roughness from 10 nm to 4 nm rms. Using undiluted AZ 5214E photoresist, the substrates were spin-coated with a thickness of 1.5 µm which was baked softly for 50 seconds at a temperature of 110 ^oC. The photoresist was then exposed by a laser lithography system which used acousto-optic laser beam deflection for the precise patterning of the microring with a diameter of less than 200 µm. The developed structured photoresist mask was then transferred into $LiNbO_3$ film by the process of Ar^+ ion-etching down to below the BCB layer. A net etch rate of 1.8 nm/min was selected for $LiNbO_3$ films. The samples were then put into a standard clean-1 solution at 100 ^oC after removing the remaining photoresists from them. At this point, the adhesion between the microring and the BCB is reduced due to oxidation and as a result, the $LiNbO_3$ microring is detached from the substrate. The microring remaining on the donor substrate is easily moveable and ready to be transferred to any arbitrary substrate by using a thin wire. However, the positioning of the microring on the host substrates is materialized by

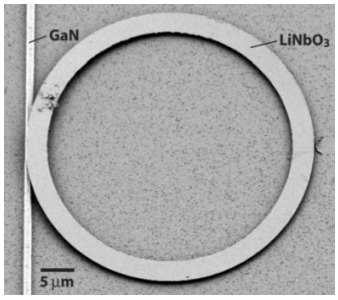

Fig. 7.11: SEM picture of a GaN microring positioned vertically on GaN waveguide. Reproduced with permission from Ref. [161].

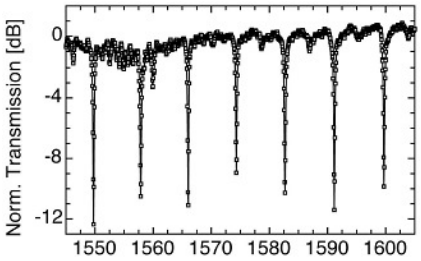

Fig. 7.12: Measured transmission spectrum through the GaN port waveguide of the microring resonator. The resonances are separated by a FSR of 8.1 nm at 1.55 µm wavelength. Reproduced with permission from Ref. [161].

using micropositioning tools. The host substrate was chosen as a c-plane sapphire wafer having 600 mm thick GaN film grown on AlN layer. GaN waveguide was chosen due to its refractive index similarity with that of $LiNbO_3$ and these properties were helpful in symmetric coupling between the two devices. For the development of GaN port waveguides, the same procedure as mentioned above was followed. Here the etch rate of 8 nm/min was followed for GaN film.

Figure 7.11 shows such a SEM picture of a microring resonator consisting of $LiNbO_3$ microring (600 nm thick, 3 µm wide and 20 µm radius) and a GaN coupling waveguide (600 nm thick and 1.1 µm wide). Using a commercially available mode solver program, the width of the GaN waveguide was adjusted so that the effective refractive indices of GaN become close to that of $LiNbO_3$ microring in TE mode. For small amount of adhesive forces, the $LiNbO_3$ microring which was laid vertically on the GaN waveguide was stable in the experiment, but for better stability, thin SiO_2 cladding layer could be used for a preset position of the microring. To do the characterization of this kind of hybrid microring resonator, an infrared laser (single longitudinal and transversal mode) tuneable from 1530 nm to 1610 nm was used. The laser was end-fire coupled with the GaN waveguide using a microscope objective having the magnification of 100. The spectrum measured is shown in the Fig. 7.12.

This shows resonance dips separated by a free spectral range (FSR) of 1 THz which corresponds to 8.1 nm at the wavelength of 1.55 μm. The above experiment, shows that the combination of ferroelectric microring like $LiNbO_3$ with any arbitrary material such as that of GaN is feasible, which leads to the development of hybrid integrated optics in future.

8 Concluding Remarks and Future Directions

Exploiting optical nonlinearity has been important for the development of all-optical ultrafast devices in optical broadband communication to perform all-optical wavelength conversion, switching, routing and other functionalities in order to enhance performance of optical networks. Optical waveguides have the advantage of achieving the amount of required nonlinearity at very short distances if compared to traditional optical fibre.

As has been shown, the GaN platform possesses all types of optical nonlinearity whereas, the second order nonlinearity is absent in Si. Also for the indirect bandgap properties of Si, it is not possible to achieve some of the desired functionalities allowing the development of all-optical photonic chips under the single platform. Here, carrier induced FCA, FCI, TPA effects are responsible for preventing ultrahigh speed operation in Si.

On other hand, GaN, also being CMOS compatible as Si, shows very good prospect for enabling all-optical ultrafast device operation. Additionally, very high conduction band offset, ultrafast relaxation time, and robustness of GaN platform could be advantageous for building future devices. Moreover TPA related absorption losses are absent because this platform is direct band-gap material.

A novel demonstrated waveguides made of GaN semiconductor material grown on sapphire are very promising. The refractive index contrast between the GaN and the sapphire is very high. This is advantageous in making small size and compact optical devices.

Various waveguide structures can be constructed using GaN as the core as high refractive index and $Al_xGa_{1-x}N$ as the cladding layer with lower refractive index. Here $Al_xGa_{1-x}N$ is made by engineering the band-gap energy of GaN and AlN alloys with different Al concentrations. In this way, direct bandgap GaN semiconductor material and its alloys are used for the development of lasers, photodetectors using the waveguides which are transparent for the spectrum of communication wavelength (1.5 μm). We have seen that the refractive indices of GaN materials and their alloys can support the design and fabrication of the above desired devices.

We have illustrated that fabrication of GaN on Si waveguides, GaN crystal waveguides, GaN nanowires, GaN electro-optic and electro-absorption modulators could be the building blocks for ultrafast communication devices as well as GaN photodetectors, GaN VCSELs, GaN amplifiers, GaN AWGs. All the above suggest that there is a strong possibility leading to integrated photonic chips made of GaN materials as the unique solution for all-optical signal processing. This would ensure the performance enhancement of the existing routers and switches for future ultrafast broadband networks.

As for the final remark, the current lack of Integrated Photonic Circuits is the consequence of the fact that until now there has not been a relevant common material platform available which would support all the desired functionalities in photonic devices (a direct contrast to CMOS-based microelectronics) [159]. However, it can be argued that the GaN platform holds this promise. Being also CMOS compatible, nearly all basic functionalities we are looking for could be realized by using this compound semiconductor material and at the end of the road we may have the photonic platform we have been all for so long looking for.

Acknowledgment:
This work was supported by the Royal Society under the International Exchanges Scheme 2012/R2.

References

[1] D. Barney. The Great Cloud Bottleneck: How Capacity Issues Can Kill Your Cloud Project. Redmondmag.com., Online Achieve, 2011. http://redmondmag.com/articles/2011/12/01/cloud-bottleneck-issues.aspx.

[2] A. Davidson, I. Glesk, and A. Buis. Has Silicon Reached Its Limit? *Advances in Electrical and Electronic Engineering*, 12(6):590 – 598, 2015.

[3] A. Liu, L. Liao, H. Rong, R. Jones, D. Samara-Rubio, D. Rubin, R. Cohen et al. Recent development in silicon photonics: 2.5 Gb/s silicon optical modulator and silicon Raman laser. In *Integrated Optoelectronic Devices 2005*, International Society for Optics and Photonics, pages 80 – 93, 2005.

[4] J. Leuthold, C. Koos, and W. Freude. Nonlinear silicon photonics. *Nature Photonics*, 4(8):535 – 544, 2010.

[5] J. P. Sokoloff, P. R. Prucnal, I. Glesk, and M. Kane. A Terahertz Optical Asymmetric Demultiplexer (TOAD). *IEEE Photonics Technology Letters,* 5(7):787 – 790, 1993.

[6] R. W. Boyd. *Nonlinear Optics*. 3rd edn /Academic Press, 2008.

[7] M. Foster, A. Turner, M. Lipson, and A. Gaeta. Nonlinear optics in photonic nanowires. *Optics Express*, 16(2):1300 – 1320, 2008.

[8] H. Hsieh, K. Feng, and M. Lee. Study of cross-phase modulation and free-carrier dispersion in silicon photonic wires for Mamyshev signal regenerators. *Optics Express*, 18(9):9613 – 9621, 2010.

[9] J. Phillips and J. Van Vechten. Nonlinear Optical Susceptibilities of Covalent Crystals. *Physical Review*, 183(3):709 – 711, 1969.

[10] B. Levine. Electrodynamical Bond-Charge Calculation of Nonlinear Optical Susceptibilities. *Physical Review Letters*, 22(15):787 – 790, 1969.

[11] J. A. Miragliott and D. K. Wickenden. Nonlinear Optical Properties of Gallium Nitride. *Semiconductors and Semimetals*, 57: 319 – 370, 1998.

[12] H Hora, Y. R. Shen. The Principles of Nonlinear Optics. *Laser and Particle Beams* 4(2):318-319, 1986.

[13] V. A. Yariv. *Quantum Electronics*. John Wiley and Sons, New York-London-Toronto, 1975.

[14] R. W. Boyd. *Nonlinear Optics*. New York: Academic Press, 1992.

[15] M. D. Levenson and S. S. Kano. *Introduction Nonlinear Laser Spectroscopy*. New York: Academic Press, 1988.

[16] Y. R. Shen. Recent advances in nonlinear optics. *Reviews of Modern Physics*, 48(1): 1 – 32, 1976.

[17] I. Glesk, C. W. Bing, X. Lei, B. Varghese, and P. R. Prucnal. Ultra-fast all-optical switching in optical networks. *Progress in Optics*, 45:53 – 118, 2003.

[18] R. J. Manning, I. D. Phillips, A. D. Ellis, A. E. Kelly, A. J. Poustie, and K. J. Blow. 10 Gbit/s all-optical regenerative memory using single SOA-based logic gate. *Electronics Letters*, 35(2):158 – 159, 1999.

[19] I. Glesk, J. P. Sokoloff, and P. R. Prucnal. Demonstration of All-Optical Demultiplexing of TDM Data at 250 Gb/s. *Electronics Letters*, 30(4):339 – 341, 1994.

[20] I. Glesk, J. P. Sokoloff, and P. R. Prucnal. All-Optical Address Recognition and Self-Routing in a 250 Gb/s Packet-Switched Network. *Electronics Letters*, 30(16):1322 – 1323, 1994.

[21] G. K. Maity, T. Chattopadhyay, D. K. Gayen, C. Taraphdar, A. K. Maiti, S. P. Maity, and J. N. Roy. All-optical binary flip-flop with the help of Terahertz Optical Asymmetric Demultiplexer. *Natural Computing*, 9(4):903 – 916, 2010.

[22] P. Toliver, K. -L. Deng, I. Glesk, and P. R. Prucnal. Simultaneous Optical Compression and Decompression of 100 Gb/s OTDM Packets Using a Single TOAD and a Bi-directional Optical Delay Line Lattice. *IEEE Photonics Technology Letters*, 11(9):1183 – 1185, 1999.

[23] K. -L. Deng, R. Runser, I. Glesk, and P. R. Prucnal. Single-Shot Optical Sampling Oscilloscope for Ultrafast Optical Waveforms. *IEEE Photonics Technology Letters*, 10(3):397 – 399, 1998.

[24] I. Glesk, K. I. Kang, and P. R. Prucnal. Demonstration of Ultrafast All-Optical Packet Routing. *Electronics Letters*. 33(9):794 – 795, 1997.

[25] K. -L. Deng, I. Glesk, K. I. Kang, and P. R. Prucnal. Unbalanced TOAD for Optical Data and Clock separation in Self-Clocked Transparent OTDM Networks. *IEEE Photonics Technology Letters*, 9(6):830 – 832, 1997.

[26] I. Glesk and P. R. Prucnal. 250 Gb/s Self-Clocked Optical TDM with a Polarization-Multiplexed Clock. *Fiber and Integrated Optics*, 14(1):71 – 82, 1995.

[27] C. Koos, L. Jacome, C. Poulton, J. Leuthold, and W. Freude. Nonlinear silicon-on-insulator waveguides for all-optical signal processing. *Optics Express*, 15(10):5976 – 5990, 2007.

[28] M. Foster, K. Moll, and A. Gaeta. Optimal waveguide dimensions for nonlinear interactions. *Optics Express*, 12(13): 2880 – 2887, 2004.

[29] T. Vallaitis, S. Bogatscher, L. Alloatti, P. Dumon, R. Baets, M. Scimeca, I. Biaggio, F. Diederich, C. Koos, W. Freude and J. Leuthold. Optical properties of highly nonlinear silicon-organic hybrid (SOH) waveguide geometries. *Optics Express*, 17(20):17357 – 17368, 2009.

[30] Y. Kuo, H. Rong, V. Sih, S. Xu, M. Paniccia, and O. Cohen. Demonstration of wavelength conversion at 40 Gb/s data rate in silicon waveguides. *Optics Express*, 14(24):11721 – 11726, 2006.

[31] V. R. Almeida, Q. Xu, C. A. Barrios, and M. Lipson. Guiding and confining light in void nanostructure. *Optics Letters*, 29(11):1209 – 1211, 2004.

[32] N. J. Doran and D. Wood. Nonlinear-optical loop mirror. *Optics Letters*, 13(1):56 – 58, 1988.

[33] B. P. Nelson, K. J. Blow, P. D. Constantine, N. J. Doran, J. K. Lucek, I. W. Marshall, and K. Smith. All-optical Gbit/s switching using nonlinear optical loop mirror. *Electronics Letters*, 27(9): 704 – 705, 1991.

[34] P. A. Andrekson, N. A. Olsson, J. R. Simpson, D. J. Digiovanni, P. A. Morton, T. Tanbun-Ek, R. A. Logan, and K. W. Wecht. 64 Gb/s all-optical demultiplexing with the nonlinear optical-loop mirror. *Photonics Technology Letters, IEEE* 4(6):644 – 647, 1992.

[35] D. J. Barros, A. P. Almeida, F. S. Pinto, J. P. Carvalho, O. Frazão, and H. M. Salgado. Four-Wave Mixing in Photonic Crystal Fibres for Wavelength Conversion in Optical Networks.

[36] K. Uchiyama, S. Kawanishi, and M. Saruwatari. 100-Gb/s multiple-channel output all-optical OTDM demultiplexing using multichannel four-wave mixing in a semiconductor optical amplifier. *IEEE Photonics Technology Letters*, 10(6):890 – 892, 1998.

[37] Encyclopedia of Laser Physics and Technology - supercontinuum generation, supercontinua, nonlinear, spectral broadening, laser rainbow. [online] Rp-photonics.com., 2015. Available at: http://www.rp-photonics.com/supercontinuum_generation.html [Accessed 24 Feb. 2015].

[38] G. Genty, S. Coen, and J. M. Dudley. Fiber supercontinuum sources (Invited). *J. Opt. Soc. Am. B*, 24(8):1771 – 1785, 2007.

[39] S. Li, A. B. Ruffin, D. V. Kuksenkov, M-J Li, and D. A. Nolan. Supercontinuum generation in optical fibers. In *Asia-Pacific Optical Communications*, International Society for Optics and Photonics, 2007, pages 678105 – 678105, 2007.

[40] N. Iizuka, K. Kaneko, N. Suzuki, T. Asano, S. Noda, and O. Wada. Ultrafast intersubband relaxation (≤150 fs) in AlGaN/GaN multiple quantum wells. *Applied Physics Letters*, 77(5):648 – 650, 2000.

[41] J. D. Heber, C. Gmachl, H. M. Ng, and A. Y. Cho. Comparative study of ultrafast intersubband electron scattering times at ∼ 1.55 μm wavelength in GaN/AlGaN heterostructures. *Applied Physics Letters*, 81(7):1237 – 1239, 2002.

[42] N. Iizuka, K. Kaneko, and N. Suzuki. Near-infrared intersubband absorption in GaN/AlN quantum wells grown by molecular beam epitaxy. *Applied Physics Letters*, 81(10): 1803 – 1805, 2002.

[43] D. D. Yang, F. H. Julien, P. Boucaud, J. M. Lourtioz, and R. Planel. Intersubband absorption of GaAs/AlGaAs quantum wells in MBE grown mid-infrared slab waveguides. *IEEE Photonics Technology Letters*, 2(3):181 – 183, 1990.

[44] F. H. Julien, P. Vagos, J-M. Lourtioz, D. D. Yang, and R. Planel. Novel all-optical 10 μm waveguide modulator based on intersubband absorption in GaAs/AlGaAs quantum wells. *Applied Physics Letters*, 59(21):2645 – 2647, 1991.

[45] R. Hui, Y. Wan, J. Li, S. X. Jin, J. Y. Lin, and H. X. Jiang. Birefringence of GaN/AlGaN optical waveguides. *Applied Physics Letters*, 83(9):1698 – 1700, 2003.

[46] A. D. L. Bugallo. Fabrication and Characterization of nanodevices based on III-V nanowires. PhD dissertation, Université Paris Sud-Paris XI, 2012.

[47] C. Xiong, W. Pernice, K. K. Ryu, C. Schuck, K. Y. Fong, T. Palacios, and H. X. Tang. Integrated GaN photonic circuits on silicon (100) for second harmonic generation. *Optics Express*, 19(11):10462 – 10470, 2011.

[48] C. Xiong, W. Pernice, C. Schuck, and H. X. Tang. Integrated Photonic Circuits in Gallium Nitride and Aluminum Nitride. *International Journal of High Speed Electronics and Systems*, 23(01n02):1450001-1 – 1450001-8, 2014.

[49] S. Pal, and C. Jacob. Silicon—a new substrate for GaN growth. *Bulletin of Materials Science*, 27(6):501 – 504, 2004.

[50] N. V. Triviño, U. Dharanipathy, J-F. Carlin, Z. Diao, R. Houdre, and N. Grandjean. Integrated photonics on silicon with wide bandgap GaN semiconductor. *Applied Physics Letters*, 102(8):081120-1 – 081120-4, 2013.

[51] I. Saraswati, , A. Stolz, S. Ko, E. Dogheche, N. R. Poespawati, R. Wigajatri, and D. Decoster. Optical Properties of Gallium Nitride Heterostructures Grown on Silicon for Waveguiding Application. In *Advanced Materials Research*, volume 980, pages 41 – 45, 2014.

[52] I. Saraswati, N. R. Poepawati, R. Wigajatri, E. Dogheche, D. Decoster, S. Ko, Y.H. Cho, L. Considine, D. Pavlidis. Investigation of Structural, Morphological and Optical Properties of GaN/AlGaN Heterostructures on Si. In *Photonic Global Conference, Singapore.* 2012.

[53] Q. Wang. Design and Experimental Characterization of an Erbium Doped GaN Waveguide. PhD dissertation, University of Kansas, 2012.

[54] R. Hui, S. Taherion, Y. Wan, J. Li, S. X. Jin, J. Y. Lin, and H. X. Jiang. GaN-based waveguide devices for long-wavelength optical communications. *Applied Physics Letters*, 82(9): 1326 – 1328, 2003.

[55] S. Ghosh, P. Waltereit, O. Brandt, H. T. Grahn, and K. H. Ploog. Polarization-dependent spectroscopic study of M-plane GaN on γ-$LiAlO_2$. *Applied Physics Letters*, 80(3):413 – 415, 2002.

[56] R. Hui, Y. Wan, J. Li, S. Jin, J. Lin, and H. Jiang. III-nitride-based planar lightwave circuits for long wavelength optical communications. *IEEE Journal of Quantum Electronics*, 41(1):100 – 110, 2005.

[57] B. R. Bennett, R. A. Soref, and J. A. Del Alamo. Carrier-induced change in refractive index of InP, GaAs and InGaAsP. *IEEE Journal of Quantum Electronics*, 26(1):113 – 122, 1990.

[58] M. Okuno, K. Kato, Y. Ohmori, M. Kawachi, and T. matsunaga. Improved 8x8 integrated optical matrix switch using silica-based planar lightwave circuits. *Journal of Lightwave Technology*, 12(9):1597 – 1606, 1994.

[59] N. Takato, T. Kominato, A. Sugita, K. Jinguji, H. Toba, and M. Kawachi. Silica-based integrated optic Mach-Zehnder multi/demultiplexer family with channel spacing of 0.01-250 nm. *IEEE Journal on Selected Areas in Communications,* 8(6):1120 – 1127, 1990.

[60] C. R. Doerr, C. H. Joyner, L. W. Stulz, and R. Monnard. Wavelength-division multiplexing cross connect in InP. *IEEE Photonics Technology Letters,* 10(1):117 – 119, 1998.

[61] M. K. Smit and C. V. Dam. PHASAR-based WDM-devices: Principles, design and applications. *IEEE Journal of Selected Topics in Quantum Electronics*, 2(2):236 – 250, 1996.

[62] R. Das. Ultra-broadband optical parametric amplification by tailoring the group-velocity dispersion of Bragg reflection waveguides. *Journal of Physics D: Applied Physics*, 42(23):235106, 2009.

[63] R. Das and K. Thyagarajan. A high efficiency scheme for phase-matched second-harmonic generation in GaN-based Bragg reflection waveguide. *IEEE Photonics Technology Letters,* 19(19):1526 – 1528, 2007.

[64] E. Yablonovitch and T. J. Gmitter. Photonic band structure: the face-centered-cubic case. *Physical Review Letters*, 63(18):1950 – 1953, 1989.

[65] T. F. Krauss, M. Richard, and Stuart Brand. Two-dimensional photonic-bandgap structures operating at near-infrared wavelengths. *Nature*, 383(6602):699 – 702, 1996.

[66] D. Labilloy, H. Benisty, C. Weisbuch, T. F. Krauss, R. M. De La Rue, V. Bardinal, R. Houdré, U. Oesterle, D. Cassagne, and C. Jouanin. Quantitative measurement of transmission, reflection, and diffraction of two-dimensional photonic band gap structures at near-infrared wavelengths. *Physical Review Letters*, 79(21):4147 – 4150, 1997.

[67] N. V. Triviño, U. Dharanipathy, J-F. Carlin, Z. Diao, R. Houdre, and N. Grandjean. Integrated photonics on silicon with wide bandgap GaN semiconductor. *Applied Physics Letters*, 102(8):081120-1 – 081120-4, 2013.

[68] J. C. Knight, J. Broeng, T. A. Birks, and P. St J. Russell. Photonic band gap guidance in optical fibers. *Science* 282(5393):1476 – 1478, 1998.

[69] E. Yablonovitch, T. J. Gmitter, R. D. Meade, A. M. Rappe, K. D. Brommer, and J. D. Joannopoulos. Donor and acceptor modes in photonic band structure. *Physical Review Letters*, 67(24):3380 – 3383, 1991.

[70] P. R. Villeneuve, F. Shanhui, J. D. Joannopoulos, Kuo-Yi Lim, G. S. Petrich, L. A. Kolodziejski, and R. Reif. Air-bridge microcavities. *Applied Physics Letters*, 67(2):167 – 169, 1995.

[71] P. R. Villeneuve, F. Shanhui, and J. D. Joannopoulos. Microcavities in photonic crystals: Mode symmetry, tunability, and coupling efficiency. *Physical Review B* 54(11):7837 – 7842, 1996.

[72] R. D. Meade, A. Devenyi, J. D. Joannopoulos, O. L. Alerhand, D. A. Smith, and K. Kash. Novel applications of photonic band gap materials: Low-loss bends and high Q cavities. *Journal of Applied Physics*, 75(9):4753 – 4755, 1994.

[73] S-Yu Lin, E. Chow, V. Hietala, P. R. Villeneuve, and J. D. Joannopoulos. Experimental demonstration of guiding and bending of electromagnetic waves in a photonic crystal. *Science*, 282(5387):274 – 276, 1998.

[74] L. G. Baird. Near field imaging of gallium nitride nanowires for characterization of minority carrier diffusion. *Naval Postgraduate School Monterey Ca Dept Of Physics*, 2009.

[75] S. Arafin, X. Liu, and Z. Mi. Review of recent progress of III-nitride nanowire lasers. *Journal of Nanophotonics*, 7(1):074599 – 074599, 2013.

[76] J. J. Coleman, A. C. Bryce, and C. Jagadish, eds. *Advances in semiconductor lasers*, Volume 86. Academic Press, 2012.

[77] H. Xu. Controlled Lasing in Gallium Nitride Nanowires. PhD dissertation, The University of New Mexico, 2013.

[78] P. Yang. The chemistry and physics of semiconductor nanowires. *MRS Bulletin*, 30(02): 85 – 91, 2005.

[79] A. Motayed. Gallium nitride nanowire based electronic and optical devices. PhD dissertation, University of Maryland, College Park, 2007.

[80] R. S. Wagner and W. C. Ellis. Vapor-liquid-solid mechanism of single crystal growth. *Applied Physics Letters*:89 – 90, 1964.

[81] M. C. Gupta and J. Ballato. *The Handbook of Photonics: Second Edition.* CRC Press, Taylor & Francis Group, Boca Raton, FL, USA, 2007.

[82] C. Kumtornkittikul. GaN/AlN Multiple Quantum Wells and Nitride-Based Waveguide Structures for Ultrafast All-Optical Switch Utilizing Intersubband Transition. PhD dissertation, 2006.

[83] Y. Li, A. Bhattacharyya, C. Thomidis, T. D. Moustakas, and R. Paiella. Intersubband nonlinear optical processes in GaN/AlN quantum-well waveguides. In *Conference on Lasers and Electro-Optics*, Optical Society of America, page CTuH3, 2008.

[84] Y. Li, A. Bhattacharyya, C. Thomidis, T. D. Moustakas, and R. Paiella. Nonlinear optical waveguides based on near-infrared intersubband transitions in GaN/AlN quantum wells. *Optics Express*, 15(9):5860 – 5865, 2007.

[85] N. Iizuka, K. Kaneko, and N. Suzuki. All-optical switch utilizing intersubband transition in GaN quantum wells. *IEEE Journal of Quantum Electronics*, 42(8):765 – 771, 2006.

[86] J. Liu, Y. Bai, and G. Xiong. Studies of the second-order nonlinear optical susceptibilities of GaN/AlGaN quantum well. *Physica E: Low-dimensional Systems and Nanostructures*, 23(1):70 – 74, 2004.

[87] D. Passeri, M. C. Larciprete, A. Belardini, S. Paoloni, A. Passaseo, C. Sibilia, and F. Michelotti. Second harmonic generation in AlGaN, GaN and AlxGa1–xN/GaN multiple quantum well structures. *Applied Physics B*, 79(5):611 – 615, 2004.

[88] R. Rapaport, G. Chen, O. Mitrofanov, C. Gmachl, H. M. Ng, and S. N. G. Chu. Resonant optical nonlinearities from intersubband transitions in GaN/AlN quantum wells. *Applied Physics Letters*, 83(2):263 – 265, 2003.

[89] J. D. Heber, C. Gmachl, H. M. Ng, and A. Y. Cho. Comparative study of ultrafast intersubband electron scattering times at ∼1.55 µm wavelength in GaN/AlGaN heterostructures. *Applied Physics Letters*, 81(7):1237 – 1239, 2002.

[90] L. J. McKnight. Waveguides in large bandgap materials for lasers and quantum photonics. PhD dissertation, University of Strathclyde, 2012.

[91] N. Iizuka, K. Kaneko, and N. Suzuki. Sub-picosecond all-optical gate utilizing an intersubband transition. *Optics Express*, 13(10):3835 – 3840, 2005.

[92] N. Suzuki and N. Iizuka. Feasibility study on ultrafast nonlinear optical properties of 1.55-µm intersubband transition in AlGaN/GaN quantum wells. *Japanese Journal of Applied Physics*, 36(8A):L1006 – L1008, 1997.

[93] N. Suzuki and N. Iizuka. Electron scattering rates in AlGaN/GaN quantum wells for 1.55-µm inter-subband transition. *Japanese Journal of Applied Physics*, 37(4A):L369 – L371, 1998.

[94] C. Kumtornkittikul, M. Sugiyama, and Y. Nakano. GaN/AIN multiple quantum wells grown on GaN-AIN waveguide structure by metalorganic vapor-phase epitaxy. *Journal of Electronic Materials*, 35(4):744 – 749, 2006.

[95] C. Kumtornkittikul, T. Shimizu, N. Iizuka, N. Suzuki, M. Sugiyama, and Y. Nakano. AlN waveguide with GaN/AlN quantum wells for all-optical switch utilizing intersubband transition. *Japanese Journal of Applied Physics*, 46(4L):L352 – L355, 2007.

[96] G. Ghione. *Semiconductor devices for high-speed optoelectronics*. Cambridge University Press, 2009.

[97] H. Machhadani, P. Kandaswamy, S. Sakr, A. Vardi, A. Wirtmüller, L. Nevou, F. Guillot et al. GaN/AlGaN intersubband optoelectronic devices. *New Journal of Physics*, 11(12): 125023, 2009.

[98] O. Skorka, B. Meyler, and J. Salzman. Propagation loss in GaN-based ridge waveguides. *Applied Physics Letters*, 84(19):3801 – 3803, 2004.

[99] C-Y Huang, Y-D Lin, A. Tyagi, A. Chakraborty, H. Ohta, J. S. Speck, S. P. DenBaars, and S. Nakamura. Optical waveguide simulations for the optimization of InGaN-based green laser diodes. *Journal of Applied Physics*, 107(2):023101-1 – 023101-7, 2010.

[100] R. Geiss, A. Chowdhury, C. M. Staus, H. M. Ng, S. S. Park, and J. Y. Han. Low loss GaN at 1550 nm. *Applied Physics Letters*, 87(13):132107 – 132107, 2005.

[101] A. Stolz, L. Considine, E. Dogheche, D. Decoster, and D. Pavlidis. Prospective for Gallium Nitride-Based Optical Waveguide Modulators. *IEICE Transactions on Electronics*, 95(8):1363 – 1368, 2012.

[102] M. Kumar, J. T. Boyd, H. E. Jackson, J. M. Zavada, H. A. Jenkinson, R. G. Wilson, B. Theys, and J. Chevallier. Channel optical waveguides formed by deuterium passivation in GaAs and InP. *Journal of Applied Physics*, 82(7):3205 – 3213, 1997.

[103] J. C. Johnson, H-J. Choi, K. P. Knutsen, R. D. Schaller, P. Yang, and R. J. Saykally. Single gallium nitride nanowire lasers. *Nature Materials*, 1(2):106 – 110, 2002.

[104] D. J. Gargas, M. E. Toimil-Molares, and P. Yang. Imaging single ZnO vertical nanowire laser cavities using UV-laser scanning confocal microscopy. *Journal of the American Chemical Society*, 131(6):2125 – 2127, 2009.

[105] F. Qian, Y. Li, S. Gradečak, H-G. Park, Y. Dong, Y. Ding, Z. L. Wang, and C. M. Lieber. Multi-quantum-well nanowire heterostructures for wavelength-controlled lasers. *Nature Materials*, 7(9):701-706, 2008.

[106] H. Gao, A. Fu, S. C. Andrews, and P. Yang. Cleaved-coupled nanowire lasers. In *Proceedings of the National Academy of Sciences* volume 110, number 3, pages 865 – 869, 2013.

[107] A. Javan, W. R. Bennett Jr, and D. R. Herriott. Population Inversion and Continuous Optical Maser Oscillation in a Gas Discharge Containing a He-Ne Mixture. *Physical Review Letters*, 6(3):106, 1961.

[108] W. H. Loh, B. N. Samson, L. Dong, G. J. Cowle, and K. Hsu. High performance single frequency fiber grating-based erbium: ytterbium-codoped fiber lasers. *Journal of Lightwave Technology*, 16(1):114 – 118, 1998.

[109] J. J. Zayhowski, and A. Mooradian. Single-frequency microchip Nd lasers. *Optics Letters*, 14(1):24 – 26, 1989.

[110] G. T. Wang, Q. Li, J. Huang, A. A. Talin, A. Armstrong, P. C. Upadhya, and R. P. Prasankumar. III-nitride nanowires: novel materials for solid-state lighting. In *SPIE OPTO*, International Society for Optics and Photonics, page 79540T – 79540T, 2011.

[111] M. Graf. Design and characterisation of far-and mid-infrared quantum cascade detectors. PhD dissertation, Université de Neuchâtel, 2008.

[112] S. Sakr, Y. Kotsar, S. Haddadi, M. Tchernycheva, L. Vivien, I. Sarigiannidou, N. Isac, E. Monroy, and F. H. Julien. GaN-based quantum cascade photodetector with 1.5 μm peak detection wavelength. *Electronics Letters*, 46(25):1685 – 1686, 2010.

[113] E. A. DeCuir, M. O. Manasreh, Elena Tschumak, J. Schormann, D. J. As, and K. Lischka. Cubic GaN/AlN multiple quantum well photodetector. *Applied Physics Letters*, 92(20): 201910 – 201910, 2008.

[114] D. Hofstetter, E. Baumann, F. R. Giorgetta, F. Guillot, S. Leconte, and E. Monroy. Optically nonlinear effects in intersubband transitions of GaN/AlN-based superlattice structures. *Applied Physics Letters*, 91(13):131115 – 131115, 2007.

[115] D. Hofstetter, R. Theron, E. Baumann, F. R. Giorgetta, S. Golka, G. Strasser, F. Guillot, and E. Monroy. Monolithically integrated AlGaN/GaN/AlN-based solar-blind ultraviolet and near-infrared detectors. *Electronics Letters*, 44(16):986 – 988, 2008.

[116] D. Hofstetter, E. Baumann, F. R. Giorgetta, R. Théron, F. Guillot, E. Monroy, S. Golka, and G. Strasser. Monolithically integrated UV/IR-photodetectors based on an AlN/GaN-based superlattice grown on an AlGaN buffer layer. *Physica Status Solidi (c)*, 6(S2):S818 – S821, 2009.

[117] A. Vardi, G. Bahir, F. Guillot, C. Bougerol, E. Monroy, S. E. Schacham, M. Tchernycheva, and F. H. Julien. Near infrared quantum cascade detector in GaN/ AlGaN/ AlN heterostructures. *Applied Physics Letters*, 92(1):011112-1 – 011112-3, 2008.

[118] A. Vardi, N. Kheirodin, L. Nevou, H. Machhadani, L. Vivien, P. Crozat, M. Tchernycheva et al. High-speed operation of GaN/AlGaN quantum cascade detectors at $\lambda \approx 1.55$ μm. *Applied Physics Letters*, 93(19):193509 – 193509, 2008.

[119] S. Sakr, P. Crozat, D. Gacemi, Y. Kotsar, A. Pesach, P. Quach, N. Isac et al. GaN/AlGaN waveguide quantum cascade photodetectors at $\lambda \approx 1.55$ μm with enhanced responsivity and ~ 40 GHz frequency bandwidth. *Applied Physics Letters*, 102(1):011135-1 – 011135-4, 2013.

[120] S. Sakr, Y. Kotsar, S. Haddadi, M. Tchernycheva, L. Vivien, I. Sarigiannidou, N. Isac, E. Monroy, and F. H. Julien. GaN-based quantum cascade photodetector with 1.5 μm peak detection wavelength. *Electronics Letters*, 46(25):1685 – 1686, 2010.

[121] E. Desurvire. The golden age of optical fiber amplifiers. *Physics Today*, 47(1):20 – 27, 1994.

[122] A. J. Kenyon. Recent developments in rare-earth doped materials for optoelectronics. *Progress in Quantum Electronics*, 26(4):225 – 284, 2002.

[123] R. Dahal, C. Ugolini, J. Y. Lin, H. X. Jiang, and J. M. Zavada. Erbium-doped GaN optical amplifiers operating at 1.54 μm. *Applied Physics Letters*, 95(11):111109-1 – 111109-3, 2009.

[124] R. Dahal, J. Y. Lin, H. X. Jiang, and J. M. Zavada. Er-Doped GaN and $In_xGa_{1-x}N$ for Optical Communications. In *Rare Earth Doped III-Nitrides for Optoelectronic and Spintronic Applications*, Springer Netherlands, pages 115 – 157, 2010.

[125] R. Dahal, J. Y. Lin, H. X. Jiang, and J. M. Zavada. Near infrared photonic devices based on Er-doped GaN and InGaN. *Optical Materials*, 33(7):1066 – 1070, 2011.

[126] K Iga. "Surface-emitting laser-its birth and generation of new optoelectronics field." *IEEE Journal of Selected Topics in Quantum Electronics*, 6(6):1201 – 1215, 2000.

[127] T-C. Lu, C-C. Kao, H-C. Kuo, G-S. Huang, and S-C. Wang. CW lasing of current injection blue GaN-based vertical cavity surface emitting laser. *Applied Physics Letters*, 92(14): 141102 – 141102, 2008.

[128] T-C. Lu, S-W. Chen, T-T. Wu, P-M. Tu, C-K. Chen, C-H. Chen, Z-Y. Li, H-C. Kuo, and S-C. Wang. Continuous wave operation of current injected GaN vertical cavity surface emitting lasers at room temperature. *Applied Physics Letters*. 97(7):071114 – 071114, 2010.

[129] Y. Higuchi, K. Omae, H. Matsumura, and T. Mukai. Room-temperature CW lasing of a GaN-based vertical-cavity surface-emitting laser by current injection. *Applied Physics Express*, 1(12):121102-1 – 121102-3, 2008.

[130] J. Piprek. What is the problem with GaN-based VCSELs? In *Numerical Simulation of Optoelectronic Devices (NUSOD), 2013 13th International Conference on*, IEEE, 2013, pages 89 – 90, 2013.

[131] G. M. Yang, M. H. MacDougal, and P. D. Dapkus. Ultralow threshold current vertical-cavity surface-emitting lasers obtained with selective oxidation. *Electronics Letters*, 31(11):886 – 888, 1995.

[132] A. V. Krishnamoorthy, K. W. Goossen, L. M. F. Chirovsky, R. G. Rozier, P. Chandramani, S. P. Hui, J. Lopata, J. A. Walker, and L. A. D'Asaro. 16 × 16 VCSEL array flip-chip bonded to cmos vlsi circuit. *IEEE Photonics Technology Letters*, 12(8):1073 – 1075, 2000.

[133] U. Eriksson, P. Evaldsson, and K. Streubel. A novel technology for monolithic integration of VCSELs and heterojunction bipolar transistors (HBTs) at 1.55μm. In *CLEO Pacific Rim*, volume 97, pages 14 – 18.

[134] J. S. Harris Jr. GaInNAs long-wavelength lasers: progress and challenges. *Semiconductor Science and Technology*, 17(8):880 – 891, 2002.

[135] N. V. Triviño, U. Dharanipathy, J-F. Carlin, Z. Diao, R. Houdre, and N. Grandjean. Integrated photonics on silicon with wide bandgap GaN semiconductor. *Applied Physics Letters*, 102(8):081120 – 081124, 2013.

[136] New concept for the monolithic integration of optoelectronic circuits on Silicon substrate: Silicon Photonics. [Online]. http://www.nasp.de/publications.html., 2015. Available at: http://www.nasp.de/publications.html?file=files/downloads/Silicon_Photonics.pdf. [Accessed 19 Jan. 2015].

[137] J. E. Bowers, D. Liang, A. W. Fang, H. Park, R. Jones, and M. J. Paniccia. Hybrid silicon lasers: The final frontier to integrated computing. *Optics and Photonics News*, 21(5):28 – 33, 2010.

[138] L. Pavesi, L. D. Negro, C.Mazzoleni, G. Franzo, and F. Priolo. Optical gain in silicon nanocrystals. *Nature*, 408(6811):440 – 444, 2000.

[139] G. Franzo, F. Priolo, S. Coffa, A. Polman, and A. Carnera. Room-temperature electroluminescence from Er-doped crystalline Si. *Applied Physics Letters*, 64(17):2235 – 2237, 1994.

[140] O. Boyraz and B. Jalali. Demonstration of a silicon Raman laser. *Optics Express*, 12(21):5269 – 5273, 2004.

[141] R. Jones, O. Cohen, M. Paniccia, A. W. Fang, and J. Bowers. A Hybrid Silicon Laser-The first electrically pumped, hybrid silicon laser overcomes one of the last major hurdles to silicon photonic chips. *Photonics Spectra*, 41(1):54 – 64, 2007.

[142] H. Yonezu. Control of structural defects in group III–V–N alloys grown on Si. *Semiconductor Science and Technology*, 17(8):762 – 768, 2002.

[143] T. T. Nguyen. Sillicon photonics based on monolithic integration of III-V nanostructures on silicon. PhD dissertation, INSA de Rennes, 2013.

[144] B. Kunert, S. Reinhard, J. Koch, M. Lampalzer, K. Volz, and W. Stolz. "First demonstration of electrical injection lasing in the novel dilute nitride Ga (NAsP)/GaP-material system." *Physica Status Solidi (c)*, 3(3):614 – 618, 2006.

[145] B. Kunert, A. Klehr, S. Reinhard, K. Volz, and W. Stolz. Near room temperature electrical injection lasing for dilute nitride Ga (NAsP)/GaP quantum-well structures grown by metal organic vapour phase epitaxy. *Electronics Letters*, 42(10):601 – 603, 2006.

[146] S. Mishra, N. K. Chaudhary, and K. Singh. *Overview of optical interconnect technology*. arXiv preprint arXiv:1303.3954, 2013.

[147] R. A. Soref and J. P. Lorenzo. All-silicon active and passive guided-wave components for lambda=1.3 and 1.6 microns. *IEEE Journal of Quantum Electronics*, 22:873 – 879, 1986.

[148] R. Soref. The past, present, and future of silicon photonics. *IEEE Journal of Selected Topics in Quantum Electronics*, 12(6):1678 – 1687, 2006.

[149] B. Jalali and S. Fathpour. Silicon photonics. *Journal of Lightwave Technology*, 24(12):4600 – 4615, 2006.

[150] M. Lipson. Guiding, modulating, and emitting light on silicon-challenges and opportunities. *Journal of Lightwave Technology*, 23(12):4222 – 4238, 2005.

[151] J.Yang. *High-performance quantum dot lasers and integrated guided-wave devices on silicon*. ProQuest, 2008.

[152] J. Ma. Nonlinear Integrated Photonics On Silicon And Gallium Arsenide Substrates. PhD dissertation, University of Central Florida Orlando, Florida, 2014.

[153] G. D. Miller, R. G. Batchko, W. M. Tulloch, D. R. Weise, M. M. Fejer, and R. L. Byer. 42%-efficient single-pass cw second-harmonic generation in periodically poled lithium niobate. *Optics Letters*, 22(24):1834 – 1836, 1997.

[154] K. Noguchi, O. Mitomi, and H. Miyazawa. Millimeter-wave Ti: LiNbO3 optical modulators. *Journal of Lightwave Technology*, 16(4):615 – 619, 1998.

[155] A. Chiba, T. Sakamoto, T. Kawanishi, K. Higuma, M. Sudo, and J. Ichikawa. 16-level quadrature amplitude modulation by monolithic quad-parallel Mach-Zehnder optical modulator. *Electronics Letters*, 46(3):220 – 222, 2010.

[156] P. Rabiei, J. Ma, S. Khan, J. Chiles, and S. Fathpour. Heterogeneous lithium niobate photonics on silicon substrates. *Optics Express*, 21(21):25573 – 25581, 2013.

[157] A. Guarino, G. Poberaj, D. Rezzonico, R. Degl'Innocenti, and P. Günter. Electroopti-cally tunable microring resonators in lithium niobate. *Nature Photonics*, 1(7): 407 – 410, 2007.

[158] J. Kondo, A. Kondo, K. Aoki, M. Imaeda, T. Mori, Y. Mizuno, S. Takatsuji, Y. Kozuka, and M. Minakata. 40-Gb/s X-cut LiNbO3 optical modulator with two-step back-slot structure. *Journal of Lightwave Technology*, 20(12):2110 – 2114, 2002.

[159] B. E. Little and S. T. Chu. Toward very large-scale integrated photonics. *Optics and Photonics News*, 11(11):24 – 29, 2000.

[160] M. Koechlin. Electro-optical microresonators in ion-sliced lithium niobate. PhD Dissertation, Eidgenössische Technische Hochschule ETH Zürich, Nr. 18811, 2009.

[161] M. Koechlin, F. Sulser, Z. Sitar, G. Poberaj, and P. Gunter. Free-standing lithium niobate microring resonators for hybrid integrated optics. *IEEE Photonics Technology Letters*, 22(4): 251 – 253, 2010.